S100A1 AND S100B: NOVEL DRUG TARGETS FOR ALZHEIMER'S DISEASE THERAPY

A Dissertation

by

EMILY ANNA ROLTSCH

Submitted to the Office of Graduate Studies of
Texas A&M University
in partial fulfillment of the requirements for the degree of

DOCTOR OF PHILOSOPHY

December 2011

Major Subject: Veterinary Microbiology

S100A1 and S100B: Novel Drug Targets for Alzheimer's Disease Therapy

S100A1 AND S100B: NOVEL DRUG TARGETS FOR ALZHEIMER'S DISEASE THERAPY

A Dissertation

by

EMILY ANNA ROLTSCH

Submitted to the Office of Graduate Studies of
Texas A&M University
in partial fulfillment of the requirements for the degree of

DOCTOR OF PHILOSOPHY

Approved by:

Chair of Committee,	Danna B. Zimmer
Committee Members,	C. Jane Welsh
	Brian Porter
	Farida Sohrabji
Head of Department,	Linda Logan

December 2011

Major Subject: Veterinary Microbiology

ABSTRACT

S100A1 and S100B: Novel Drug Targets for Alzheimer's Disease Therapy.

(December 2011)

Emily Anna Roltsch, B.S.; M.S, Texas A&M University

Chair of Advisory Committee: Dr. Danna B. Zimmer

Numerous factors/gene products, including S100A1 and S100B, have been implicated in the onset and progression of Alzheimer's disease (AD). However, deciphering S100A1/S100B's role in AD has been hampered by their antipodal effects and ability to act as both intracellular calcium receptors and secreted neuropeptides. This study utilizes two approaches, genetic ablation and passive immunotherapy, to inhibit S100A1 and/or S100B in the PSAPP AD mouse model to ascertain the net contribution of these proteins to AD pathology. In addition, a combination of microarray profiling, post-array validation and bioinformatics were used to identify changes in miRNA expression in response to S100A1/S100B ablation. In 6 month old mice, S100B ablation resulted in a 3-fold decrease in cortical but not hippocampal plaque load while S100A1 ablation resulted in a 3.5-fold reduction in cortical and a 2.4-fold reduction in hippocampal plaque load. Interestingly, ablation of both S100A1 and S100B was synergistic resulting in an age-, region- and end point- specific manner. Diminished plaque load was accompanied by decreased GFAP-positive astrocytes and Iba-1 positive microglia. The effects of S100A1/S100B on plaque load were not limited

to early stages of plaque deposition. Even though older (12 month old) PSAPP animals had over 6-fold increase in plaque load, S100A1 or S100A1/S100B ablation still diminished cortical/hippocampal plaque load by 60-65%. Similar results were observed when passive immunotherapy was used to inhibit S100A1/S100B function. Anti-S100 treatment of mice from 3-6 months of age decreased cortical/hippocampal plaque load, and decreased cortical but not hippocampal GFAP staining. The effects of passive immunotherapy with S100A1/S100B antibodies were not limited to pre-plaque treatment. Anti-S100 treated mice from 6-9 months of age exhibited decreased cortical, but not hippocampal, plaque load and cortical/hippocampal GFAP staining. In addition, these S100A1/S100B mediated decreases were accompanied by downregulated expression of miR- 448, miR-133a, miR-204, and miR-206 as well as upregulated expression of miR-34a. Collectively, these data demonstrate that inhibition of S100A1 and S100B synergistically reduce AD pathology and suggest that the detrimental gain of function of S100A1/S100B contributes to AD. Therefore, development of drugs to inhibit S100 function in patients will be beneficial in the treatment of AD and slowing disease progression.

To my family for their endless love and support and to all the loved ones around the world suffering from this debilitating disease

ACKNOWLEDGEMENTS

I would like to thank my committee chair, Dr. Danna Zimmer, and my committee members, Drs. Jane Welsh, Brian Porter and Farida Sohrabji, for their support and guidance throughout the course of this project. I am indebted to Dr. Zimmer for her tireless efforts and determination to make a decided dental school applicant into a neuroscientist and giving me the opportunity to work on this amazing project. Words cannot express my appreciation for her support, encouragement and patience throughout this project and program. Thank you to Dr. Mike Criscitiello for allowing me space in his lab after Dr. Zimmer left for Maryland. I would like to thank my parents, Jenny and Scott, for their love, encouragement and support and my brother Zachary who, despite my many meltdowns, was the best brother I could have asked for, providing encouragement and support, and making me laugh when I wanted so badly to cry. Words cannot express what it means to me to have such wonderful friends, too many to name herein, who have supported, encouraged and influenced me over the years and made my time at Texas A&M University such a wonderful experience.

NOMENCLATURE

Aβ	Amyloid Beta
AD	Alzheimer's Disease
APP	Amyloid Precursor Protein
BACE1	β-site of APP Cleaving Enzyme
BDNF	Brain-Derived Neurotrophic Factor
BP	Base Pair
Ca^{2+}	Calcium
CDK5	Cyclin-Dependent Kinase 5
CNS	Central Nervous System
CX	Cortex
CR	Cerebellum
DAPI	4',6-diamidino-2-phenylindole
GFAP	Glial Fibrillary Acidic Protein
GSK3β	Glycogen Synthase Kinase 3 Beta
HCV	Hepatitis C Virus
HP	Hippocampus
IBA1	Ionized Calcium Binding Adaptor Molecule 1
IFNβ	Interferon β
KLF5	Kruppel-like Factor 5
miRNA	Micro-ribonucleic Acid

miR-	Micro-ribonucleic Acid
mESC	Mouse Embryonic Stem Cells
NaCl	Sodium Chloride
NaOH	Sodium Hydroxide
NF-κB	Nuclear Factor Kappa-light-chain-enhancer of Activated B Cells
NIH	National Institutes of Health
OLF	Olfactory Bulb
PBS	Phosphate Buffered Saline
PCR	Polymerase Chain Reaction
PKA	Protein Kinase A
Pre-miRNA	Precursor Micro-ribonucleic Acid
Pri-miRNA	Primary Micro-ribonucleic Acid
PSEN1	Presenilin 1 Gene
PS-1	Presenilin 1
PSEN2	Presenilin 2 Gene
RNA	Ribonucleic Acid
SATB1	Special AT-rich Sequence-binding Protein-1
SEM	Standard Error of the Mean
UTR	Untranslated Region

TABLE OF CONTENTS

CHAPTER Page

CHAPTER Page

LIST OF FIGURES

FIGURE Page

LIST OF TABLES

CHAPTER I

INTRODUCTION

Calcium (Ca^{2+}) signaling is responsible for a multitude of cellular functions, including gene expression, cell growth, development, survival and ultimately cell death. In neuronal cells, an increase in intracellular calcium $[Ca^{2+}]_i$ levels triggers vesicle fusion and neurotransmitter release (Berridge, 1998). Ca^{2+} receptor proteins convert changes in $[Ca^{2+}]_i$ into responses. Members of the S100/calmodulin/troponin superfamily of Ca^{2+} receptor proteins contain a highly conserved 12 amino acid EF-hand Ca^{2+} binding domain. S100 proteins also contain a Ca^{2+} binding loop comprised of 14 amino acids called the 'pseudo EF-hand' (Marenholz, et al., 2004; Zimmer, et al., 2005). Like all Ca^{2+} receptor proteins, S100 proteins undergo a conformational change after binding Ca^{2+}, exposing a hydrophobic patch necessary for interacting with numerous intra- and extra-cellular protein targets and the subsequent exertion of their biological effects (Figure 1) (Marenholz, et al., 2004; Zimmer, et al., 2003; Zimmer, et al., 2005; Zimmer and Weber, 2010).

The first S100 family members were isolated as a brain-specific fraction in 1965 and called S100 to denote their solubility in 100% saturated ammonium sulfate (Moore, 1965). This original fraction was composed of two 10,000 molecular weight proteins,

---

This dissertation follows the style of The Journal of Neuroscience.

S100A1 and S100B (Marenholz, et al., 2004; Zimmer, et al., 1995; Zimmer, et al., 2005). A total of 21 S100 proteins are encoded in the human genome, seventeen (S100A1-S100A16) of which are encoded in a gene cluster on human chromosome 1q21. The remaining family members are encoded on other chromosomes: S100B

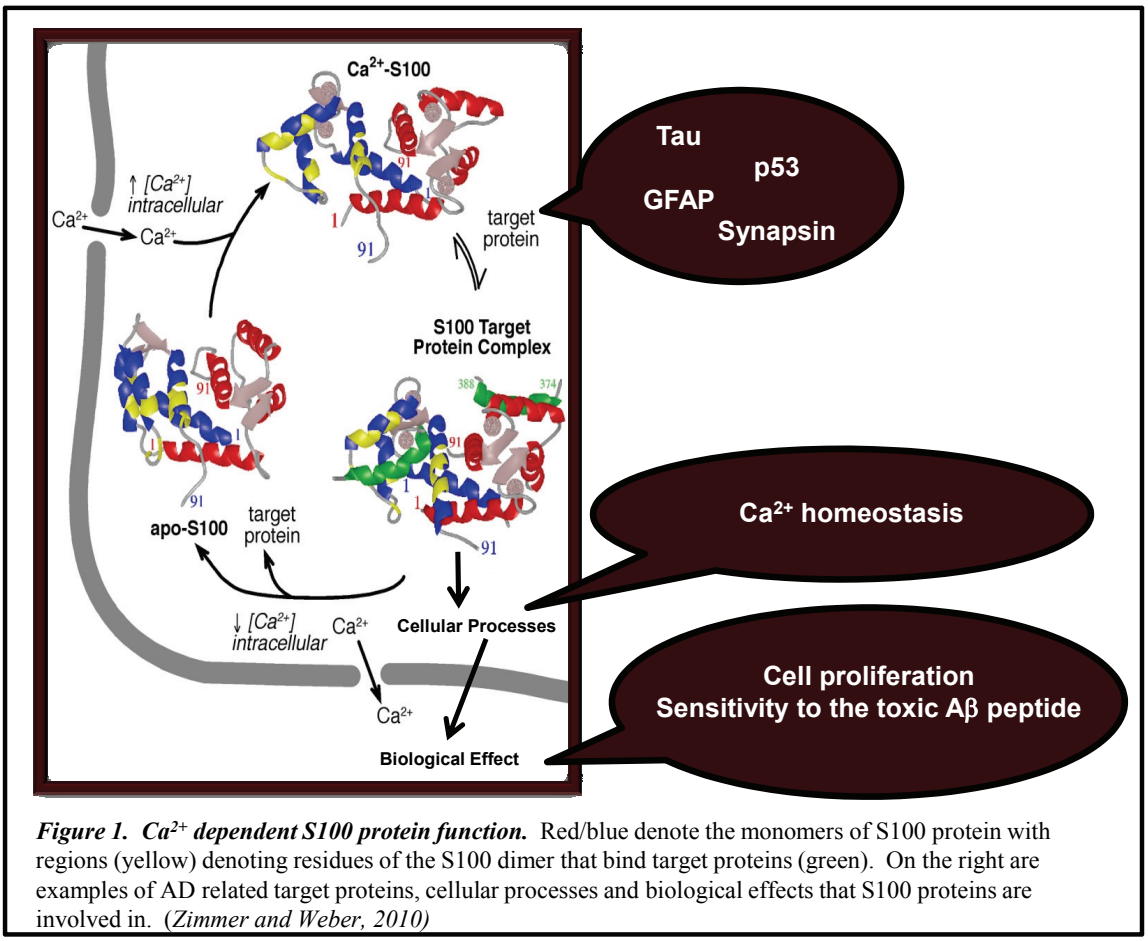

Figure 1. Ca^{2+} dependent S100 protein function. Red/blue denote the monomers of S100 protein with regions (yellow) denoting residues of the S100 dimer that bind target proteins (green). On the right are examples of AD related target proteins, cellular processes and biological effects that S100 proteins are involved in. (*Zimmer and Weber, 2010)*

(human chromosome 21q22), S100G (human chromosome Xp22), S100P (human chromosome 4p16), S100Z (human chromosome 5q13). Interestingly, the mouse

genome contains a region on chromosome 3 syntenic to the human cluster on chromosome 1q21 and lacks only 3 family members, S100A7, S100A12 and S100P (Marenholz, et al., 2004; Marenholz, et al., 2006; Wright, et al., 2009). Each S100 family member exhibits a unique cell-type specific expression pattern. For example, ten family members are expressed in the brain: S100A1, S100A2, S100A4, S100A5, S100A6, S100A10, S100A11, S100A13, S100B and S100Z (Zimmer, et al., 2005). Of these, S100A1 and S100B exhibit the highest levels of expression. Over 20 intracellular targets have been reported for S100A1/S100B. In addition, S100A1 and S100B regulate a large number of diverse cellular processes including energy metabolism, cell proliferation and differentiation, cytoskeletal organization, Ca^{2+} homeostasis and signal transduction pathways (Donato, 2001; Heizmann and Cox, 1998; Roltsch, et al., 2010; Santamaria-Kisiel, et al., 2006).

S100B is reported to localize to several cell structure elements, in fact, S100B is found dispersed throughout the cytoplasm and associated with microtubules, type III filaments and intracellular membranes (Sorci, et al., 2010). *In vitro* studies on S100B have been conducted in several cell lines. A recent study reports that PC12 cells over expressing S100B exhibit enhanced cell proliferation, as well as reduced apoptosis and sensitivity to nerve growth factor (NGF) when compared to control PC12 cells (Arcuri, et al., 2005). In addition, it was reported that astrocytes with reduced S100B expression exhibited a decrease in cell proliferation and migration in addition to the acquisition of a differentiating phenotype when compared to control astrocytes (Brozzi, et al., 2009).

Within the cell, S100B regulates movement and cytoskeletal organization, cell proliferation, differentiation and cell signaling (Donato, et al., 2009).

S100B functions not only as an intracellular regulator, but as an extracellular peptide as well. S100B release/secretion by astrocytes is regulated by forskolin, lysophosphatidic acid, serotonin, glutamate, IL-6β, metabolites and the neurotoxic amyloid beta (Aβ) peptide (Pena, et al., 1995; Pinto, et al., 2000; Quincozes-Santos, et al., 2010; Tramontina, et al., 2006; Whitaker-Azmitia, et al., 1990). Extracellular S100B levels are also gender-, age- and concentration-dependent (Hu, et al., 1996; Leclerc, et al., 2010; Nogueira, et al., 2009). Nanomolar S100B levels beneficially promote neuronal survival while micromolar levels detrimentally promote apoptosis (Hu, et al., 1996). These effects are thought to be mediated mostly, but not exclusively, by the receptor for advanced glycation end products (RAGE) (Hofmann, et al., 1999; Leclerc, et al., 2010; Sorci, et al., 2010).

Reports linking S100A1 with neuronal cell differentiation and function have renewed interest in S100A1 function in the brain (Zimmer and Landar, 1995). Recent studies have reported that S100A1 colocalizes with synapsin I, one of its many target proteins, suggesting a role in vesicle trafficking (Benfenati, et al., 2004). *In vitro* studies in PC12 cells have reported that S100A1 is up-regulated in response to NGF suggesting that S100A1 has a role in neuronal cell differentiation (Zimmer and Landar, 1995). It has also been reported that S100A1 ablation in PC12 cells results in increased levels of soluble and polymerized tubulin, decreased proliferation, increased neurite extension (length and number), increased resistance to Aβ-induced cell death, stabilization of

intracellular Ca^{2+} levels and downregulation of amyloid precursor protein (APP) expression (Zimmer, et al., 1998; Zimmer, et al., 2005). Collectively, these studies indicate S100A1 links cytoskeletal organization, proliferation and differentiation. Numerous neurological diseases have been associated with altered expression and/or function of S100A1 including multiple sclerosis, amyotrophic lateral sclerosis, and Alzheimer's disease (AD) (Verma, et al., 2007; Zimmer, et al., 2005).

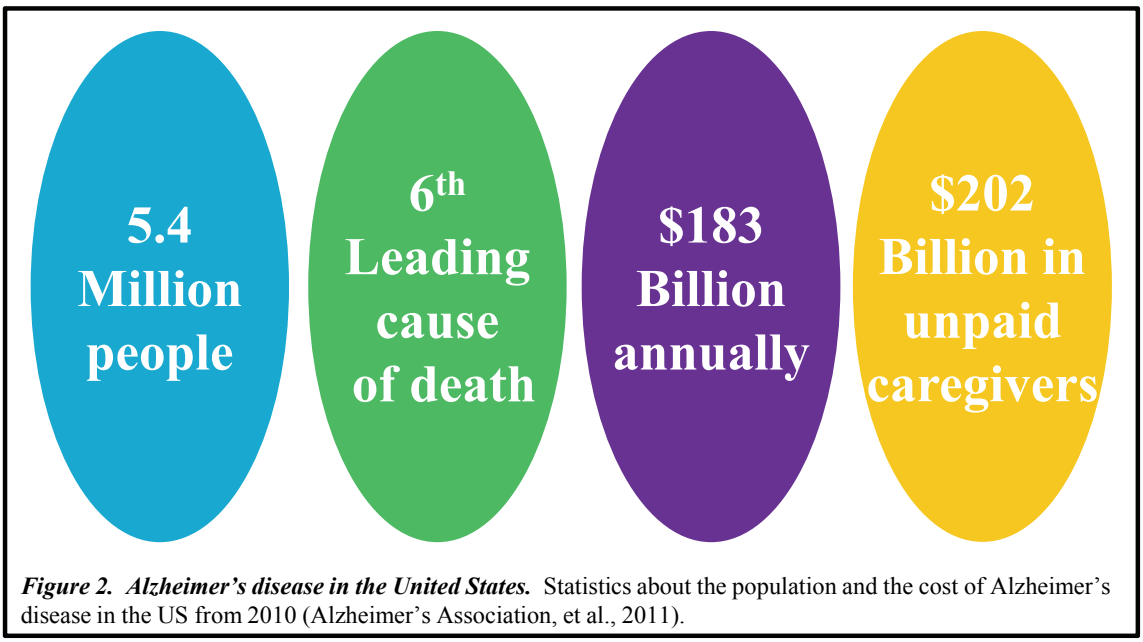

Figure 2. Alzheimer's disease in the United States. Statistics about the population and the cost of Alzheimer's disease in the US from 2010 (Alzheimer's Association, et al., 2011).

Alzheimer's disease (AD) is a progressive neurodegenerative disorder and the sixth leading cause of death in the United States (Alzheimer's Association, 2011). Over 35 million people worldwide, 5.4 million in the United States alone, have been diagnosed with AD costing the country an estimated $183 billion annually in health care costs. In addition, there are over 14 million unpaid care givers that provided 17 billion

hours of unpaid care in 2010, valued at $202 billion (Figure 2). By mid-century, the number of individuals in the United States diagnosed with AD is projected to reach 11-16 million and the annual cost of health care will reach $1.1 trillion. Currently, there are no treatments available to slow or stop the progression of AD. The five FDA-approved drugs available (Table 1) "temporarily slow worsening of symptoms for about six to 12 months, on average, for about half the individuals that take them" (Alzheimer's Association, et al., 2011). The identification of a therapy that will slow the progression of AD is significant because even a one year delay in onset will reduce health care costs by $250 billion/year (Alzheimer's Association, et al., 2011).

Table 1. FDA approved drugs for Alzheimer's disease

Drug Name (generic)	Type	Use	Side Effects
Cognex (tacrine)	Cholinesterase inhibitor	Rarely prescribed due to safety concerns	
Razadyne (galantamine)	Cholinesterase inhibitor	Symptomatic treatment for mild to moderate AD	Nausea, vomiting, diarrhea, weight loss, loss of appetite
Exelon (rivastigmine)	Cholinesterase inhibitor	Symptomatic treatment for mild to moderate AD	Nausea, vomiting, diarrhea, weight loss, loss of appetite, muscle weakness
Aricept (donepezil)	Cholinesterase inhibitor	Symptomatic treatment for mild to moderate AD	Nausea, vomiting, diarrhea
Namenda (memantine)	N-methyl D-aspartate (NMDA) antagonist	Symptomatic treatment for moderate to severe AD	Dizziness, headache, constipation, confusion

The most common, or "hallmark", pathological features of AD are extracellular senile plaques, comprised primarily of misfolded amyloid beta (Aβ) peptides, intracellular neurofibrillary tangles (NFTs), comprised of hyperphosphorylated tau

protein and brain atrophy resulting from neuronal and dendritic loss (Figure 3) (Castellani, et al., 2010; Querfurth and LaFerla, 2010). AD presents in one of two forms, sporadic or familial AD, which are clinically indistinguishable, differing only in their ages of onset (Reitz, et al., 2011). We do not know the cause of sporadic AD, although it is believed that a combination of environmental and genetic risk factors exist,

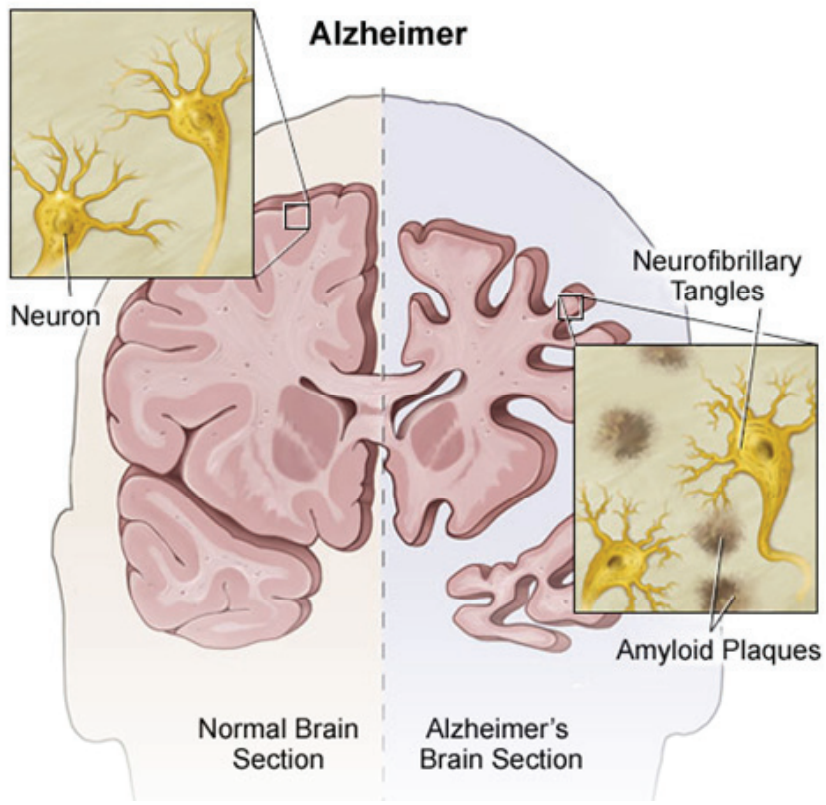

Figure 3. Alzheimer's disease in the brain. Image depicts a normal age matched brain section on the left and an Alzheimer's disease brain section on the right. In Alzheimer's disease, protein mishandling causes a buildup of extracellular senile plaques comprised of Amyloid β (Aβ), intracellular neurofibrillary tangles form with in the neurons due to hyperphosphorylation of the Tau protein and resulting neuronal cell loss causes brain atrophy. (Alzheimer's Association, et al., 2011)

such as cardiovascular disease, elevated blood pressure, type 2 diabetes, smoking, history of depression, traumatic brain injury and the APOE ε4 gene allele (Castellani, et al., 2010; Reitz, et al., 2011). Over 95% of AD cases are of the sporadic, or late onset form, that presents in patients >65 years old, while 1-5% are of the familial, or early onset form, that presents as early as 30 years old (Bekris, et al., 2010; Reitz, et al., 2011). Early-onset AD is hereditary and associated with known mutations in several genes, namely APP, PSEN1 and PSEN2 (Bertram, et al., 2010). The APP gene encodes the Amyloid Precursor Protein (APP) which is cleaved to produce Aβ peptides and the presenilin genes (PSEN1 and PSEN2) encode proteins that are involved in APP breakdown and Aβ generation (Bekris, et al., 2010; Reitz, et al., 2011). The clinical

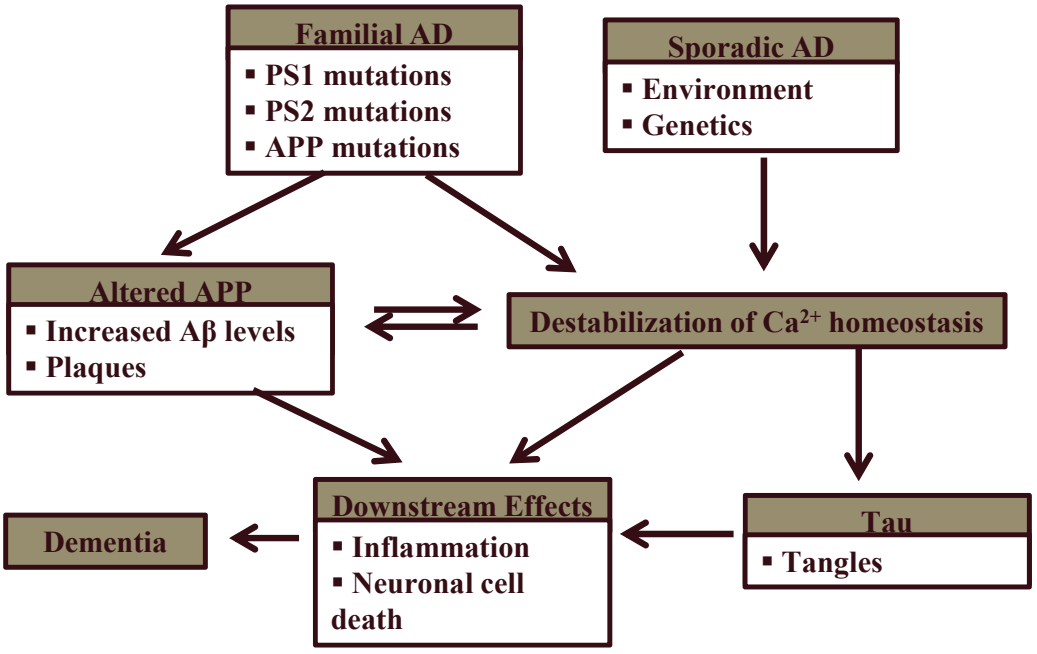

Figure 4. Histopathological development of Alzheimer's disease. Depicted above is the progression of AD pathobiology in both forms, sporadic (early) and familial (late) onset AD.

presentation and pathology of both forms include initial disturbances in Ca^{2+} homeostasis. The altered APP processing caused by the genetic mutations in early-onset AD causes a remodeling of the Ca^{2+} signaling pathways (Berridge, 2010; 2011). In both forms, dysregulated Ca^{2+} homeostasis is followed by inflammation, neurodegeneration, senile plaque deposition comprised of Aβ peptide, intracellular hyperphosphorylated tau and ultimately cognitive dysfunction (Figure 4) (Berridge, 2010; 2011; Demuro, et al., 2010; Querfurth and LaFerla, 2010; Supnet and Bezprozvanny, 2010).

Inflammation is an early and critical event in the pathology of AD. The inflammatory response in the brain includes activation of microglia, astrocytes, macrophages and lymphocytes that results in the release of inflammatory mediators that further recruit immune cells through the blood brain barrier (BBB) as well as additional microglia (Cameron and Landreth, 2010; Lee, et al., 2010). Activated microglia overexpress interleukin 1β (IL-1β) leading to the production of APP by neurons and subsequent activation of astrocytes, which overexpress S100B and leads to increased Ca^{2+} dysregulation (Griffin, 2006). In addition, activated astrocytes and microglia are found surrounding Aβ plaques in the brain, and the Aβ peptide functions as an activation signal for astrocytes (Combs, 2009) (Heneka, et al., 2010; Verkhratsky, et al., 2010). Furthermore, this activation of microglia and astrocytes is initially beneficial, but chronic activation and recruitment of microglia and astrocytes contribute to pathology and disease progression (Heneka, et al., 2010; Lee, et al., 2010; Wyss-Coray and Mucke, 2002).

Another early event in the pathology of AD is amyloid plaque deposition. Amyloid plaques are comprised of Aβ peptides, which are a natural metabolic product of Amyloid Precursor Protein (APP), typically 36-43 amino acids in length (Querfurth and LaFerla, 2010). The toxic form, $A\beta_{42}$, is formed by the sequential cleavage of APP by beta-site amyloid precursor protein-cleaving enzyme 1 (β-secretase), encoded by BACE1, and γ-secretase, a protein complex involving the protein products of PSEN1 and/or PSEN2 (Bekris, et al., 2010; Querfurth and LaFerla, 2010; Zhang, et al., 2011). Aβ begins as a monomer, but spontaneously aggregates to form oligomers (2-6 peptides), which coalesce to form intermediate assemblies and eventually insoluble fibrils in a β-sheet formation that comprise the extracellular Aβ plaques (Iwatsubo, et al., 1994; Jarrett, et al., 1993; Querfurth and LaFerla, 2010). Not only does Aβ form insoluble plaques, but soluble dimers and trimmers have also been reported to be toxic to neuronal synapse (Querfurth and LaFerla, 2010). Collectively, all of these disease pathways lead to cognitive decline and ultimately dementia. One possible avenue of treatment is to prevent the transduction of destabilized Ca^{2+} homeostasis in to pathology, and this is possible through the inhibition of the S100 family of Ca^{2+} signaling proteins.

The goal of this project is to ascertain the potential of S100A1/S100B inhibition as a treatment for AD and to identify an intracellular mechanism of S100A1/S100B function to aid in the development of drug targets for AD therapy. The central hypothesis is that inhibition of intra- and extra-cellular S100A1/S100B will decrease plaque load and inflammation as well as normalize miRNA expression. The specific

objectives for this study are:

1) Quantify the effects of S100A1/S100B ablation on AD histopathology
2) Determine the efficacy of S100A1/S100B immunotherapy on AD pathology
3) Identify miRNA's that contribute to S100A1/S100B mediated reversal of AD pathobiology.

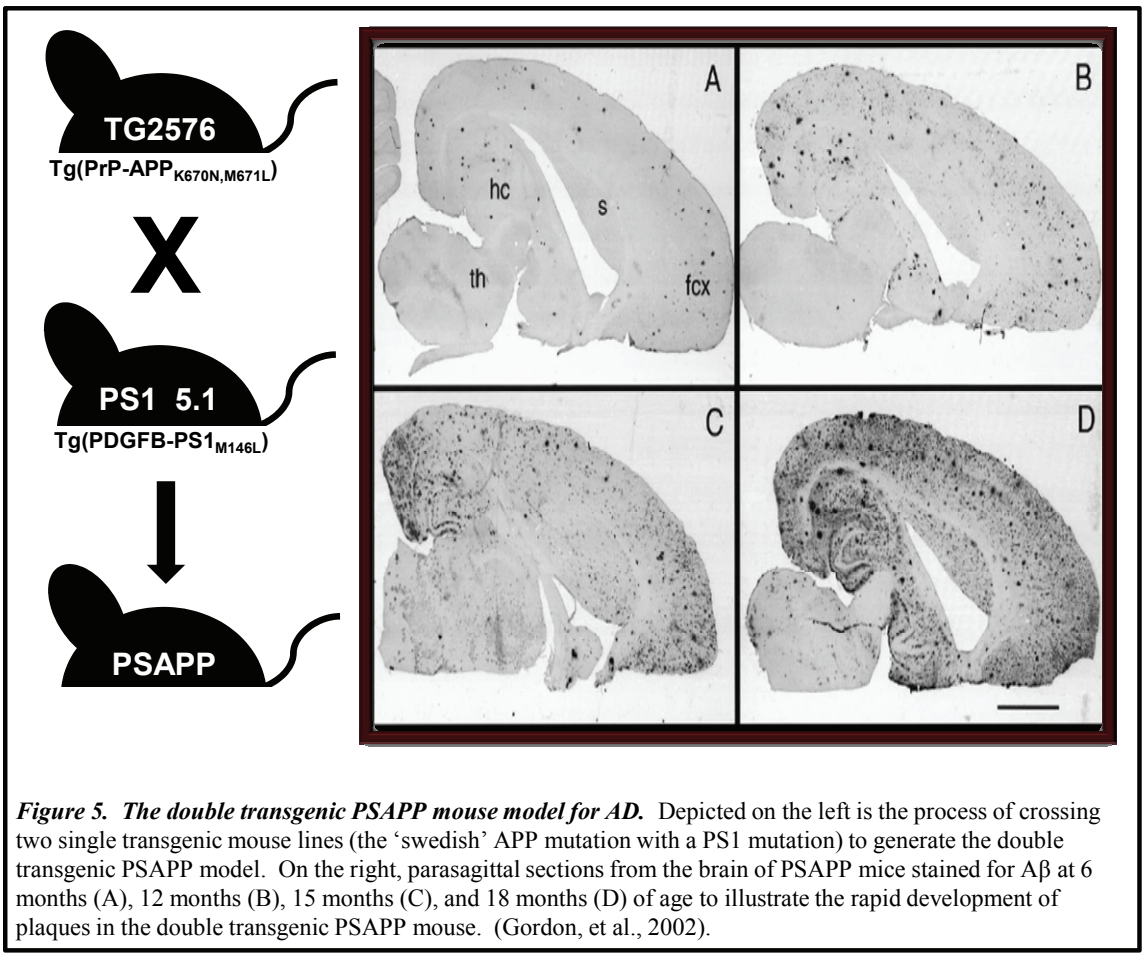

Figure 5. The double transgenic PSAPP mouse model for AD. Depicted on the left is the process of crossing two single transgenic mouse lines (the 'swedish' APP mutation with a PS1 mutation) to generate the double transgenic PSAPP model. On the right, parasagittal sections from the brain of PSAPP mice stained for Aβ at 6 months (A), 12 months (B), 15 months (C), and 18 months (D) of age to illustrate the rapid development of plaques in the double transgenic PSAPP mouse. (Gordon, et al., 2002).

Because there are no S100 specific inhibitors, this study uses two approaches to ascertain the net effect of S100A1 and S100B on *in vivo* AD histopathology, genetic ablation and passive immunotherapy. We will use genetic ablation to recapitulate the entire spectrum of S100A1 and/or S100B function (detrimental and beneficial) in an AD mouse line. The overt phenotypes of S100A1 and S100B knockout mice are normal and the only cellular phenotypes reported are modulatory changes in Ca^{2+} homeostasis (Prosser, et al., 2008; Xiong, et al., 2000). We will also use passive immunotherapy to inhibit S100A1/S100B in the mouse model to ascertain the ability of S100 antibodies to mimic the genetic effects since passive immunotherapy is a viable treatment option for patients. There are several different mouse models available to study AD but all express mutations that are found in the human early-onset form of AD. Transgenic mouse models have had difficulty in reproducing the entire spectrum of AD pathologies, especially neuronal cell loss (Elder, et al., 2010). Nonetheless mouse models have been instrumental in deciphering the molecular mechanisms of AD pathology and developing new therapies (Elder, et al., 2010; Gotz and Ittner, 2008; Morrissette, et al., 2009; Radde, et al., 2008). The PSAPP double transgenic mouse used in this study expresses the "Swedish" APP mutation ($APP_{K670N/M671L}$) and a PSEN1 mutation ($PS\text{-}1_{M146L}$) (Figure 5) (Gordon, et al., 2001; Gordon, et al., 2002; Holcomb, et al., 1998; Holcomb, et al., 1999). Because this line has two overexpressing transgenes, the model has a rapid disease onset and mimics many facets of the human disease including plaque deposition, dystrophic neurites, glial activation, and memory deficits (Gordon, et al., 2001; Gordon, et al., 2002; Holcomb, et al., 1998; Holcomb, et al., 1999; Holcomb, et al., 2006). In

order to generate the mice for this study, the PSAPP model was crossed to three different knockout lines, S100A1$^{-/-}$ to determine if S100A1 has an effect on AD pathology, S100B$^{-/-}$ in order to address the controversy in the field as to whether or not S100B has a role in AD pathology and S100A1$^{-/-}$/S100B$^{-/-}$ to ascertain any synergistic effects of S100A1 and S100B (Figure 6).

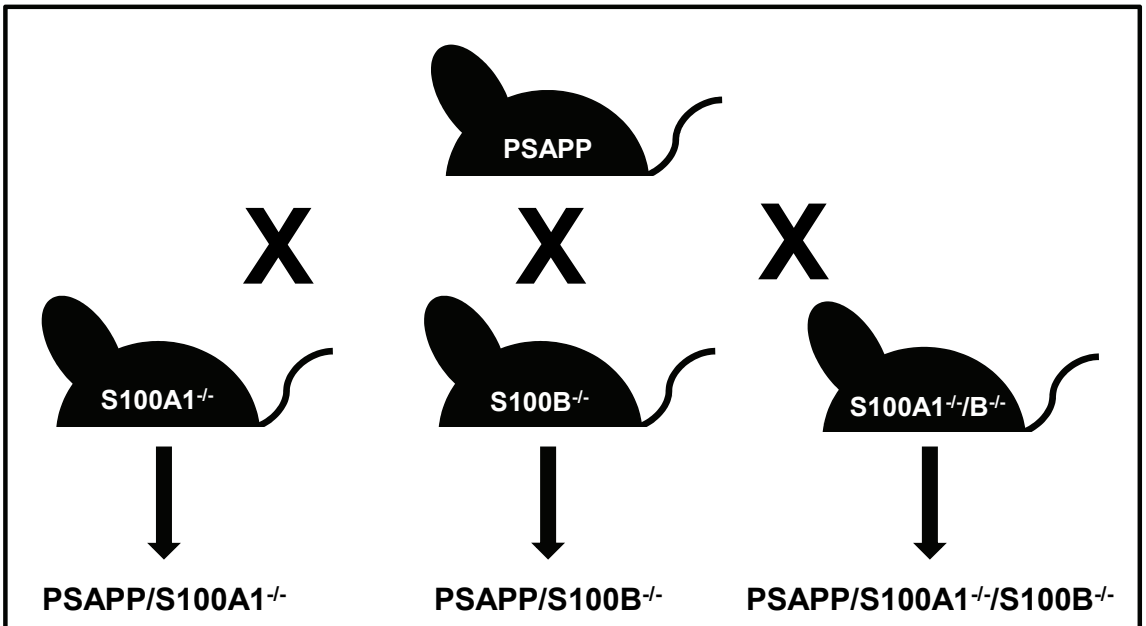

Figure 6. Development of the PSAPP/S100 knockout mouse models. Depicted above is the strategy for developing the PSAPP/S100 genetic models utilized in these studies. Double transgenic PSAPP mice will be crossed with each of the following lines to produce the PSAPP/S100 knockout lines: S100A1$^{-/-}$, S100B$^{-/-}$ and S100A1$^{-/-}$/S100B$^{-/-}$ (Prosser, et al., 2008; Roltsch, et al., 2010)

CHAPTER II

PSAPP MICE EXHIBIT REGIONALLY SELECTIVE DECREASES IN GLIOSIS AND PLAQUE DEPOSITION IN RESPONSE TO S100B ABLATION*

Background

S100B, a member of the S100 protein family, is expressed predominantly in astrocytes and functions as both an intracellular Ca^{2+} receptor and an extracellular neuropeptide (Mrak and Griffin, 2004; Van Eldik and Wainwright, 2003; Zimmer, et al., 2005). The term S100 to refers to the solubility of these 10,000 molecular weight proteins in saturated ammonium sulfate (Moore, 1965). S100 proteins are distinguished from other members of the S100/calmodulin/ troponin superfamily of EF-hand Ca2+ binding proteins by their 3 D structure and highly conserved 14 amino acid Ca^{2+} binding loop (Zimmer, et al., 2003). Upon binding Ca^{2+}, S100 proteins undergo a conformational change which exposes a hydrophobic patch necessary for interacting with numerous intra- and extracellular protein targets and subsequent exertion of their biological effects (Zimmer, et al., 2003; Zimmer and Weber, 2010). Over 20 intracellular targets have been reported for S100B suggesting that it regulates a large number of diverse cellular processes, including energy metabolism, cell proliferation, cytoskeleton organization, Ca^{2+} homeostasis and signal transduction pathways. The extracellular effects of S100B

---

*Reprinted with permission from: Roltsch E, Holcomb L, Young KA, Marks A, Zimmer DB. PSAPP mice exhibit regionally selective reductions in gliosis and plaque deposition in response to S100B ablation. J Neuroinflammation 7:78 (2010) Copyright 2010 by BioMed Central Ltd.

are concentration dependent; nanomolar S100B levels beneficially promote neuronal survival while micromolar levels detrimentally promote apoptosis (Hofmann, et al., 1999; Hu, et al., 1996; Leclerc, et al., 2010). S100B's extracellular effects are thought to be mediated by the receptor for advanced glycation end products (RAGE) (Hofmann, et al., 1999; Leclerc, et al., 2010). S100B release/secretion is regulated by forskolin, lysophosphatidic acid, serotonin, glutamate, IL-6b, metabolites and the neurotoxic Aβ peptide (Pena, et al., 1995; Pinto, et al., 2000; Quincozes-Santos, et al., 2010; Tramontina, et al., 2006; Whitaker-Azmitia, et al., 1990) as well as being gender- and age-dependent (Nogueira, et al., 2009). Increased S100B levels are associated with a variety of neurological disorders including Alzheimer's disease (AD), multiple sclerosis, amyotrophic lateral sclerosis, schizophrenia, epilepsy, alcoholism, drug abuse, hypoxia and traumatic brain injury (Mori, et al., 2010; Mrak and Griffin, 2004; Sorci, et al., 2010; Van Eldik and Wainwright, 2003; Zimmer, et al., 2005).

Altered S100B function is associated with AD pathobiology. The clinical presentation and pathology of early- and late-onset AD include early disturbances in Ca^{2+} homeostasis followed by inflammation, neurodegeneration, senile plaques comprised of aggregated amyloid β (Aβ) peptide, intracellular neurofibrillary tangles comprised of aggregated hyperphosphorylated tau, and ultimately cognitive dysfunction (Demuro, et al., 2010; Querfurth and LaFerla, 2010; Small and Duff, 2008; Supnet and Bezprozvanny, 2010). In human autopsy specimens, the highest levels of S100B expression are observed in the most severely affected regions and S100B associates with plaques (Marshak, et al., 1992; Van Eldik and Griffin, 1994; Van Eldik and Wainwright,

2003). Serum/CSF S100B levels inversely correlate with cognitive function, i.e. patients with lower S100B levels exhibit lower Clinical Dementia Rating scores and higher Mini-Mental State Examination scores (Chaves, et al., 2010). In addition, the rs2300403 single nucleotide polymorphism (SNP) in the S100B gene is associated with low cognitive performance, dementia and AD (Lambert, et al., 2007). While the cellular events/molecular mechanisms whereby S100B contributes to AD pathobiology have not yet been elucidated, S100B has been reported to regulate Aβ biogenesis, amyloid precursor protein expression/processing and tau hyperphosphorylation (Anderson, et al., 2009; Esposito, et al., 2008; Mori, et al., 2010). In turn, the Aβ peptide increases S100B levels (Chow, et al., 2010) resulting in a positive feedback loop. Thus, S100B may be a key contributor to a detrimental "cytokine cycle" that drives the progression of AD (Leclerc, et al., 2010; Mrak and Griffin, 2004; Querfurth and LaFerla, 2010; Sen and Belli, 2007; Small and Duff, 2008; Sorci, et al., 2010; Van Eldik and Wainwright, 2003; Zimmer and Weber, 2010).

In vivo studies in genetically modified mouse models have yielded conflicting results regarding the contribution of increased S100B expression to AD pathology. Transgenic TghuS100B mice express 4-5 fold more S100B protein (Friend, et al., 1992) and exhibit increased hippocampal gliosis with no change in plaque load upon hippocampal Aβ infusion when compared to non-transgenic controls (Craft, et al., 2005). However, TghuS100B/Tg2576 mice exhibit increased plaque load/gliosis in the hippocampus as well as the cortex when compared to Tg2576 mice (Mori, et al., 2010). The mechanism(s) responsible for the differential effects of increased S100B expression

on hippocampal pathology in the two AD models have not been elucidated. Pharmacological inhibition and genetic ablation have also produced contradictory results. Treatment of Tg2576 mice with arundic acid, an inhibitor of S100B expression (40-45% decrease), reduces plaque load/gliosis in the hippocampus and cortex (Mori, et al., 2006). Surprisingly, S100B ablation has no effect on hippocampal plaque load, gliosis or dystrophic neurons in an Aβ infusion model (Craft, et al., 2005). Thus, the ability of S100B inhibitors to prevent/reverse AD histopathology is not completely understood.

While specific inhibitors that block the interaction of S100B with its target proteins are under development, currently available compounds do not cross the blood brain barrier and cannot be used to inhibit CNS S100B (Markowitz, et al., 2007). Therefore, this study uses an in vivo genetic approach which recapitulates the entire spectrum of S100 function (detrimental, beneficial, intracellular, and extracellular) to ascertain the net effect of S100B ablation on AD histopathology in the PSAPP AD mouse line. Although no AD mouse model exhibits all aspects of the human disease, the PSAPP double transgenic ($APP_{K670NM671L}$/$PS\text{-}1_{M146L}$) line has a rapid disease onset and mimics many facets of the human disease including plaque deposition, dystrophic neurites, glial activation, and memory deficits (Gordon, et al., 2001; Gordon, et al., 2002; Holcomb, et al., 1998; Holcomb, et al., 1999). PSAPP/S100B knockout mice exhibited a regionally selective decrease in cortical but not hippocampal plaque load. Reductions in plaque load were accompanied by decreases in plaque number, GFAP-positive astrocytes, Iba1-positive microglia and phospho-tau positive neurons. Finally,

S100B immunoreactivity in cortex and hippocampus of PSAPP mice was plaque associated and co-localized with astrocytes/microglia. These results suggest that secreted and intracellular forms of S100B contribute to AD pathology and that pharmacological strategies which selectively block S100B action in the CNS may be effective in treating AD.

Methods

PSAPP X S100B knockout mice. The PSAPP double transgenic line was generated by crossing the Tg2576 line ("Swedish" $APP_{K670N/M671L}$ mutation) with the 6.2 line (PS-1_{M146L}) (Gordon, et al., 2001; Gordon, et al., 2002; Holcomb, et al., 1998; Holcomb, et al., 1999). The $S100B^{-/-}$ line has been described previously (Xiong, et al., 2000). The PSAPP/$S100B^{-/-}$ line was generated by crossing PSAPP double transgenic males with $S100B^{-/-}$ females and subsequent interbreeding of the PSAPP/$S100B^{+/-}$ heterozygous offspring (PSAPP/$S100B^{+/-}$ X PSAPP/$S100B^{+/-}$). To control for changes in genetic background, all experiments used PSAPP/$S100B^{+/+}$ and PSAPP/$S100B^{-/-}$ littermates. Procedures involving animals were approved by the Texas A&M University Institutional Animal Care and Use Committee and comply with the NIH Guide for the Care and Use of Laboratory Animals.

For genotyping, amplification of a 500 bp product using PCR primers for the mouse β-casein gene (forward primer 5' GAT GTG CTC AG GCT AAA GTT 3' and reverse primer 5' AGA AAC GGA ATG TTG TGG AGT 3') was used to assess genomic DNA quality. The PS-1 and APP transgenes were detected as previously described [36]. Amplification of 250 bp band (forward primer 5' GCA AAG AAC AGG

GTA GAA AAC ATG AAA AAC G 3'; reverse primer 5' GCC ATT CAA ACT AAT ATC CAG AAG CAA CCC 3') was used to detect the wild-type S100B allele. PCR programs contained a 5 minute denaturation step at 95°C; followed by thirty cycles consisting 1 minute at 94°C, 2 minutes at 60°C, and 3 minutes at 72°C; as well as a final 7 minute extension step at 72°C.

Sample acquisition/processing. Brains were removed from anesthetized animals, rinsed in phosphate buffered saline (PBS) and fixed in 4% (wt/vol) paraformaldehyde in PBS for 30 minutes. Sagittal slices, 2 mm in thickness, were prepared using an acrylic brain matrix (Ted Pella, Redding CA) and post-fixed for an additional 30 minutes. Slices were then permeabilized in 2 mM MgCl2, 0.01% (wt/vol) sodium deoxycholate, 0.02% (vol/vol) Nonidet P-40 in 100 mM sodium phosphate buffer pH 7.5 for 36-48 hours. After post-fixation in 10% buffered formalin for 16 hours, tissues were embedded in paraffin and 5 micron sagittal sections were mounted on glass slides for subsequent staining. This processing procedure, originally developed for visualization of β-galactosidase reporter gene activity in transgenic mouse tissues, provides optimum S100B antibody specificity/sensitivity without compromising the detection of other antigens.

Immunohistochemical and Congo red staining. To minimize variability, sections from experimental and control groups were processed simultaneously. Consecutive slides (2/animal) each containing sections at Allen Brain Atlas Sagittal Levels 8 and 17 were depariffinized and rehydrated to distilled water. For Congo red staining, slides were incubated in 0.02 M NaOH in 80% ethanol saturated with NaCl for 20 minutes

followed by a 30 minute incubation in 0.2% (wt/vol) Congo Red (Cat. 150711, MP Biomedicals, LLC, Solon, OH) in 0.02 M NaOH in 80% ethanol saturated with NaCl, dehydration and mounting. Immunostaining was performed on a DAKO autostainer (Dako, Carpentaria, CA) using a biotin-free polymer detection kit (MACH 2, Biocare Medical, Walnut Creek, CA) and conditions recommended by the primary antibody manufacturer. Primary antibodies for immunohistochemistry included a mouse monoclonal S100B antibody (1-1000 dilution of Z0311 Dako); rabbit polyclonal GFAP antibody (1-1000 dilution of Z0334, Dako); mouse monoclonal Iba1antibody (1-300 dilution of SC-32725, Santa Cruz Biotechnology, Santa Cruz, CA); and mouse monoclonal Ser202/Thr205 phosphorylated tau antibody (1-20 dilution of MN1020, Pierce Chemical Co., Rockford, IL). For immunofluorescence microscopy, the anti-Iba1 antibody was diluted 1-10, the anti-GFAP antibody 1-100, and the anti-S100B antibody 1-50 (612377 from BD Transduction Laboratories, San Jose, CA). Secondary antibodies included an Alexa Fluor 546 donkey anti-rabbit (1-200 dilution of A10040, Molecular Probes, Carlsbad, CA); Alexa Fluor 488 rabbit anti-mouse (1-200 dilution of A11059, Molecular Probes); and Alexa Fluor 546 donkey anti-mouse (1-200 dilution of A10036, Molecular Probes).

For quantification, digital images were captured at 10× magnification on an Olympus IX70 Imaging System using a single exposure setting as follows: the entire hippocampus (2 images); the visual (1 image), somatosensory (1 image) and somatomotor (1 image) cortex as well as representative areas of the cerebellum and olfactory bulb. Images were converted to gray scale and the threshold intensity was set

to the intensity observed in areas without tissue. Image J software (NIH Image, Bethesda, MD) was used to quantify positive pixels, plaque size, plaque number and total area. Plaque load and immunoreactivity were defined as the % area, i.e. the area of positive pixels/total pixels × 100. The data were expressed as the mean ± SEM (n= 8 for PSAPP and n= 6 for PSAPP/S100B$^{-/-}$). An independent samples t-test (SPSS Inc., Chicago, IL) was used to determine the significance ($p < 0.05$) of measured differences between the two genotypes. Pearson's Correlation Coefficient and scatter plots of the mean hippocampal and cortical GFAP/Iba1 staining versus plaque load for each animal were used to determine the relationship between plaque load and astrocytosis/microgliosis.

Images for colocalization experiments were obtained on a Zeiss 510 META NLO laser scanning microscope. The following settings were used for fluorophore detection: DAPI excitation G 365, Dichroic FT 395, BP 445/50; for Alexa 488, exciter BP 470/20, Dichroic FT 493, Emission BP 505-530; and Alexa 568, Exciter BP 560/40, Dichroic FT 585, Emission BP 630/75. Images were collected, corrected for background and bleed through (reference images) and colocalization (overlap coefficient) of GFAP/S100B and Iba1/S100B determined using the LSM software.

Results

S100B ablation reduces cortical but not hippocampal plaque load. To determine if S100B ablation altered amyloidogenesis, plaque load was quantified in PSAPP/S100B knockout and PSAPP mice. Congo red stained fibrillar plaques were observed in the hippocampus and cortex of 6 month old PSAPP/S100B$^{-/-}$ and PSAPP mice (Figure 7A).

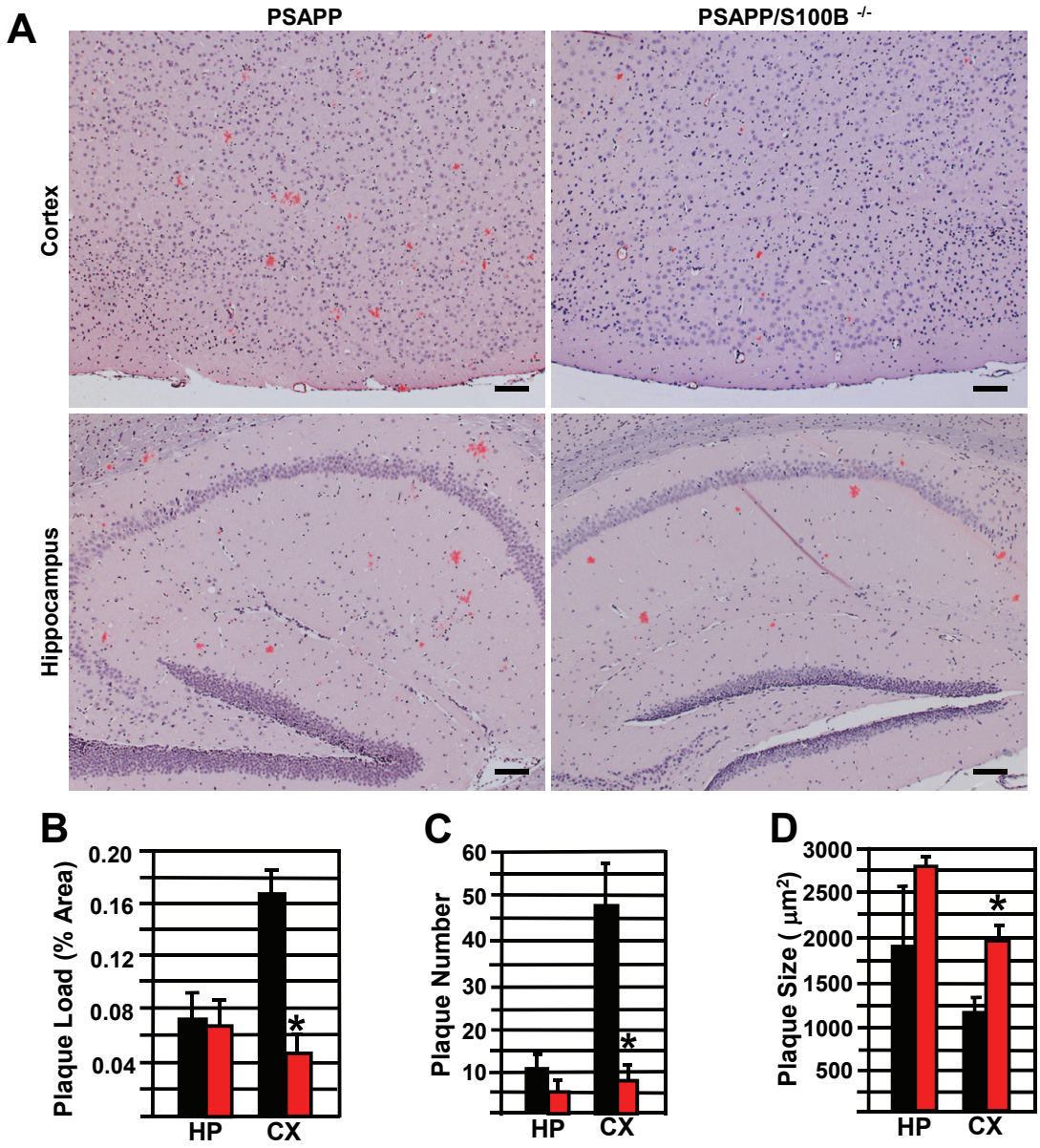

Figure 7: S100B ablation reduces cortical, but not hippocampal plaque load. Panel A contains representative micrographs of parasagittal cortical/hippocampal sections from 6 month old PSAPP and PSAPP/S100B$^{-/-}$ mice stained with congo red (pink) and hematoxylin (blue) to visualize plaques and nuclei, respectively. The histograms depict the mean congophilic plaque load (Panel B), plaque number (Panel C), and plaque size (Panel D) $\pm$ SEM in PSAPP (black bars, n=8), and PSAPP/S100B$^{-/-}$ (red bars, n=6) mice. Scale bars represent 50 microns and asterisks denote $p \leq 0.05$ when compared to the PSAPP group.

In fact, congophilic plaque load in the control PSAPP littermates was indistinguishable from previous reports (Gordon, et al., 2001; Gordon, et al., 2002; Holcomb, et al., 1998). Furthermore, hippocampal plaque load in the two genotypes was indistinguishable: 0.070 ± 0.020 and 0.075 ± 0.022 percent area in the PSAPP/S100B$^{-/-}$ and PSAPP controls, respectively (Figure 7B). Hippocampal plaque size and number were also similar in the two genotypes (Figure 7C and 7D). In contrast, there was a 3-fold reduction in cortical plaque load in PSAPP/S100B$^{-/-}$ mice (0.050 ± 0.016 percent area) when compared to PSAPP mice (0.168 ± 0.016 percent area) (Figure 7B). This decrease in cortical plaque load was accompanied by an 5-fold reduction in plaque number (47.78 ± 9.42 vs. 8.78 ± 2.07) and a slight increase in plaque size (1162 ± 141 vs. 1955 ± 196 μm2) (Figure 7C and 7D). In summary, this is the first demonstration that S100B ablation selectively reduces cortical plaque load.

S100B ablation reduces cortical, but not hippocampal, gliosis. S100B's deleterious effects in the central nervous system have been attributed to reactive gliosis (astrocytosis and microgliosis) (Craft, et al., 2005; Mori, et al., 2006; Mori, et al., 2010; Van Eldik and Griffin, 1994). The microglial marker Iba1 and astrocytic marker GFAP were used to determine if S100B ablation in PSAPP mice also reduced gliosis. Plaque-associated Iba1 staining of small cell bodies and long processes was observed in the cortex and hippocampus of PSAPP and PSAPP/S100B$^{-/-}$ mice (Figure 8A and 8B). This staining pattern was similar to previous reports for AD mouse models (Tg2576) (Mori, et al., 2006; Mori, et al., 2010). Hippocampal Iba1 staining in the two genotypes was similar (0.51 ± 0.12 vs. 0.51 ± 0.10 percent area) (Figure 8C). However, cortical Iba1 staining

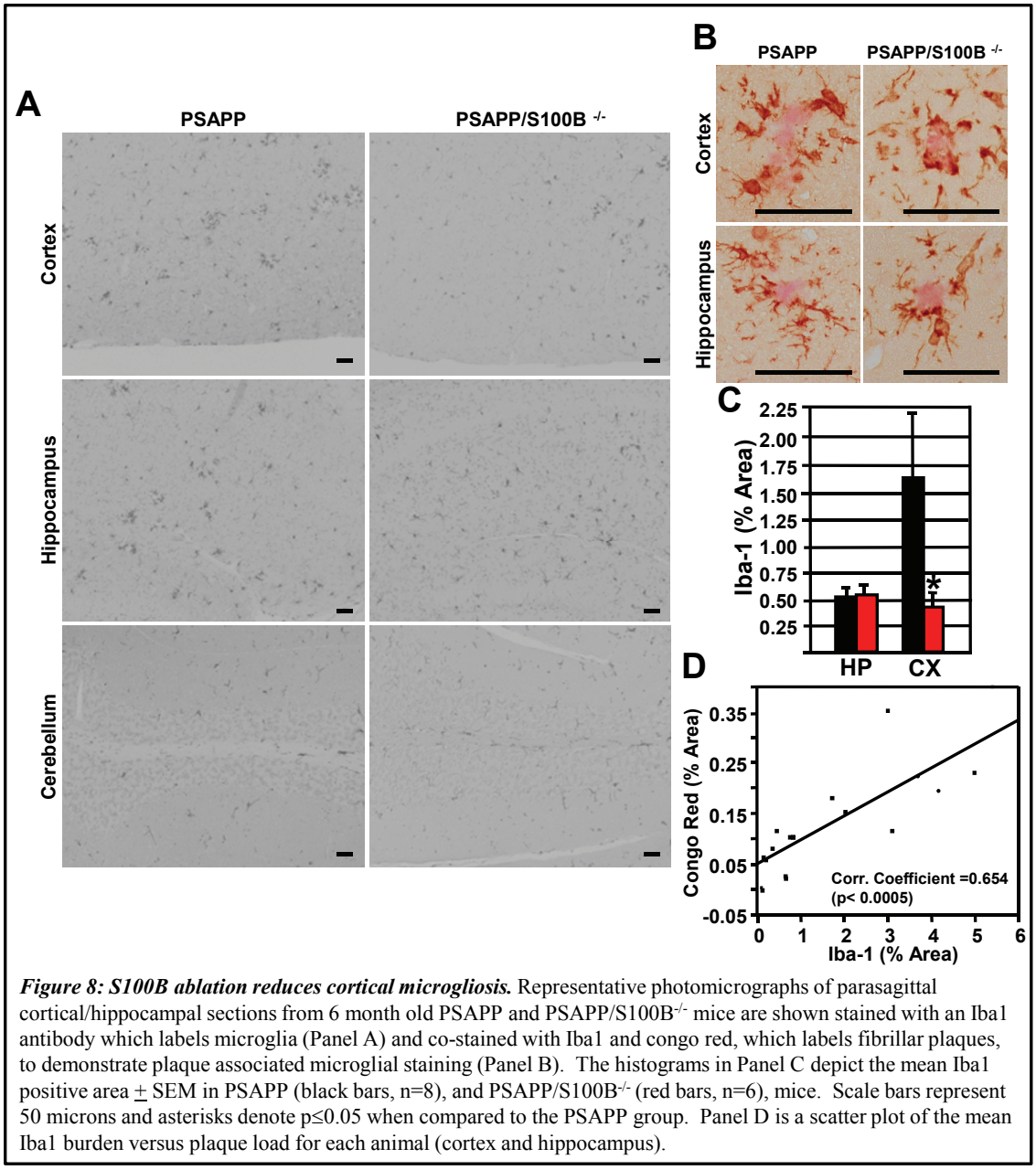

Figure 8: S100B ablation reduces cortical microgliosis. Representative photomicrographs of parasagittal cortical/hippocampal sections from 6 month old PSAPP and PSAPP/S100B$^{-/-}$ mice are shown stained with an Iba1 antibody which labels microglia (Panel A) and co-stained with Iba1 and congo red, which labels fibrillar plaques, to demonstrate plaque associated microglial staining (Panel B). The histograms in Panel C depict the mean Iba1 positive area $\pm$ SEM in PSAPP (black bars, n=8), and PSAPP/S100B$^{-/-}$ (red bars, n=6), mice. Scale bars represent 50 microns and asterisks denote $p \leq 0.05$ when compared to the PSAPP group. Panel D is a scatter plot of the mean Iba1 burden versus plaque load for each animal (cortex and hippocampus).

was 4-fold less (0.45 ± 0.09 vs. 1.69 ± 0.49 percent area) in PSAPP/S100B$^{-/-}$ mice when compared to PSAPP control mice (Figure 8C). In both genotypes, the Iba1 staining was similar in non-plaque containing regions such as the cerebellum (Figure 8A) and

olfactory bulb (data not shown). Furthermore, there was a direct correlation between Iba1 staining and plaque load (Pearson's Correlation Coefficient 0.654, $p < 0.0005$)

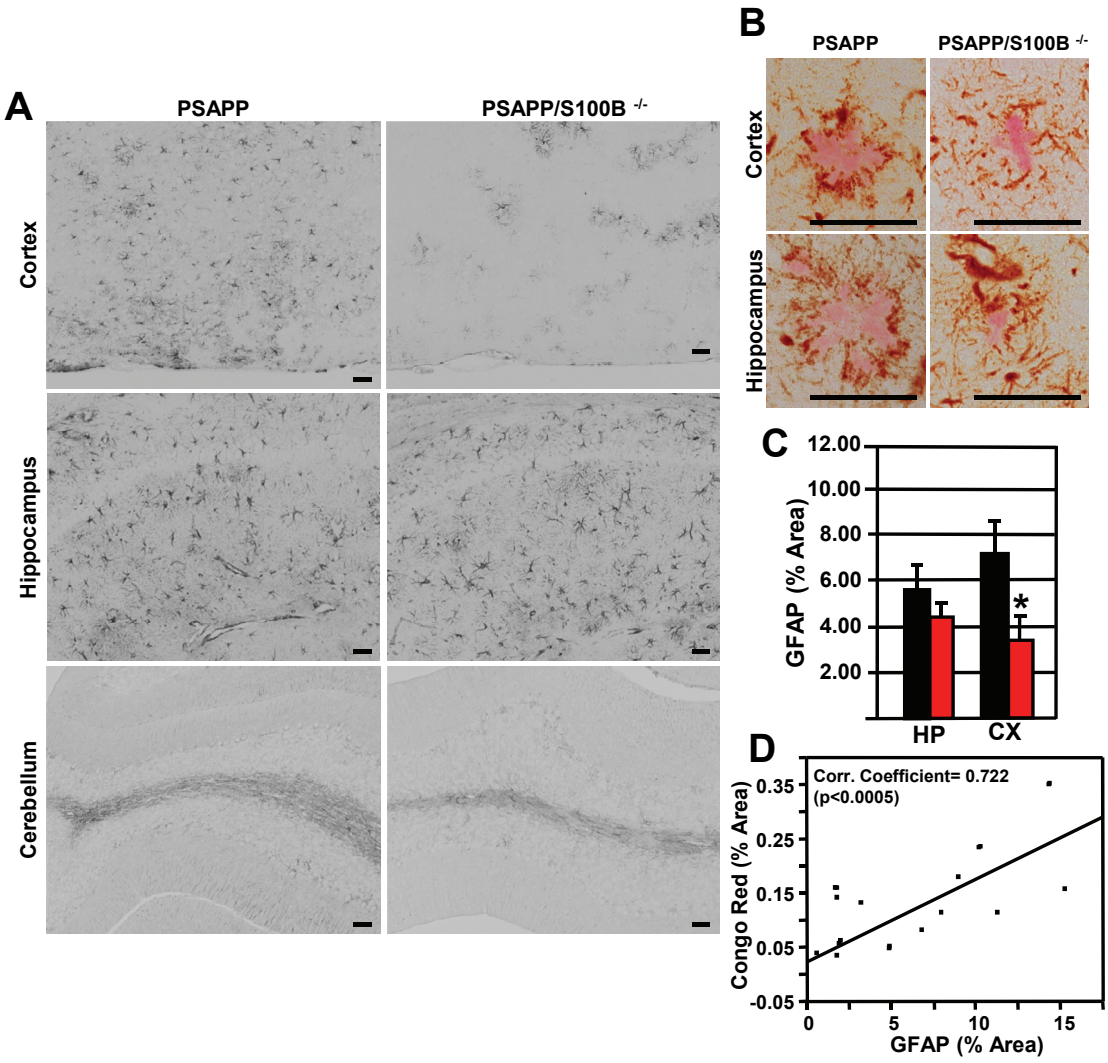

Figure 9: S100B ablation reduces cortical astrocytosis. Representative photomicrographs of parasagittal cortical/hippocampal sections from 6 month old PSAPP and PSAPP/S100B$^{-/-}$ mice shown stained with a GFAP antibody which recognizes activated astrocytes (Panel A) and co-stained with GFAP and congo red which recognizes fibrillar plaques to demonstrate plaque associated astrocytic staining (Panel B). The histogram in Panel C illustrates the mean GFAP positive area $\pm$ SEM in PSAPP (black bars, n=8), and PSAPP/S100B$^{-/-}$ (red bars, n=6) mice. Scale bars represent 50 microns and asterisks denote $p \leq 0.05$ when compared to the PSAPP group. Panel D is a scatter plot of the mean GFAP burden versus plaque load for each animal (cortex and hippocampus).

(Figure 8D). Hippocampal/ cortical plaque-associated GFAP positive astrocytes were also observed in both genotypes (Figure 9A and 9B) and the staining pattern (somata and processes) was indistinguishable from previous reports for AD mouse models (Mori, et al., 2006; Mori, et al., 2010). Hippocampal GFAP staining was similar (4.53 ± 0.67 vs. 5.52 ± 1.35 percent area) while cortical GFAP staining was 2-fold less (3.56 ± 0.92 vs. 7.26 ± 1.40 percent area) in PSAPP/S100B$^{-/-}$ mice when compared to PSAPP control mice (Figure 9C). In addition, GFAP staining in non-plaque containing regions such as the cerebellum (Figure 9A) and olfactory bulb (data not shown) was similar in the two genotypes. Like Iba1, there was a direct correlation between GFAP staining and plaque load (Pearson's Correlation Coefficient 0.722 $p < 0.0005$) (Figure 9D). Collectively, these findings demonstrate that S100B ablation results in regionally selective decreases in microgliosis and astrocytosis that directly correlate with plaque load.

Effects of S100B ablation on dystrophic neurons. Although the correlation between plaque load and cognitive function remains controversial, decreases in plaque load are commonly accompanied by reductions in dystrophic neurons/neurites and improvements in cognitive function. In fact, changes in phospho-tau levels/ staining are used to detect dystrophic neurons in PSAPP and Tg2576 mice despite the fact that these models do not develop tangles (Giunta, et al., 2009; Ricobaraza, et al., 2009; Tomiyama, et al., 2010). Therefore, the AT8 phospho-tau antibody, which detects phospho-Ser202/Thr205, was used to ascertain the effect of S100B ablation on dystrophic neurons. The hippocampal and cortical phospho-tau staining patterns in both genotypes was indistinguishable from

previous reports: punctate plaque-associated staining (Figure 10). These results demonstrate that S100B ablation does not prevent the development of plaque-associated

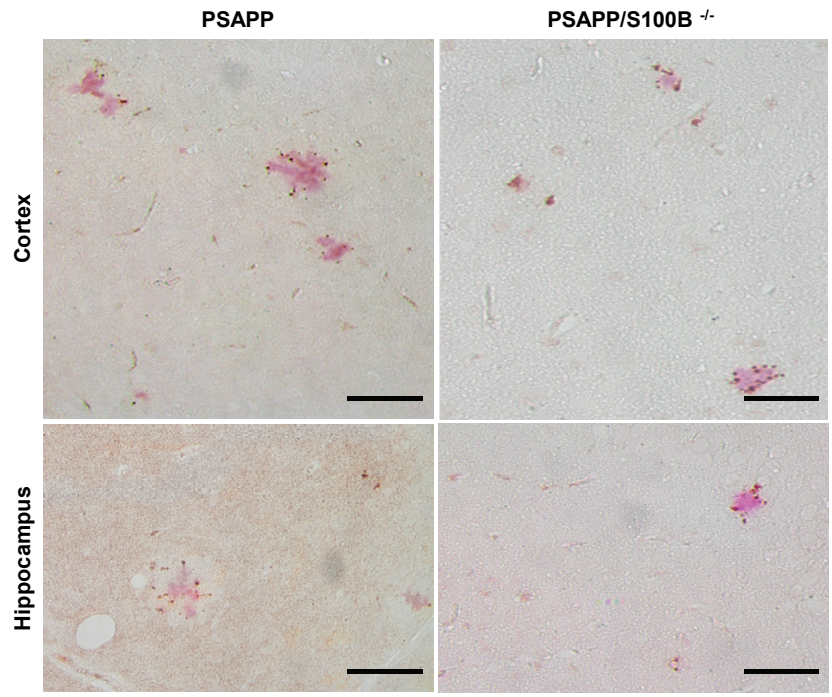

Figure 10: S100B ablation reduces cortical phospho-tau staining. Representative photomicrographs of parasagittal cortical and hippocampal sections from 6 month old PSAPP and PSAPP/S100B$^{-/-}$ mice co-stained with the AT8 antibody which recognizes tau phosphorylated at Ser202/Thr205 and congo red to visualize plaque associated dystrophic neurites. Scale bars represent 50 microns.

dystrophic neurons. However, as predicted by the plaque load results, PSAPP/S100B$^{-/-}$ mice exhibited fewer cortical but similar numbers of hippocampal phospho-tau foci/plaques when compared to PSAPP mice (Figure 10).

S100B colocalizes with hippocampal as well as cortical astrocytes, microglia, and plaques. In human autopsy specimens and the Tg2576 mouse model, S100B staining is associated with astrocytes and plaques (Marshak, et al., 1992; Mori, et al., 2010; Van

Eldik and Griffin, 1994). In addition, in human AD the highest levels of S100B are observed in the most severely affected regions (Van Eldik and Griffin, 1994). Therefore, S100B immunohistochemistry was used to determine if differences in S100B

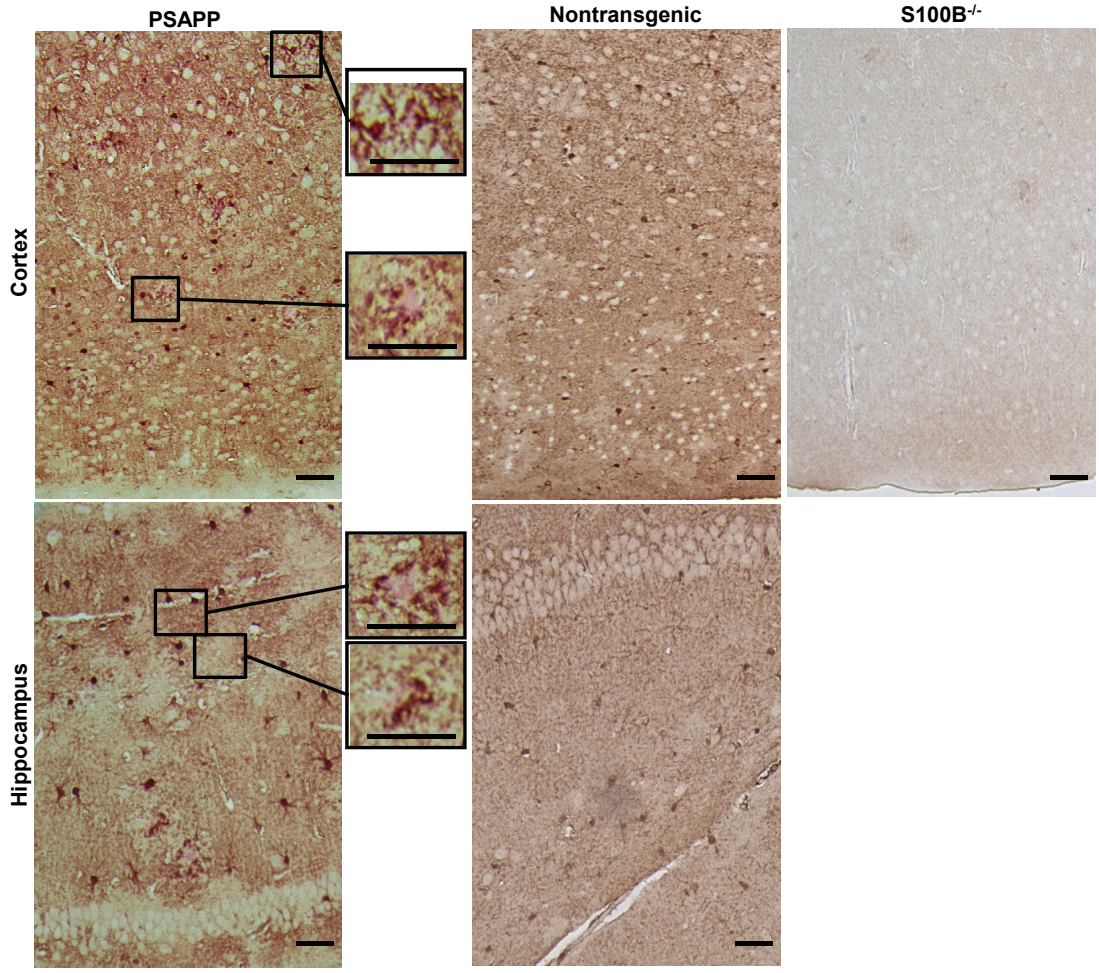

Figure 11: S100B distribution in PSAPP mice. Representative photomicrographs of parasagittal cortical and hippocampal sections from 6 month old PSAPP, non-transgenic littermates or S100B$^{-/-}$ mice co-stained with an S100B antibody and congo red. Insets provide higher magnification of representative plaques. Scale bars represent 50 microns.

distribution were responsible for the regionally selective effects of S100B ablation on histopathology in PSAPP mice. In nontransgenic mice, intense staining of astrocytic cell bodies/processes and diffuse cytoplasmic/extracellular S100B staining was observed in the hippocampus and cortex (Figure 11). PSAPP mice exhibited a similar staining pattern as well as punctate plaque-associated staining (Figure 11). The increased staining intensity in PSAPP mice when compared to nontransgenic mice is consistent with previous reports of increased S100B expression in AD (Mrak and Griffin, 2004; Van Eldik and Wainwright, 2003; Zimmer, et al., 2005). Sections from PSAPP/S100B$^{-/-}$ mice exhibited no detectable staining (Figure 11) indicating that plaque associated and diffuse cytoplasmic/extracellular staining were not attributable to non-specific antibody binding and/or high background. The S100B staining pattern observed in PSAPP mice was similar to staining patterns observed in the Tg2576 AD mouse model (Mori, et al., 2006) and human autopsy specimens (Sheng, et al., 1996). The cellular distribution of S100B in PSAPP mice was confirmed by double immunofluorescence staining with astrocytic (GFAP, overlap coefficient 0.8083 ± 0.0149) and microglial (Iba1, overlap coefficient 0.8476 ± 0.0356) markers (Figure 12). Collectively, these findings suggest that both intracellular and extracellular forms of S100B may contribute to AD histopathology. In conclusion, the regionally selective effects of S100B ablation on histopathology are most likely attributable to regional differences in the cellular processes that are regulated by S100B and not differences in S100B expression/distribution.

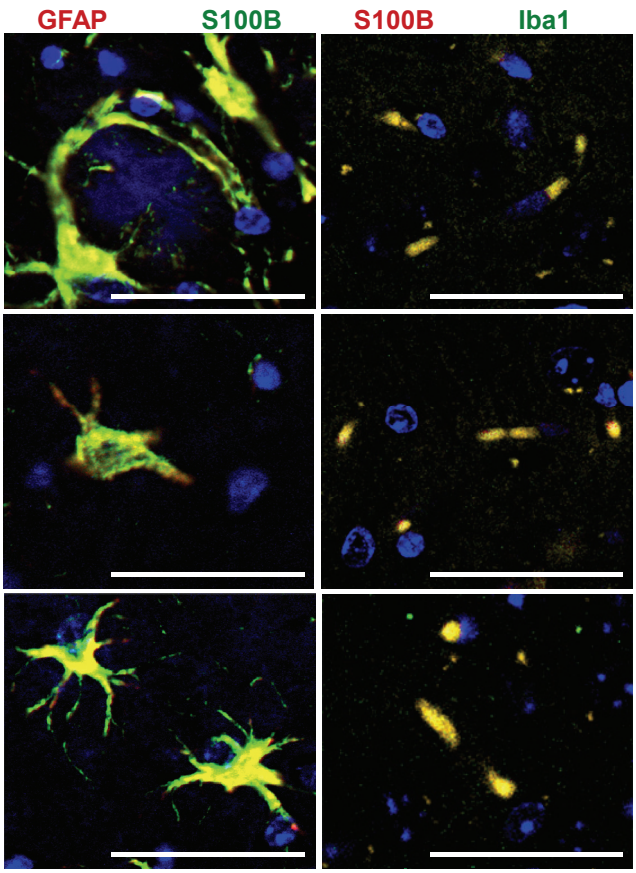

Figure 12: S100B staining co-localizes with plaques, microglia and astrocytes. Representative fluorescent micrographs of parasagittal cortical sections from 6 month old PSAPP mice co-stained with a GFAP (red) and an S100B (green) antibody or an Iba1 (green) and an S100B (red) antibody. Yellow denotes co-localization of S100B with astrocytes and microglia. Scale bars represent 50 microns.

Discussion

This study definitively demonstrates that S100B ablation/inhibition reduces AD pathology. PSAPP/S100B knockout mice exhibited a regionally selective decrease in cortical but not hippocampal plaque load that was accompanied by reductions in astrocytosis, microgliosis and dystrophic neurons. These regionally selective effects were not attributable to variations in the S100B distribution; cortical and hippocampal S100B staining patterns were indistinguishable in PSAPP mice. Finally, in PSAPP mice

S100B immunoreactivity was associated with plaques and colocalized with astrocytes as well as microglia suggesting that both intracellular and extracellular S100B contribute to AD histopathology. Interestingly, other studies have reported regionally selectively effects of S100B ablation on Ca^{2+} handling, synaptic plasticity, kainate-induced gamma amplitudes and BDNF (brain-derived neurotrophic factor) levels (Nishiyama, et al., 2002; Sakatani, et al., 2007; Sakatani, et al., 2008; Schulte-Herbruggen, et al., 2008). Ascertaining the molecular mechanisms responsible for S100B's selective effects on AD histopathology and other processes may provide new insights into the events that contribute to the non-uniform progression of AD (Gomez-Isla, et al., 1996; Hyman, et al., 1984; Romito-DiGiacomo, et al., 2007).

These findings clarify inconsistencies in the literature regarding S100B's contribution to AD histopathology. Genetic ablation (this study), pharmacological inhibition (Mori, et al., 2006) and genetic overexpression (Mori, et al., 2010) approaches consistently indicate that decreases in S100B reduce AD histopathology in the cortex. The larger effects observed with genetic ablation may be due to maximal inhibition; pharmacological inhibition reduces S100B levels by 40-50% and genetic overexpression increases S100B levels by 30% (Mori, et al., 2006; Mori, et al., 2010). In all $S100B^{-/-}$ mice, hippocampal plaque load remains unchanged regardless of the mechanism used to induce plaque deposition, i.e. Aβ infusion (Craft, et al., 2005) or overexpression of mutant proteins (APP and PS-1) in transgenic mice (this study). However, pharmacological inhibition of S100B synthesis with arundic acid in mice that overexpress mutant APP (TG2576 line) reduces hippocampal plaque load/gliosis (Mori,

et al., 2006) and overexpression of S100B in the same model increases hippocampal plaque load/gliosis (Mori, et al., 2010). These differential effects may be due to alternative mechanisms of action for arundic acid (Asano, et al., 2005), upregulation of compensatory mechanisms in knockout models, gain of function in overexpression models, differences in the AD mouse models and/or variations the ages of the animals.

A consistent finding in this and previous studies is a direct correlation between changes in plaque load and gliosis/inflammation in response to alterations in S100B expression. It is unclear, however, whether changes in plaque load are the cause or the result of changes in gliosis. Furthermore, it is unclear how these histopathological changes impact cognitive function. Microglia are an essential component of the inflammatory response and exist in many forms (Morgan, 2006; Perry, et al., 2010). They beneficially phagocytize plaques and suppress inflammation as well as detrimentally promote inflammation and neuronal cell death (Fuhrmann, et al., 2010; Heneka, et al., 2010; Lee and Landreth, 2010). Detailed analyses of microglial/glial phenotypes in PSAPP/S100B$^{-/-}$ mice will be instrumental in identifying S100B-regulated events that contribute to AD pathology and in discerning the relationship between plaques and inflammation. Behavioral data are not available for any of the S100B/AD mouse models. Strengthened synaptic plasticity and enhanced spatial memory in S100B$^{-/-}$ mice (Nishiyama, et al., 2002) suggest that PSAPP/ S100B$^{-/-}$ mice will exhibit improved cognitive function. This hypothesis is supported by the inverse correlation of serum/CSF S100B levels and the direct correlation of the rs2300403 SNP in the S100B gene with low cognitive performance, dementia and AD (Chaves, et al.,

2010; Lambert, et al., 2007). Experiments are underway to determine if pharmacological inhibition of S100B expression and/or interaction of S100B with its target proteins will improve cognitive function in AD and/or other neurological disorders.

S100B's plaque association and co-localization with cells (microglia/astrocytes) in this and previous studies (Marshak, et al., 1992; Mori, et al., 2006; Van Eldik and Griffin, 1994) suggest that both intracellular and extracellular S100B contribute to AD pathology. Inhibition of intracellular S100B would be predicted to reduce Aβ induced spontaneous calcium transients (Chow, et al., 2010), decrease inflammatory cytokine release (Mrak and Griffin, 2004; Sen and Belli, 2007; Van Eldik and Wainwright, 2003) and prevent Aβ induced increases in S100B levels (Pena, et al., 1995). Inhibition of extracellular S100B would be predicted to alter Ca^{2+} handling, synaptic plasticity long-term potentiation, neuronal apoptosis and/or BDNF levels (Fulle, et al., 2000; Nishiyama, et al., 2002; Rebaudo, et al., 2000; Sakatani, et al., 2007; Sakatani, et al., 2008; Schulte-Herbruggen, et al., 2008; Sheng, et al., 1996; Xiong, et al., 2000). Decreased extracellular S100B-RAGE/scavenger receptor signaling in glia, neurons and/or endothelial cells (Deane and Zlokovic, 2007; Hofmann, et al., 1999; Hoppmann, et al., 2010; Hu, et al., 1996; Perrone, et al., 2008; Takeuchi and Yamagishi, 2008; Yan, et al., 1996; Yan, et al., 2009) could also impact APP synthesis, APP processing and/or tau phosphorylation (GSK3β, cdk5 and/or PKA pathways) (Demuro, et al., 2010; Querfurth and LaFerla, 2010; Small and Duff, 2008; Supnet and Bezprozvanny, 2010). In fact, intracellular/extracellular S100B may link dysregulation of Ca^{2+} homeostasis with AD pathobiology and/or serve as a common upstream regulator of both tau

phosphorylation/neurofibrillary tangles and Aβ production/plaque deposition (Demuro, et al., 2010; Querfurth and LaFerla, 2010; Small and Duff, 2008; Supnet and Bezprozvanny, 2010). While astrocytes, microglia and oligodendrocytes are the most logical source of S100B, peripheral tissues such as adipose cannot be excluded (Pham, et al., 2010; Steiner, et al., 2010; Steiner, et al., 2010). Defining the source of and mechanisms of release/secretion for S100B will be important steps in delineating the S100B-regulated processes that contribute to AD histopathology.

Conclusions

Collectively, these data definitively demonstrate that S100B ablation reduces plaque load, gliosis and dystrophic neurons in the cortex but not the hippocampus. If this reduction in histopathology can be demonstrated to positivity impact cognitive changes related to AD, then additional impetus to the search for new therapeutic interventions targeted at S100B will be provided. The development of effective pharmacological strategies for modulating S100B function in patients will also require quantifying the contribution of extracellular versus intracellular forms, identifying the S100B-regulated target proteins/cellular processes, and ascertaining the contribution of the five other S100 family members implicated in AD, S100A1, S100A6, S100A7, S100A9, and S100A12 (Boom, et al., 2004; Qin, et al., 2009; Shepherd, et al., 2006; Zimmer, et al., 2005). Finally, the beneficial effects of S100B ablation/inhibition may extend to other neurological disorders that involve dysregulation of glial cell calcium homeostasis (Matute, 2010; Nedergaard, et al., 2010).

CHAPTER III

S100A1 ABLATION REDUCES ALZHEIMER'S DISEASE PATHOLOGY IN THE PSAPP MOUSE MODEL

Background

S100A1 is a member of the S100 family of Ca^{2+} and Zn^{2+} binding proteins. The term S100 to refers to the solubility of these low molecular weight (~10,000 kDa) proteins in saturated ammonium sulfate (Moore, 1965). S100 proteins are distinguished from other members of the S100/calmodulin/troponin superfamily of EF-hand Ca^{2+} binding proteins by their 3D structure and highly conserved 14 amino acid Ca^{2+} binding loop (Haass and Selkoe, 2007). Upon binding Ca^{2+}, S100 proteins undergo a conformational change which exposes a hydrophobic patch necessary for interacting with numerous intra- and extracellular protein targets and subsequent exertion of their biological effects (Haass and Selkoe, 2007). Individual S100 family members regulate a large number of diverse target proteins/cellular processes that include energy metabolism, cell proliferation, cytoskeletal organization, Ca^{2+} homeostasis and signal transduction pathways. The number/diversity of S100 target proteins, modulatory effects of S100s on target protein activity under physiological conditions and absence of overt phenotypes in knockout mice has led to the misconception that S100s are redundant and play a minor role in Ca^{2+} signaling. In reality, S100s are uniquely suited to transduce changes in a universal second messenger into spatially and temporally unique biological responses (Zimmer and Weber, 2010). The diversity among family

members coupled with their overlapping but distinct expression patterns and partial functional redundancy confers cell-type diversity/specificity to signaling. Furthermore, their interaction with and regulation of multiple components within a given pathway/process allows for cross-talk between and feedback loops within pathways. Nonetheless, the most dramatic effects of S100 signaling are observed under non-physiological conditions and often associated with increases in intracellular calcium levels. For example, increased S100A1 levels delay the conversion of beneficial cardiac hypertrophy to detrimental cardiomyopathy (Most, et al., 2007). In contrast, a detrimental gain of S100B function contributes to unregulated melanoma cell growth (Markowitz, et al., 2007).

Six members of the S100 family have been implicated in the onset/progression of AD: S100A1, S100A6, S100A7, S100A9, S100A12 and S100B (Boom, et al., 2004; Chaves, et al., 2010; Qin, et al., 2009; Shepherd, et al., 2006; Steiner, et al., 2011; Zimmer, et al., 2005). S100B is hypothesized to contribute to a "detrimental cytokine cycle" that drives the progression of AD (Leclerc, et al., 2010; Mrak and Griffin, 2004; Querfurth and LaFerla, 2010; Sen and Belli, 2007; Small and Duff, 2008; Sorci, et al., 2010; Van Eldik and Wainwright, 2003; Zimmer and Weber, 2010) and recent studies have identified inhibition of S100B as a novel strategy for reducing plaque load, gliosis and neuronal dysfunction (Roltsch, et al., 2010). S100A9 and S100A12 are inflammation associated proteins, constitutively expressed in neutrophils and induced in plaque associated macrophages (Shepherd, et al., 2006). S100A6 is upregulated in astrocytes that surround plaques in human autopsy specimens and transgenic mice

(Boom, et al., 2004). S100A7, originally characterized as a marker for psoriasis (Ruse, et al., 2001), is present in the CSF of AD patients and promotes non-amyloidogenic APP processing (Qin, et al., 2009). In the case of S100A1, there is no information regarding S100A1expression/function in the AD brain. However, S100A1 does regulate numerous cellular processes/target proteins that have been implicated in AD.

S100A1 is expressed primarily in neurons and functions as both an intracellular Ca^{2+} receptor and an extracellular neuropeptide (Wright, et al., 2009; Zimmer, et al., 1998; Zimmer, et al., 2005). S100A1 has been reported to regulate several cellular processes that are involved in AD including APP expression, tau phosphorylation, neuronal cell sensitivity to Aβ, dendrite/synapse formation, neuronal survival and Ca^{2+} homeostasis (Zimmer, et al., 1998; Zimmer, et al., 2005). In addition, many S100A1-target proteins exhibit altered function in AD including the ryanodine receptor, tau, RAGE-receptor and Akt (Bruno, et al., 2011; Castellani, et al., 2010; Huttunen, et al., 2000; Leclerc, et al., 2009; Prosser, et al., 2011; Querfurth and LaFerla, 2010; Srikanth, et al., 2011; Wright, et al., 2009; Zimmer, et al., 2005). However, we do not know if S100A1 is expressed in the AD brain and if so, is it beneficial or detrimental.

This study uses an *in vivo* genetic approach to ascertain the net effect of S100A1 ablation on AD histopathology in the PSAPP AD mouse line. Although no AD mouse model exhibits all aspects of the human disease, the PSAPP double transgenic ($APP_{K670NM671L}$/$PS\text{-}1_{M146L}$) line has a rapid disease onset and mimics many facets of the human disease including plaque deposition, dystrophic neurites, glial activation, and memory deficits (Gordon, et al., 2001; Gordon, et al., 2002; Holcomb, et al., 1998;

Holcomb, et al., 1999). Immunohistochemistry confirmed that PSAPP and human autopsy specimens contain S100A1, some of which is plaque-associated. PSAPP/S100A1 knockout mice exhibited reductions in cortical and hippocampal plaque load that were attributable to decreases in plaque number, not plaque size. These reductions in plaque load were accompanied by decreased inflammation, i.e. GFAP-positive astrocytes and Iba1-positive microglia. Finally, ablation of both S100A1 and S100B had synergistic effects on plaque load in 6 but not 12 month old animals. These results suggest that S100A1 and S100B act via different mechanisms in young animals and that their mechanisms of action in AD are dynamic/flexible. In summary, this is the first report of *in vivo* synergy among S100 family members. These findings suggest that intracellular as well as extracellular forms of S100A1 contribute to AD pathology and that pharmacological strategies which selectively block S100A1 action in the CNS may be effective treatments for AD.

Methods

PSAPP X S100A1 knockout mice. The PSAPP double transgenic line (Gordon, et al., 2001; Gordon, et al., 2002; Holcomb, et al., 1998; Holcomb, et al., 1999) and S100A1 knockout line (Prosser, et al., 2008) have been described previously. The PSAPP/S100A1$^{-/-}$ and PSAPP S100 double knockout (PSAPP/S100A1$^{-/-}$/S100B$^{-/-}$) lines were generated by crossing PSAPP double transgenic males with S100A1$^{-/-}$/S100B$^{-/-}$ knockout females and subsequent interbreeding of the heterozygous offspring (PSAPP/S100A1$^{+/-}$/S100B$^{+/-}$ X PSAPP/S100A1$^{+/-}$/S100B$^{+/-)}$. To control for genetic background, all experiments used PSAPP/S100A1$^{+/+}$/S100B$^{+/+}$, PSAPP/S100A1$^{-/-}$

/S100B$^{+/+}$, and PSAPP/S100A1$^{-/-}$/S100B$^{-/-}$littermates. Genotyping was performed as previously described (Gordon, et al., 2001; Prosser, et al., 2008; Roltsch, et al., 2010). All procedures involving animals were approved by the Texas A&M University Institutional Animal Care and Use Committee and comply with the *NIH Guide for the Care and Use of Laboratory Animals*.

Sample acquisition/processing. Brains were removed from anesthetized animals and processed as previously described (Roltsch, et al., 2010). Briefly, brains were rinsed in phosphate buffered saline (PBS), fixed in 4% (wt/vol) paraformaldehyde in PBS for 30 minutes and sliced into 2 mm sagittal sections. After a second 30 minute fixation in 4% (wt/vol) paraformaldehyde in PBS, slices were permeablized in 2mM $MgCl_2$, 0.01% (wt/vol) sodium deoxycholate, 0.02% (vol/vol) Nonidet P-40 in 100mM sodium phosphate buffer pH 7.5 (permeabilization buffer), post-fixed in 10% buffered formalin for 16 hours and embedded in paraffin. Five micron sagittal sections were mounted on glass slides for subsequent staining. Alzheimer's tissue arrays containing parietal cortex, temporal cortex, prefrontal cortex, and hippocampal specimens from age- and gender-matched normal and AD patients (CERAD semi-quantitative assessment criteria confirmed) were obtained as a catalog item from Folio Biosciences (ARY-HH0116) (Columbus, OH).

Immunohistochemical and Congo red staining. Congo-red (plaque load), Iba1 (microgliosis), GFAP (astrocytosis) and S100A1 staining were performed as previously described (Roltsch, et al., 2010). Primary antibodies included a mouse monoclonal S100A1 antibody (1-300 dilution of SC-58840, Santa Cruz Biotechnology, Santa Cruz,

CA), a rabbit polyclonal GFAP antibody (1-1000 dilution of Z0311, Dako, Carpentaria, CA) and mouse monoclonal Iba1 antibody (1-300 dilution of SC32735, Santa Cruz Biotechnology). For quantification, digital images were captured, converted to gray scale, and positive pixels, plaque size, plaque number and total plaque load were quantified using Image J software (NIH Image, Bethesda, MD). Plaque load and immunoreactivity were defined as the % area, i.e. the area of positive pixels/total pixels X 100. The data were expressed as the mean $\pm$ SEM (n=8 for 6 and 12 month old PSAPP, n=8 for 6 month old PSAPP/S100A1$^{-/-}$ and n=3 for 12 month PSAPP/S100A1$^{-/-}$, n=6 for 6 month old PSAPP/S100A1$^{-/-}$/S100B$^{-/-}$ and n=4 for 12 month old PSAPP/S100A1$^{-/-}$/S100B$^{-/-}$). A multicomparison ANOVA with the Tukey HSD post hoc test or an independent samples t-test (JMP by SAS, Cary, NC) was used to determine the significance ($p<0.05$) of measured differences between genotypes. The Orthogonal Regression Correlation and scatter plots of the mean hippocampal and cortical GFAP/Iba1 staining/animal versus plaque load were used to determine the relationship between plaque load and astrocytosis/microgliosis.

Results

Mouse and human AD brain specimens contain S100A1. Immunohistochemistry was used to determine if S100A1 is present in the AD brain. In PSAPP mice, S100A1 staining was detectable in the cerebellum (Figure 13A), cortex and hippocampus (data not shown) at 6 and 12 months of age. In addition, the concentrated perinuclear as well as diffuse cytoplasmic/extracellular staining in the gray matter with little or no staining in the white matter pattern was similar to previous reports (Benfenati, et al., 2004;

Zimmer and Landar, 1995; Zimmer, et al., 1995). However there was one notable exception, plaque-associated S100A1 staining. PSAPP/S100A1 knockout mice exhibited

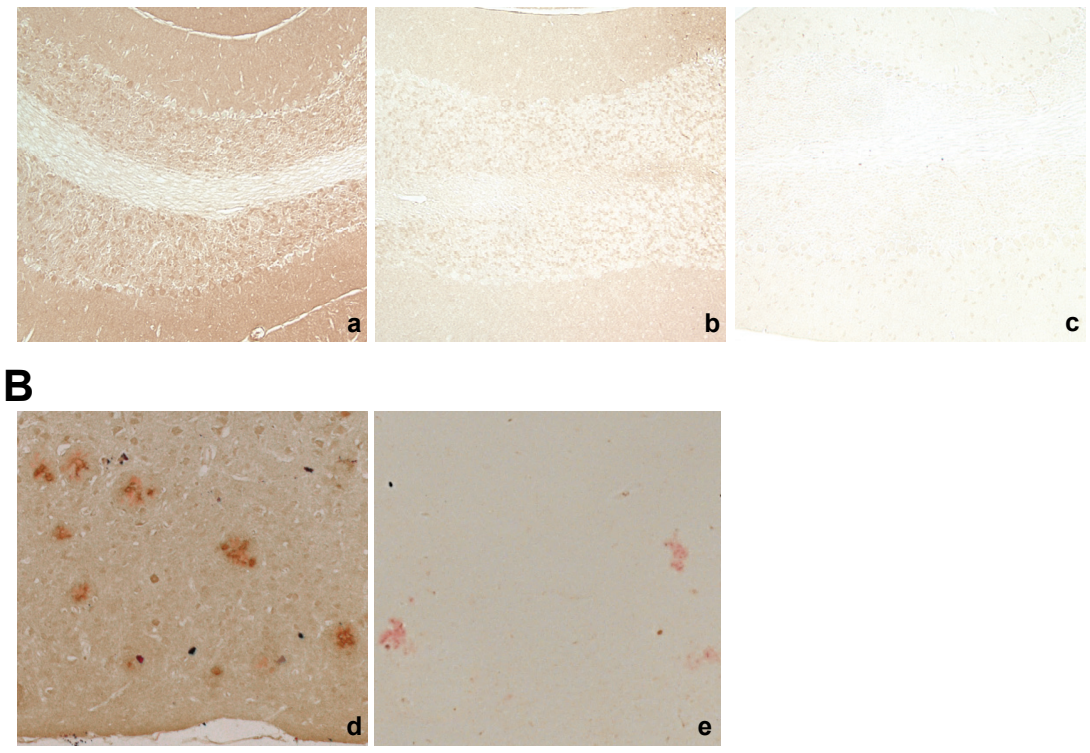

Figure 13. S100A1 distribution in PSAPP mice. Representative photomicrographs of parasagittal cerebellar (Panel A) and cortical (Panel B) sections from PSAPP (a and d), nontransgenic (b) and PSAPP/S100A1$^{-/-}$ (c and e) mice either stained with an S100A1 antibody (a, b and c) or co-stained with an S100A1 antibody and Congo red (d and e).

no detectable S100A1 staining (Figure 13) indicating that the cellular and plaque-associated S100A1 staining was not attributable to non-specific antibody binding and/or high background. Since no AD mouse model recapitulates all aspects of pathology observed in human patients (Elder, et al., 2010), age- and gender-matched control/CERAD AD confirmed human tissue arrays were used to determine if human

AD brains contained S100A1. S100A1 staining was detected in the parietal cortex, temporal cortex, prefrontal cortex and hippocampus in AD and control specimens (Figure 14). Furthermore, the staining pattern was similar to that observed in the mouse: concentrated perinuclear staining, diffuse/extracellular cytoplasmic staining and plaque-associated staining in the gray matter. Additional studies will be needed to determine if plaque associated staining in mouse models and human AD represents intracellular

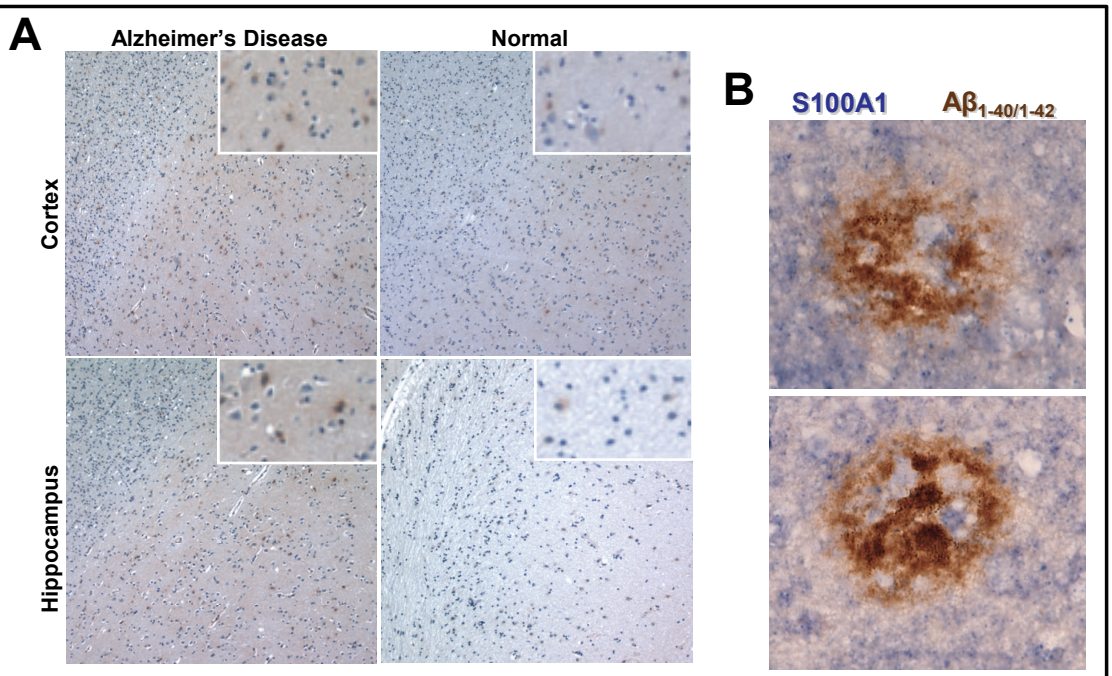

Figure 14. S100A1 distribution in human AD specimen. Representative photomicrographs of human tissue arrays containing cortical and hippocampal sections from Alzheimer's disease and age-matched controls stained with an S100A1 antibody (brown) and counterstained (Panel A). Panel B depicts higher magnification of representative plaques in human cortical AD specimens stained with an S100A1 antibody (blue) and an $A\beta_{1\text{-}40}$ antibody (brown) which labels plaques.

S100A1 within dystrophic neurites/activated microglia or extracellular S100A1 within the plaque. Nonetheless, this is the first demonstration that mouse and human AD brain

specimens contain S100A1 and suggests that aberrant S100A1 signaling in response to Ca^{2+} dysregulation may contribute to AD pathobiology.

S100A1 ablation decreases plaque load in PSAPP mice. To determine if S100A1 ablation altered amyloidogenesis, plaque load was quantified in PSAPP/S100A1 knockout and PSAPP mice. In 6 month old animals, Congo red positive plaques were observed in the hippocampus and cortex of both genotypes (Figure 15A). However, PSAPP/S100A1$^{-/-}$ mice exhibited a 3.5 fold reduction in cortical plaque load (0.0481 ± 0.0062 vs. 0.1676 ± 0.0156 percent area) and a 2.4 fold reduction in hippocampal plaque load (0.0351 ± 0.0800 vs. 0.0845 ±0.0220 percent area) when compared to PSAPP mice (Figure 15B). This decrease in plaque load was attributable to a decrease in plaque number, not plaque size. PSAPP/S100A1$^{-/-}$ exhibited a 3.6 fold reduction in cortical (13.3333 ± 1.4885 vs. 47.7778 ± 9.4204) and a 3 fold reduction in hippocampal (3.8889 ± 0.9562 vs. 11.2500 ± 3.8580) plaque number (Figure 15C). In contrast, the plaque size in the two genotypes was indistinguishable: 1358 ± 104 vs. 1162 ± 141 μm^2 in the cortex and 1952 ± 421 vs. 1864 ± 711 μm^2 in the hippocampus (Figure 15D). Plaque load in PSAPP littermates was indistinguishable from previously published reports (Gordon, et al., 2001; Gordon, et al., 2002; Holcomb, et al., 1998; Holcomb, et al., 1999; Roltsch, et al., 2010) indicating the these differences were not attributable to genetic background.

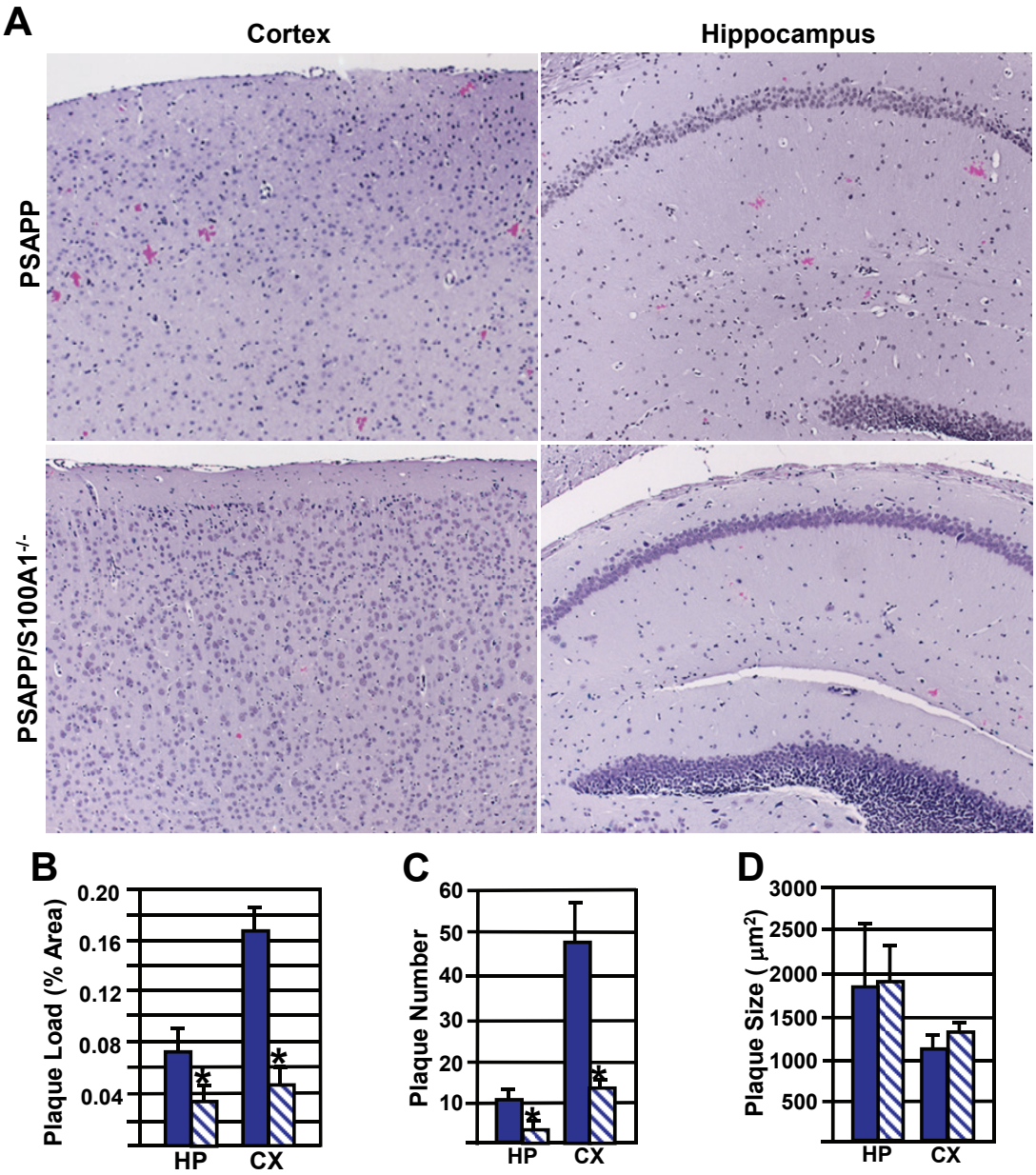

Figure 15: S100A1 ablation reduces cortical and hippocampal plaque load in six month old PSAPP mice. Panel A contains representative micrographs of parasagittal cortical/hippocampal sections from 6 month old PSAPP and PSAPP/S100A1$^{-/-}$ mice stained with congo red (pink) and hematoxylin (blue) to visualize plaques and nuclei, respectively. The histograms depict the mean congophilic plaque load (Panel B), plaque number (Panel C), and plaque size (Panel D) $\pm$ SEM in PSAPP (solid blue bars, n=8), and PSAPP/S100A1$^{-/-}$ (hatched blue bars, n=4) mice. Asterisks denote $p \leq 0.05$ when compared to the PSAPP group.

To determine if the effects of S100A1 ablation on plaque load were age-dependent, plaque load was quantified in 12 month old animals. As expected, 12 month old PSAPP littermates exhibited a 6-7 fold increase in plaque load when compared to 6 month old PSAPP mice. Nonetheless, there was a 3 fold reduction in cortical (0.3212 ± 0.0257 vs. 1.023 ± 0.0354 percent area) and a 2 fold reduction in hippocampal (0.2478 ± 0.0414 vs. 0.5511 ± 0.0684 percent area) plaque load in 12 month old PSAPP/S100A1$^{-/-}$ mice (Figure 16A and B). In addition, these reductions in plaque load were attributable to decreases in plaque number, not plaque size. PSAPP/S100A1$^{-/-}$ mice exhibited a 2 fold reduction in cortical (83.0 ± 12.3 vs. 179.8 ± 10.9) and hippocampal (24.7 ± 5.5 vs. 68.1 ± 12.7) plaque number (Figure 16C). Plaque size in the two genotypes was indistinguishable: 1299 ± 123 vs. 1816 ± 100 and 1328 ± 294 vs. 1330 ± 179 μm^2 in the cortex and hippocampus, respectively (Figure 16D). Thus, reductions in plaque load/number in response to S100A1 ablation are age-independent. In summary, this is the first demonstration that S100A1 ablation non-selectively reduces plaque load/number without altering plaque size and suggests that S100A1 accelerates new plaque deposition in the AD brain.

S100A1 ablation reduces gliosis in the PSAPP AD mouse model. Astrocytosis (Li, et al., 2011) and microgliosis (Cameron and Landreth, 2010; Wyss-Coray and Mucke, 2002) are early and critical events in the in the pathogenesis of AD (Eikelenboom, et al., 2010; Heneka, et al., 2010; Lee, et al., 2010). The astrocytic marker GFAP and microglial marker Iba1 were used to determine if S100A1 ablation also reduced gliosis.

In 6 month old PSAPP and PSAPP/S100A1$^{-/-}$ mice, cortical and hippocampal plaque-associated GFAP staining was indistinguishable from previous reports: GFAP-positive

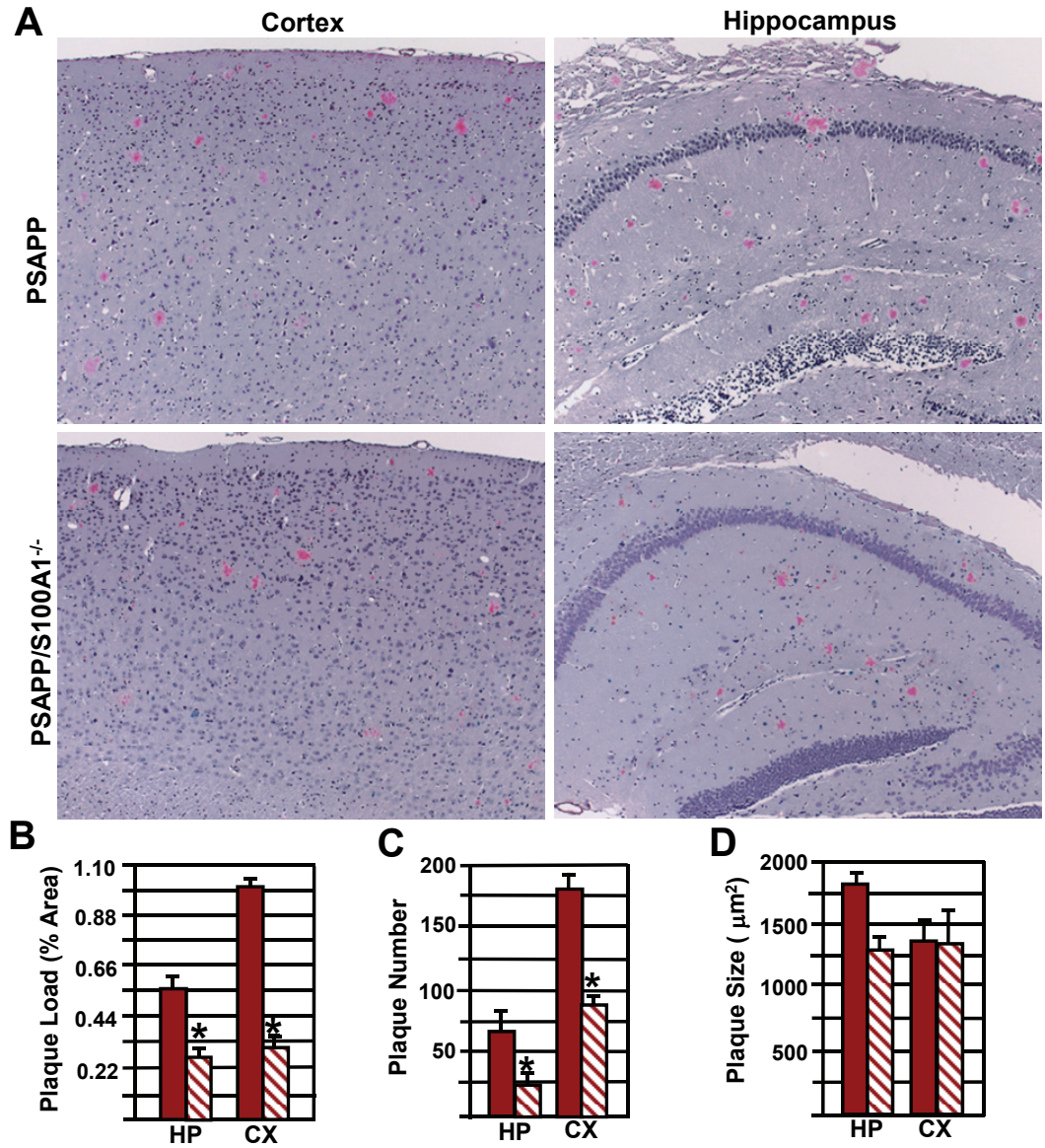

Figure 16: S100A1 ablation reduces cortical and hippocampal plaque load in twelve month old PSAPP mice. Panel A contains representative micrographs of parasagittal cortical/hippocampal sections from 12 month old PSAPP and PSAPP/S100A1$^{-/-}$ mice stained with congo red (pink) and hematoxylin (blue) to visualize plaques and nuclei, respectively. The histograms depict the mean congophilic plaque load (Panel B), plaque number (Panel C), and plaque size (Panel D) $\pm$ SEM in PSAPP (solid red bars, n=8), and PSAPP/S100A1$^{-/-}$ (hatched red bars, n=4) mice. Asterisks denote $p \leq 0.05$ when compared to the PSAPP group.

cell bodies and processes (Figure 17A and B) (Mori, et al., 2006; Mori, et al., 2010). However, 6 month old PSAPP/S100A1$^{-/-}$ mice exhibited a 3.7 fold reduction in cortical (3.2940 ± 1.0174 vs. 12.1572 ± 0.8246 percent area) and 1.5 fold reduction in hippocampal (8.3168 ± 1.3755 vs. 12.0146 ± 0.7926 percent area) GFAP staining when compared to age-matched PSAPP mice (Figure 17C). Twelve month old PSAPP/S100A1$^{-/-}$ mice exhibited a 2.3 fold reduction in cortical and (14.7362 ± 2.4743 vs. 33.3435 ± 3.0363 percent area) and 2.4 fold reduction in hippocampal (12.7549 ± 0.6016 vs. 30.8905 ± 2.8725 percent area) GFAP staining when compared to age-matched PSAPP mice (Figure 17D). Furthermore, there was there was a direct correlation between GFAP staining and plaque load (Pearson's Correlation Coefficient 0.9134 $p < 0.0001$) (Figure 17E). Interestingly, S100A1 ablation did not alter GFAP staining in non-plaque containing areas such as the cerebellum (Figure 17A). These data demonstrate that S100A1 ablation reduces astrocytosis as well as amyloidogenesis. The microglial marker Iba1 was used to determine if S100A1 ablation also reduced microgliosis. In 6 month old PSAPP and PSAPP/S100A1$^{-/-}$ mice, plaque associated Iba1 positive microglia (somata and processes) were observed in the hippocampus and cortex (Figure 18A and B) and this staining pattern was indistinguishable from previous reports for AD mouse models (Mori, et al., 2006; Mori, et al., 2010). However, PSAPP/S100A1$^{-/-}$ mice exhibited a 1.6 fold reduction in cortical (2.4590 ± 0.4860 vs. 4.0259 ± 0.3222 percent area) and a 1.4 fold reduction in hippocampal (3.3849 ± 0.0.2023 vs. 4.6109 ± 0.2560 percent area) Iba1 staining when compared to PSAPP mice

(Figure 18C). Twelve month old PSAPP/S100A1$^{-/-}$ mice exhibited a 4 fold decrease in cortical (2.0854 ± 0.4076 vs. 8.5340 ± 0.4575) and a 2.9 fold decrease in

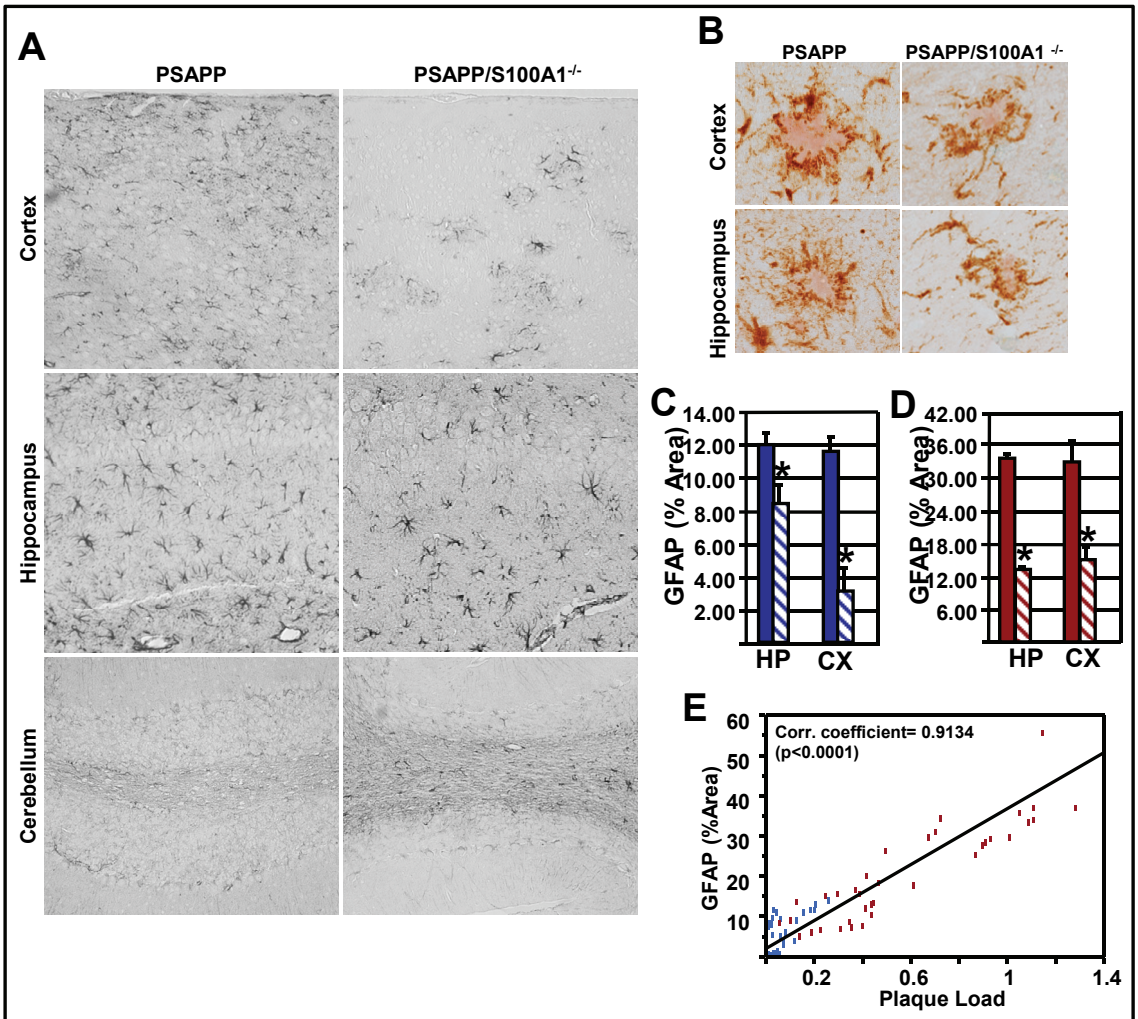

Figure 17: S100A1 ablation reduces astrocytosis. Representative photomicrographs of parasagittal cortical/hippocampal sections from 6 month old PSAPP and PSAPP/S100A1$^{-/-}$ mice are shown stained with a GFAP antibody which labels astrocytes (Panel A) and co-stained with GFAP and congo red, which labels fibrillar plaques, to demonstrate plaque associated astrocyte staining. The histograms depict the mean GFAP positive area ± SEM in six (blue, Panel C) and twelve (red, Panel D) month old PSAPP (solid bars, n=8 at 6 months, n=6 at 12 months), and PSAPP/S100A1$^{-/-}$ (hatched bars, n=4 at 6 months, n=3 at 12 months), mice. Scale bars represent 50 microns and asterisks denote p≤0.05 when compared to the PSAPP group. Panel E is a scatter plot of the mean GFAP burden versus plaque load for each animal at six (blue) and twelve (red) months (cortex and hippocampus).

hippocampal (2.4999 ± 0.3321 vs. 7.1809 ± 0.6252 percent area) Iba1 staining when compared to PSAPP mice (Figure 18D). Furthermore, there was a direct correlation

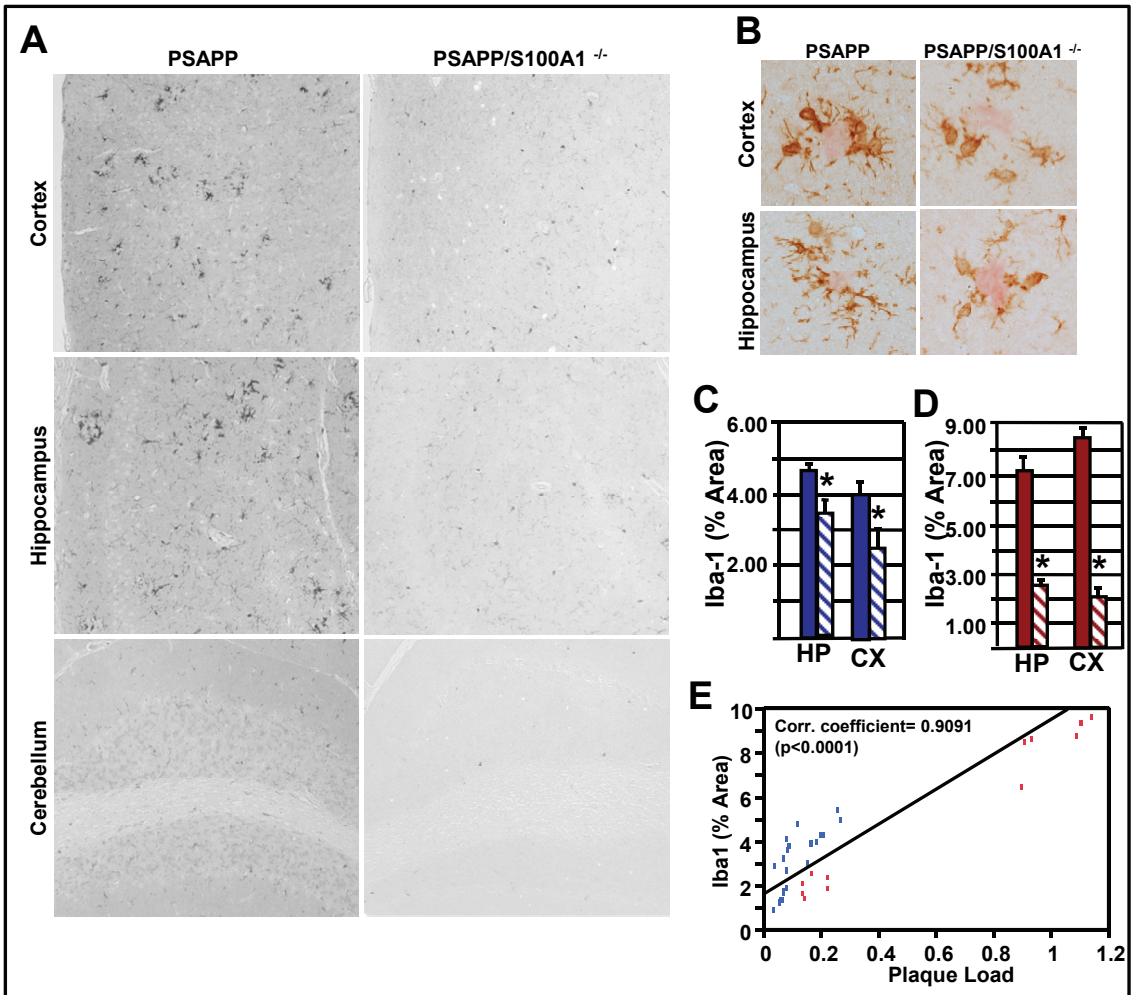

Figure 18: S100A1 ablation reduces microgliosis. Representative photomicrographs of parasagittal cortical/hippocampal sections from 6 month old PSAPP and PSAPP/S100A1$^{-/-}$ mice are shown stained with an Iba1 antibody which labels microglia (Panel A) and co-stained with Iba1 and congo red, which labels fibrillar plaques, to demonstrate plaque associated microglial staining. The histograms depict the mean Iba1 positive area ± SEM in six (Panel C) and twelve (Panel D) month old PSAPP (solid bars, n=8 at 6 months, n=6 at 12 months), and PSAPP/S100A1$^{-/-}$ (hatched bars, n=4 at 6 months, n=3 at 12 months), mice. Scale bars represent 50 microns and asterisks denote p≤0.05 when compared to the PSAPP group. Panel E is a scatter plot of the mean GFAP burden versus plaque load for each animal at six (blue) and twelve (red) months (cortex and hippocampus).

between Iba1 staining and plaque load (Pearson's Correlation Coefficient 0.9091 $p < 0.0001$) (Figure 18E). Finally, S100A1 ablation did not alter Iba1 staining in non-plaque containing regions, such as the cerebellum (Figure 18A). Collectively, these findings demonstrate that reductions in plaque load in response to S100A1 ablation directly correlate with reductions in inflammation (astrocytosis and microgliosis) and are the first report that S100A1 is pro-inflammatory.

S100A1 and S100B ablation synergistically reduce plaque load and inflammation. Previous studies have demonstrated that another member of the S100 family, S100B, selectively reduces cortical, but not hippocampal, plaque load and inflammation (Roltsch et al., 2010). Because S100A1 is expressed primarily in neurons, and S100B primarily in glial cells (Zimmer, et al., 2005), we hypothesize that the effect of concurrent ablation/inhibition of S100A1 and S100B on AD pathology would be synergistic. To test this hypothesis, plaque load, astrocytosis and microgliosis were quantified in 6 and 12 month old PSAPP/S100A1/S100B double knockout mice. There was 6.6 fold reduction in cortical and an 8.3 fold reduction in hippocampal plaque load in

Table 2. S100A1 and S100B ablation synergistically reduce plaque load and microgliosis in six month old PSAPP mice

		PSAPP/S100A1$^{-/-}$/S100B$^{-/-}$	PSAPP/S100A1$^{-/-}$	PSAPP
Plaque Load (% Area)	**Cortex**	0.0254 ± 0.0086*#	0.0481 ± 0.0062*	0.1676 ± 0.0156
	Hippocampus	0.0102 ± 0.0154*#	0.0351 ± 0.008*	0.0845 ± 0.0220
GFAP (% Area)	**Cortex**	2.1424 ± 0.7378*	3.2940 ± 1.0174*	11.7507 ± 0.7088
	Hippocampus	8.9700 ± 0.7378*	8.3168 ± 1.3755*	12.0146 ± 0.7926
Iba1 (%Area)	**Cortex**	1.1208 ± 0.1570*#	2.4590 ± 0.4860*	4.0259 ± 0.3222
	Hippocampus	2.0010 ± 0.3306*#	3.3849 ± 0.2023*	4.6109 ± 0.2560

The table depicts the mean plaque load, GFAP burden and Iba1 burden ± SEM in six month old PSAPP, PSAPP/S100A1$^{-/-}$, and PSAPP/S100A1$^{-/-}$/S100B$^{-/-}$ mice. Asterisks denote $p \leq 0.05$ when compared to the PSAPP group and number sign denotes $p < 0.05$ when compared to the PSAPP/S100A1$^{-/-}$ group.

PSAPP/S100A1$^{-/-}$/S100B$^{-/-}$ when compared to PSAPP mice and these reductions were significantly greater than the 2-4 fold reductions observed in PSAPP/S100A1$^{-/-}$ mice (Table 2). These synergistic reductions in plaque load were associated with synergistic reductions in microgliosis but not astrocytosis. PSAPP/S100A1$^{-/-}$/S100B$^{-/-}$ mice exhibited a 3.6 fold reduction in cortical and a 2.3 fold reduction in hippocampal Iba1 staining, both of which were significantly greater than the reductions observed in PSAPP/S100A1$^{-/-}$ (Table 2). In contrast, GFAP staining in 6 month old PSAPP/S100A1$^{-/-}$/S100B$^{-/-}$ and PSAPP/S100A1$^{-/-}$ mice were indistinguishable (Table 2). While direct comparisons with the previously published data for the PSAPP/S100B$^{-/-}$ line cannot be made, the fold reductions in plaque load (3-fold), Iba1 staining (4-fold) and GFAP staining (2-fold) in this study for the PSAPP/S100A1$^{-/-}$/S100B$^{-/-}$ line are greater (Roltsch, et al., 2010) and support the conclusion that effects of S100A1 and S100B are synergistic. However, this synergy was age- and region- specific. In 12 month old animals, only cortical GFAP staining exhibited a synergistic reduction in PSAPP/S100A1$^{-/-}$/S100B$^{-/-}$

Table 3. S100A1 and S100B ablation synergistically reduce cortical astrocytosis in twelve month old PSAPP mice

		PSAPP/S100A1$^{-/-}$/S100B$^{-/-}$	PSAPP/S100A1$^{-/-}$	PSAPP
Plaque Load (% Area)	**Cortex**	0.3401 ± 0.0490*	0.3212 ± 0.0257*	1.0023 ± 0.0354
	Hippocampus	0.2353 ± 0.0492*	0.2478 ± 0.0414*	0.5511 ± 0.0684
GFAP (% Area)	**Cortex**	8.9241 ± 2.3083*#	14.7363 ± 3.2256*	33.3435 ± 3.0363
	Hippocampus	15.7444 ± 1.8148*	12.7549 ± 0.6016*	33.5349 ± 1.3751
Iba1 (%Area)	**Cortex**	0.9184 ± 0.2303*	2.0854 ± 0.4076*	8.5340 ± 0.4575
	Hippocampus	1.6235 ± 0.6526*	2.5000 ± 0.3321*	7.1809 ± 0.6252

The table depicts the mean plaque load, GFAP burden and Iba1 burden ± SEM in twelve month old PSAPP, PSAPP/S100A1$^{-/-}$, and PSAPP/S100A1$^{-/-}$/S100B$^{-/-}$ mice. Asterisks denote $p \leq 0.05$ when compared to the PSAPP group and number sign denotes $p < 0.05$ when compared to the PSAPP/S100A1$^{-/-}$ group.

mice (8.5 fold) when compared to PSAPP/S100A1$^{-/-}$ mice (2.3 fold) (Table 3). Comparison data at 12 months of age for the PSAPP/S100B$^{-/-}$ line is not available. Collectively, these data demonstrate that the synergistic effects of S100A1 and S100B ablation on AD histopathology are age-, region- and endpoint-specific and support the current view in the field that S100 family members exhibit partial functional/mechanistic redundancy.

Discussion

In summary, this is the first demonstration that S100A1 ablation reduces AD histopathology. The presence of detectable S100A1 staining, some of which was plaque-associated, in PSAPP and human autopsy specimens is consistent with a detrimental gain of S100A1 function/signaling in AD in response to Ca^{2+} dysregulation. Six and twelve month old PSAPP/S100A1 knockout mice exhibited decreases in hippocampal and cortical plaque load/plaque number but not plaque size, suggesting that S100A1 promotes the formation of new plaques. Furthermore, there was a direct correlation between plaque load and inflammation, i.e. microgliosis (Iba1 staining) and astrocytosis (GFAP staining). Astrocytosis (Li, et al., 2011) and microgliosis (Cameron and Landreth, 2010; Wyss-Coray and Mucke, 2002) are early and critical events in AD pathogenesis, (Eikelenboom, et al., 2010; Heneka, et al., 2010; Lee, et al., 2010) and could be the cause or result of reductions in plaque load. Phenotypic characterization of the microglial and astrocytic populations in PSAPP/S100A1 knockout mice will provide important insights regarding the S100A1-regulated processes that contribute to AD as well as the relationship between plaques and inflammation. The increased fold

reductions in plaque load and microgliosis in 12 versus 6 month old animals suggests that S100A1 ablation/inhibition will delay and reduce the formation of new plaques even if therapy is initiated after plaques are detected. In addition, there is a strong probability that S100A1 may serve as a common upstream regulator of both tau phosphorylation/neurofibrillary tangles and Aβ production/plaque deposition (Small and Duff, 2008), since S100A1 regulates tau phosphorylation and microtubule stability (Baudier, et al., 1982; Zimmer, et al., 1998). Finally, S100A1 ablation/inhibition has been reported to alter cognitive function in normal animals (Ackermann, et al., 2006; Kubista, et al., 1999; O'Dowd, et al., 1997) suggesting that S100A1 ablation/inhibition in AD will impact cognitive function. Even though the contribution of plaques, tangles and inflammation to cognitive decline remains unresolved (Castellani, et al., 2009; Gorelick, 2010; Nelson, et al., 2009; Serrano-Pozo, et al., 2011; Thind and Sabbagh, 2007), our observations suggest that pharmacological therapies targeting S100A1 may beneficially reduce inflammation and delay plaque deposition in AD patients.

The cellular and plaque-associated S100A1 staining in AD specimens suggests that both intracellular and extracellular S100A1 contribute to the phenotypic changes observed in PSAPP S100A1 knockout mice. Upon binding Ca^{2+}, S100 proteins undergo a conformational change which exposes a hydrophobic patch necessary for interacting with numerous intra- and extracellular protein targets and subsequent exertion of their biological effects (Zimmer, et al., 2003; Zimmer and Weber, 2010). Inhibition of intracellular S100A1 signaling is predicted to increase dendrite formation/neurite extension; augment tubulin polymerization; decrease neuronal cell sensitivity to Aβ

toxicity; stimulate Akt phosphorylation and inhibit GSK3b-mediated tau phosphorylation, and normalize Ca^{2+} homeostasis (Zimmer, et al., 1998), all of which would reduce AD pathology. These beneficial effects may be attributable to S100A1 interaction with the Hsp70/Hsp90 multichaperone complex (Okada, et al., 2004), ryanodine receptor(Prosser, et al., 2008) SERCA pump (Green, et al., 2008; Vangheluwe, et al., 2005), tau (Baudier, et al., 1982), tubulin (Garbuglia, et al., 1999; Zimmer, et al., 1998) and/or p53 (Garbuglia, et al., 1999; van Dieck, et al., 2009).

Extracellular S100A1 could act in four ways: inhibition of S100A1-mediated cell death, autocrine/paracrine effects on surrounding cells, direct uptake into cells and subsequent modulation of intracellular events, and/or direct modulation of plaque deposition. Aβ exists as many distinct assemblies including monomers, low to high molecule weight oligomers, amyloid pores, protofibrils, and dense-core amyloid plaques (Glabe, 2008). Extracellular S100A1 could promote fibril assembly by increasing the local concentrations of Ca^{2+} and/or other metals which predispose protofibrils to aggregation and fibril formation (Cherny, et al., 2001; Isaacs, et al., 2006; Opazo, et al., 2003). S100 proteins are substrates for the cross-linking transglutaminases (Ruse, et al., 2001), which initiate Aβ oligomerization/aggregation, reduce clearance, and form assemblies responsible for cognitive loss (Atwood, et al., 2002; Hartley, et al., 2008). This interaction/modification may be one mechanism by which S100s enhance plaque deposition, decrease plaque clearance, and are retained in plaques. Alternatively, extracellular S100A1 could promote plaque deposition via interaction with and regulation of one or more plaque associated proteins (Aβ peptides, ApoE, LDL receptor

related protein, proteoglycans, inflammatory molecules, serum-related molecules, proteases, and/or antioxidant defense proteins) (Costa, et al., 2004; Dolev and Michaelson, 2004; Eriksson, et al., 1995; Fraser, et al., 1993; Kinghorn, et al., 2006). S100s may also act by increasing Aβ transcytosis from the serum and/or decreasing Aβ clearance via interaction with RAGE, a member of the immunoglobulin-like cell surface receptor superfamily expressed on endothelial cells, neurons, and glia (Deane and Zlokovic, 2007; Hofmann, et al., 1999; Perrone, et al., 2008; Takeuchi and Yamagishi, 2008; Yan, et al., 1996; Yan, et al., 2009). RAGE is a multiligand receptor that binds members of the S100 family (Hofmann, et al., 1999; Perrone, et al., 2008) as well as Aβ (Takeuchi and Yamagishi, 2008). Thus, paracrine/autocrine activation of RAGE receptor, by extracellular S100A1, could activate intracellular signaling pathways that ultimately result in increased Aβ levels. The development of effective pharmacological strategies for inhibiting S100A1 in patients will require quantifying the contribution of extracellular and intracellular forms of S100A1 as well as *in vivo* verification of the target proteins involved.

This is also the first report of *in vivo* synergism among S100 family members. Six month old PSAPP/S100A1$^{-/-}$/S100B$^{-/-}$ exhibited synergistic reductions in plaque load/number, astrocytosis and microgliosis when compared to PSAPP/S100A1$^{-/-}$ (this study) and PSAPP/S100B$^{-/-}$ (Roltsch, et al., 2010) suggesting that these two S100 family members regulate different target proteins/cellular processes. These results were expected because these two family members are expressed in different cell types; S100A1 is expressed primarily in neurons and S100B is expressed in glia/microglia.

Interestingly, these synergistic effects were age-, region- and endpoint-specific. This dynamic synergy may reflect changes in S100A1 and/or S100B levels, anatomical distribution, intracellular/extracellular ratios and/or subcellular distribution. Regardless of mechanism, these findings confirm the partial functional/mechanistic redundancy among family members and observed in *in vitro* systems.

Conclusions

Collectively, these data demonstrate that S100A1 ablation reduces plaque load, astrocytosis and microgliosis. The development of effective pharmacological strategies for modulating S100A1 function in patients will require quantifying the effects of S100A1 on cognitive function, delineating the contribution of extracellular vs. intracellular forms, identifying the S100A1-regulated target proteins/cellular processes in AD, and determining if changes in S100A1 expression/distribution are associated with particular stages/types of AD. Since the synergistic effects of ablating S100A1 and S100B are not universal, the effects of inhibiting multiple family members must be systematically investigated. Finally, the beneficial effects of S100A1 ablation/inhibition may extend to other neurological disorders that involve dysregulation of neuronal cell Ca^{2+} homeostasis and/or inflammation.

CHAPTER IV

PSAPP MICE EXHIBIT REDUCTIONS IN PLAQUE LOAD AND GLIOSIS IN RESPONSE TO S100A1/S100B INHIBITION WITH PASSIVE IMMUNOTHERAPY

Background

In the past decade, immunotherapy has emerged as a potential therapy for the treatment of AD (Citron, 2010; Delrieu, et al., 2011; Grill and Cummings, 2010; Solomon and Frenkel, 2010). There are two possible strategies for treatment, active and passive immunotherapy. Active immunotherapy is the administration of an antigen that stimulates an individual's immune system to develop an adaptive immunity to the disease, allowing the body to destroy that specific antigen. Passive immunotherapy is the administration of antigen specific antibodies that bind to extracellular forms of their antigen, rendering the antigen unable to interact with surrounding targets. Since the prevailing theory of AD etiology and pathogenesis is the amyloid cascade hypothesis (Hardy and Allsop, 1991; Hardy and Higgins, 1992; Karran, et al., 2011), Aβ targeted therapies have dominated the field of active and passive immunotherapy (Morgan, 2011).

Early strategies for AD immunotherapy employed active immunotherapy. In 1999, the first Aβ immunotherapy was published by Schenk and his collaborators at Elan Pharmaceuticals in which they reported that treatment of an AD mouse model with a vaccine against Aβ prior to plaque formation was sufficient to block plaque formation as the mice aged (Morgan, 2011). Since then, the development of novel immunotherapy

strategies has been a major focus of AD research. Several studies reported that treatment with an Aβ vaccine not only cleared Aβ plaques, but also improved the cognitive deficit exhibited in both murine and non-human primate models of AD (Janus, et al., 2000; Kotilinek, et al., 2002; Lemere, et al., 2004; Morgan, 2011). While studies of immunotherapy in animal models exhibited remarkable success and provided very promising results (Morgan, 2011), immunotherapy in human clinical trials resulted in a number of adverse side effects (Delrieu, et al., 2011). Although initial phase I trials with a vaccine against the full length $A\beta_{42}$ peptide produced no adverse results (Schenk, 2002), a phase IIa trial with the vaccine was stopped prematurely after a subset (6%) of patients developed aseptic meningoencephalitis, an inflammation of the brain and meninges (Orgogozo, et al., 2003). Upon further investigation, it was reported that $A\beta_{42}$ contains an epitope capable of activating T cells (Delrieu, et al., 2011; Monsonego and Weiner, 2003) and it was concluded that the meningoencephalitis response was an autoimmune reaction caused by the vaccine (Morgan, 2011; Orgogozo, et al., 2003). Although the study was interrupted, some patients did develop a significant antibody titer with no adverse effects, and the cognitive evaluations indicated less of a decline in cognition when compared to patients with no antibody titer, although these changes did not reach significance (Citron, 2010; Morgan, 2011). In spite of these adverse effects of active immunization, the cognitive results suggest that an immunotherapy approach may be effect in treating AD (Morgan, 2011).

Due to the adverse effects of active immunization, several companies have turned to passive immunotherapy. In another phase II trial, passive immunotherapy with

bapineuzumab, a humanized Aβ antibody, resulted in 9.7% of patients developing vasogenic edema (Salloway, et al., 2009). Vasogenic edema is caused by fluid leakage of the brain's blood vessels into the parenchyma through a damaged blood brain barrier (Delrieu, et al., 2011). Interestingly, the study reported a difference in response to the drug based on APOE ε4 carrier status, in that there was a potential treatment difference favoring bapineuzumab observed in noncarriers, while no difference was observed in APOE ε4 carriers (Salloway, et al., 2009). A phase III study is now in progress with bapineuzumab (Grill and Cummings, 2010). Currently there are five phase III trials being conducted for AD drug candidates, and three out of the five are passive immunotherapy trails utilizing a humanized monoclonal antibody to Aβ (Grill and Cummings, 2010). Although, the lack of improvement in cognition in patient participating in recent clinical trials targeting Aβ emphasizes the need for additional targets (Boutajangout, et al., 2011; Holmes, et al., 2008). Recent developments have also identified methods for earlier detection of AD, raising the possibility of early disease state and/or preventative treatments (Morgan, 2011).

As demonstrated in the previous studies, S100A1/S100B ablation resulted in reductions of AD pathology in PSAPP mice (Chapters II and III) (Roltsch, et al., 2010). In addition to S100B's increased expression in AD (Chaves, et al., 2010; Marshak, et al., 1992; Roltsch, et al., 2010; Van Eldik and Griffin, 1994), numerous studies have reported that S100B regulates APP expression/processing, tau hyperphosphorylation and Aβ biogenesis, as well as being regulated by Aβ (Anderson, et al., 2009; Chow, et al., 2010; Esposito, et al., 2008; Mori, et al., 2010). Furthermore, S100A1 ablation in PC 12

cells results in an increased resistance to Aβ-induced cell death, stabilization of intracellular Ca^{2+} levels and a down-regulation of APP expression (Zimmer, et al., 2005).

These data validate S100A1 and S100B as novel drug targets for AD. Because genetic ablation is not possible in the treatment of human diseases, this study uses passive immunotherapy to inhibit S100A1/S100B function in PSAPP mice. Mice treated with anti-S100 from 3-6 months of age exhibited reductions in cortical and hippocampal plaque load as well as cortical astrocytosis. In contrast, mice treated with anti-S100 from 6-9 months of age exhibited reductions in cortical, but not hippocampal, plaque load as well as cortical and hippocampal astrocytosis. These results suggest that S100A1 and S100B act via different mechanisms in young mice. In summary, this is the first report that pharmacological inhibition of S100A1/S100B is sufficient to reduce AD histopathology and that immunotherapy strategies which block S100A1/S100B function may be effective in treating AD in patients.

Methods

PSAPP mice. The PSAPP double transgenic line was generated by crossing the Tg2576 line ("Swedish" APPK670N/M671L mutation) with the 6.2 line (PS-1M146L) (Gordon, et al., 2001; Gordon, et al., 2002; Holcomb, et al., 1998; Holcomb, et al., 1999). Genotyping was performed as previously described (Gordon, et al., 2001). All procedures involving animals were approved by the Texas A&M University Institutional Animal Care and Use Committee and comply with the *NIH Guide for the Care and Use of Laboratory Animals*.

Chronic immunotherapy treatment. Cohorts of three and six month old PSAPP mice received bi-weekly 300µL intraperitoneal injections of a proprietary S100A1/S100B antibody made to the linker region of S100A1/S100B (Bethyl Laboratory Inc., Montgomery, TX), because the linker region exhibits the highest level of divergence, or IgG control (Bethyl Laboratory Inc.) at 1mg/mL for three months (6 injections total). Animals were sacrificed two weeks following the 12th injection (Figure 19).

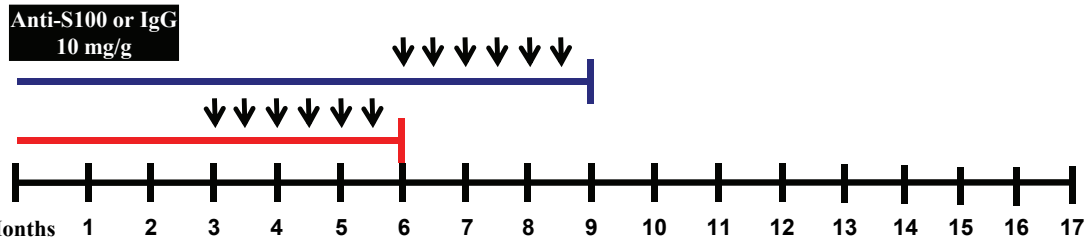

Figure 19: Timeline for anti-S100 immunotherapy treatment. Depicted above is the injection schedule for anti-S100 therapy for each treatment/age group. Red line denotes three month old treatment group and blue line denotes six month old treatment group. Black arrows denote one 300µL injection of either anti-S100 or control IgG. All animals received 6 bi-weekly injections and were sacrificed two weeks after the last injection.

Sample acquisition/processing. Brains were removed from anesthetized animals, rinsed in phosphate buffered saline (PBS) and sliced sagittally along the midline using an acrylic brain matrix (Ted Pella, Redding, CA). One hemisphere was microdissected, removing the hippocampus (HP), cerebellum (CR), olfactory bulb (OLF), and slicing the cortex into two pieces, somatomotor (CX1) and visual (CX2), and snap frozen on dry ice. The remaining hemisphere was fixed as previously described (Roltsch, et al., 2010). Briefly, brains were rinsed in phosphate buffered saline (PBS), fixed in 4% (wt/vol) paraformaldehyde in PBS for 30 minutes and sliced into 2 mm sagittal sections. After a

second 30 minute fixation in 4% (wt/vol) paraformaldehyde in PBS, slices were permeablized and post-fixed in 10% buffered formalin for 16 hours. Five micron sagittal sections of paraffin embedded sections were mounted on glass slides for subsequent staining.

Immunofluorescent and Thioflavin S staining. To minimize variability, sections from experimental and control groups were processed for plaque load and immunoreactivity together. Consecutive slides (2/animal) each containing sections at Allen Brain Atlas Sagittal Levels 8 and 17 were depariffinized and rehydrated to distilled water. Thioflavin S was used to label fibrillar plaques, and slides were incubated in 0.5% (wt/vol) Thioflavin S (T1892, Sigma, St. Louis, MO) in 50% ethanol for 10 minutes followed by two 3 minute washes in 50% ethanol. Slides will then be washed twice in distilled water for three minutes each and mounted with ProLong Gold antifade reagent with DAPI (P36935, Molecular Probes, Inc., Eugene, OR). Immunostaining was performed on a DAKO autostainer (Dako, Carpentaria, CA) using a species specific AP polymer detection kit with the Warp Red chromogen kit (Warp Red, Biocare Medical, Walnut Creek, CA), which is highly fluorescent and visualized under a Texas Red filter, with conditions recommended by the primary antibody manufacturer. Primary antibodies for immunohistochemistry included a rabbit polyclonal GFAP antibody (1-1000 dilution of Z0334, Dako).

For quantification, digital images were captured, converted to gray scale, and positive pixels and total plaque load were quantified using Image J software (NIH Image, Bethesda, MD). Plaque load and immunoreactivity were defined as the % area,

i.e. the area of positive pixels/total pixels X 100. The data were expressed as the mean ± SEM (n=4 for 3 and 6 month old Anti-S100 treated and n=3 for 3 and 6 month old IgG treated PSAPP mice). An independent samples t-test (JMP by SAS, Cary, NC) was used to determine the significance ($p<0.05$) of measured differences between each of the treatment groups. The Orthogonal Regression Correlation and scatter plots of the mean hippocampal and cortical GFAP staining/animal versus plaque load were used to determine the relationship between plaque load and astrocytosis/microgliosis.

Results

Anti-S100 therapy selectively reduces cortical and hippocampal plaque load in PSAPP mice. To determine if anti-S100 therapy altered amyloidogenesis, plaque load was quantified in PSAPP mice treated with anti-S100 or IgG antibodies. Thioflavin S positive plaques were observed in the cortex of six month old PSAPP mice treated with anti-S100 and IgG from three to six months of age (Figure 20). Passive S100 immunotherapy in 3-6 month old PSAPP mice resulted in a 4.4-fold reduction in cortical plaque load (0.0463 ± 0.0059 vs. 0.2050 ± 0.0413 percent area) with anti-S100 treatment. In addition, a 1.5-fold reduction in hippocampal plaque load (0.0560 ± 0.0112 vs. 0.0862 ± 0.0082 percent area) was exhibited when anti-S100 and IgG treated PSAPP mice were compared.

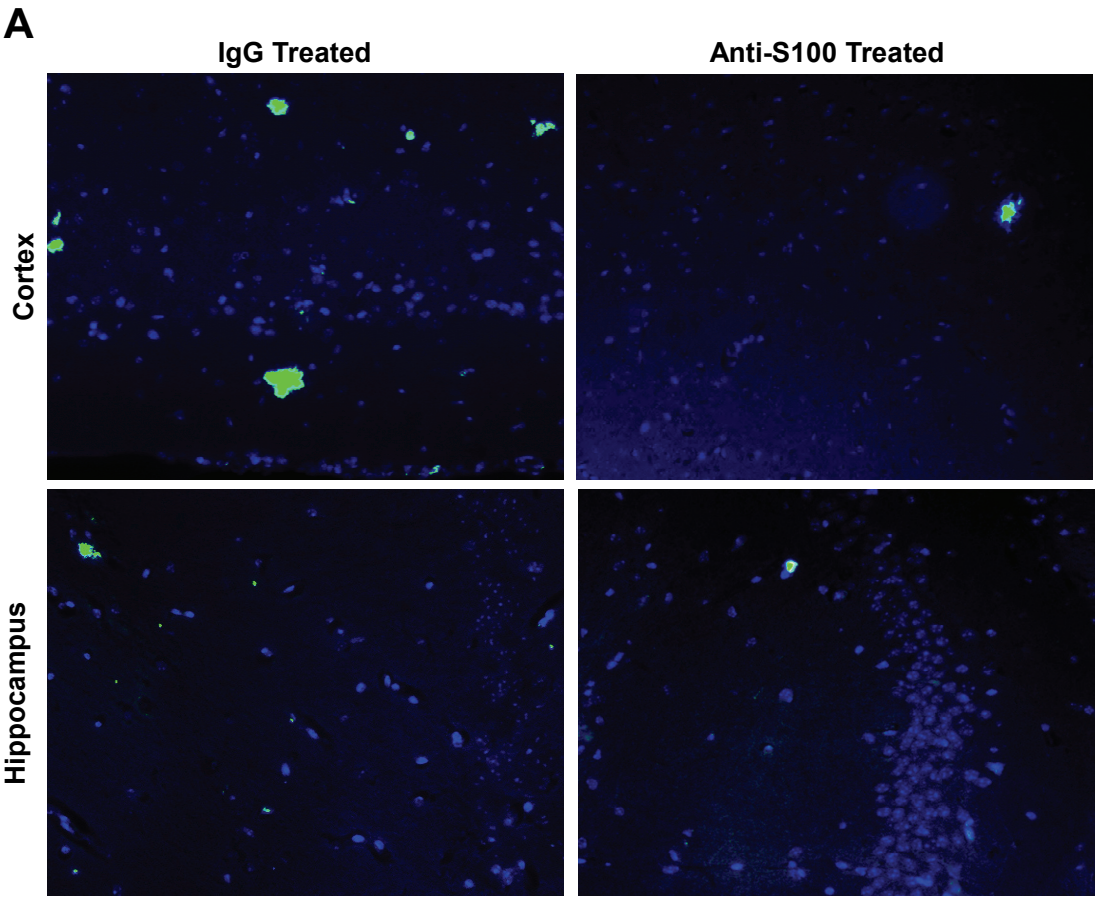

Figure 20: Anti-S100 therapy reduces cortical and hippocampal plaque load with treatment at 3-6 months of age. Panel A contains representative micrographs of parasagittal cortical/hippocampal sections from 6 month old PSAPP mice treated with Anti-S100 and IgG from ages 3-6 months stained with Thioflavin S (green) and DAPI (blue) to visualize plaques and nuclei, respectively. The histogram depicts the mean plaque load ± SEM (Panel B) in PSAPP mice treated with Anti-S100 (hatched bars, n=4), and control IgG (solid bars, n=3). Asterisks denote $p \leq 0.05$ when compared to the control group.

To determine if passive S100 immunotherapy reduces plaque load at a later stage of plaque deposition, plaque load was quantified in mice treated with anti-S100 or IgG from six to nine months of age. As in the younger mice, Thioflavin S positive plaques

were observed in the cortex of both groups (Figure 21). Passive S100 immunotherapy resulted in a 2.5-fold reduction in cortical plaque load (0.3894 ± 0.0720 vs. 0.9795 ± 0.1804 percent area) when anti-S100 is compared to IgG. Interestingly,

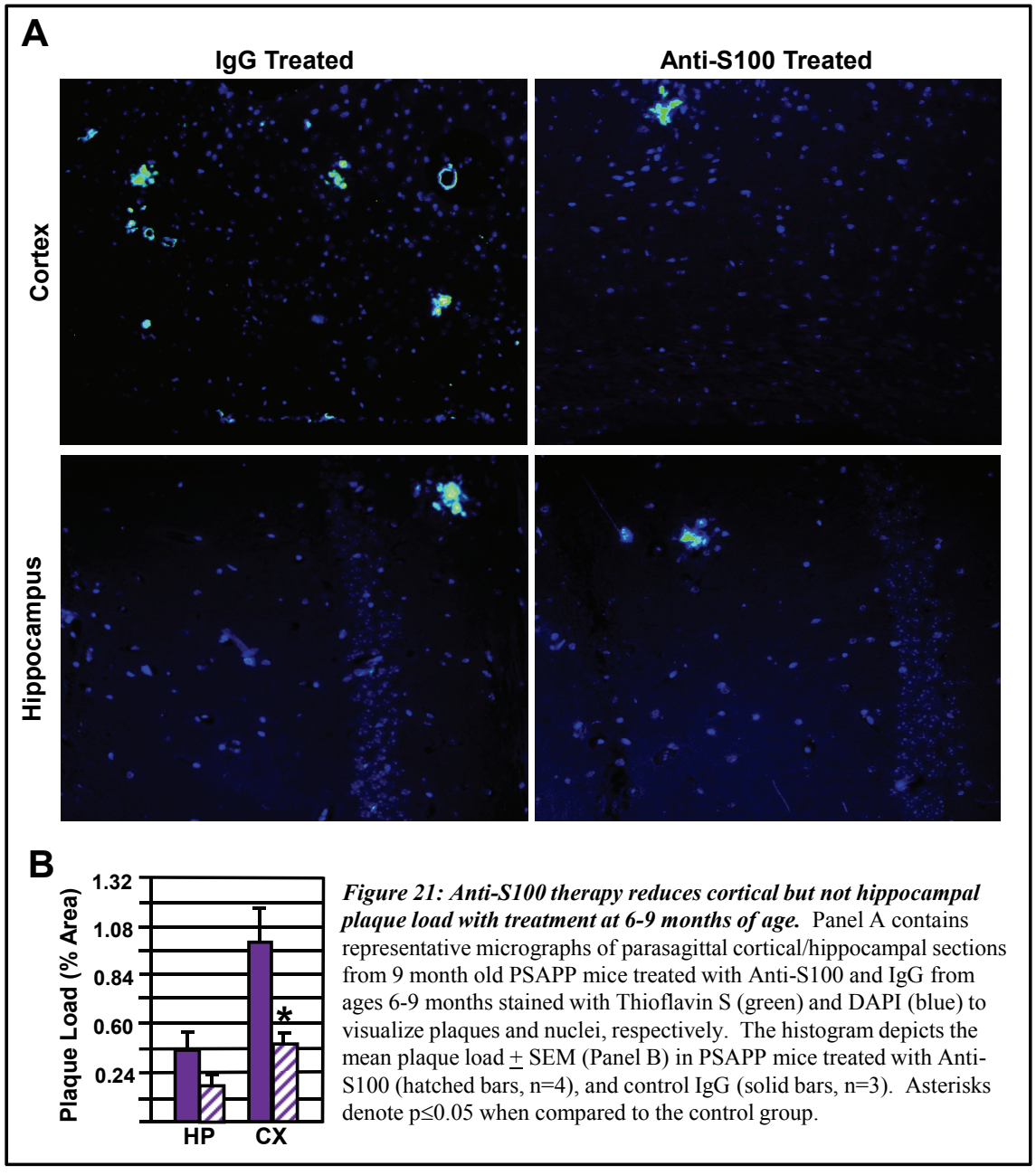

Figure 21: Anti-S100 therapy reduces cortical but not hippocampal plaque load with treatment at 6-9 months of age. Panel A contains representative micrographs of parasagittal cortical/hippocampal sections from 9 month old PSAPP mice treated with Anti-S100 and IgG from ages 6-9 months stained with Thioflavin S (green) and DAPI (blue) to visualize plaques and nuclei, respectively. The histogram depicts the mean plaque load ± SEM (Panel B) in PSAPP mice treated with Anti-S100 (hatched bars, n=4), and control IgG (solid bars, n=3). Asterisks denote $p \leq 0.05$ when compared to the control group.

there was no change in hippocampal plaque load (0.1748 ± 0.0469 vs. 0.3551 ± 0.1567 percent area) when anti-S100 is compared to IgG (Figure 21B). Thus, passive S100 immunotherapy selectively reduces plaque load in PSAPP mice.

Anti-S100 therapy selectively reduces astrocytosis in PSAPP mice. Astrocytosis is an early and critical event in AD pathogenesis (Eikelenboom, et al., 2010; Heneka, et al., 2010; Lee, et al., 2010; Li, et al., 2011). The astrocytic marker GFAP was used to

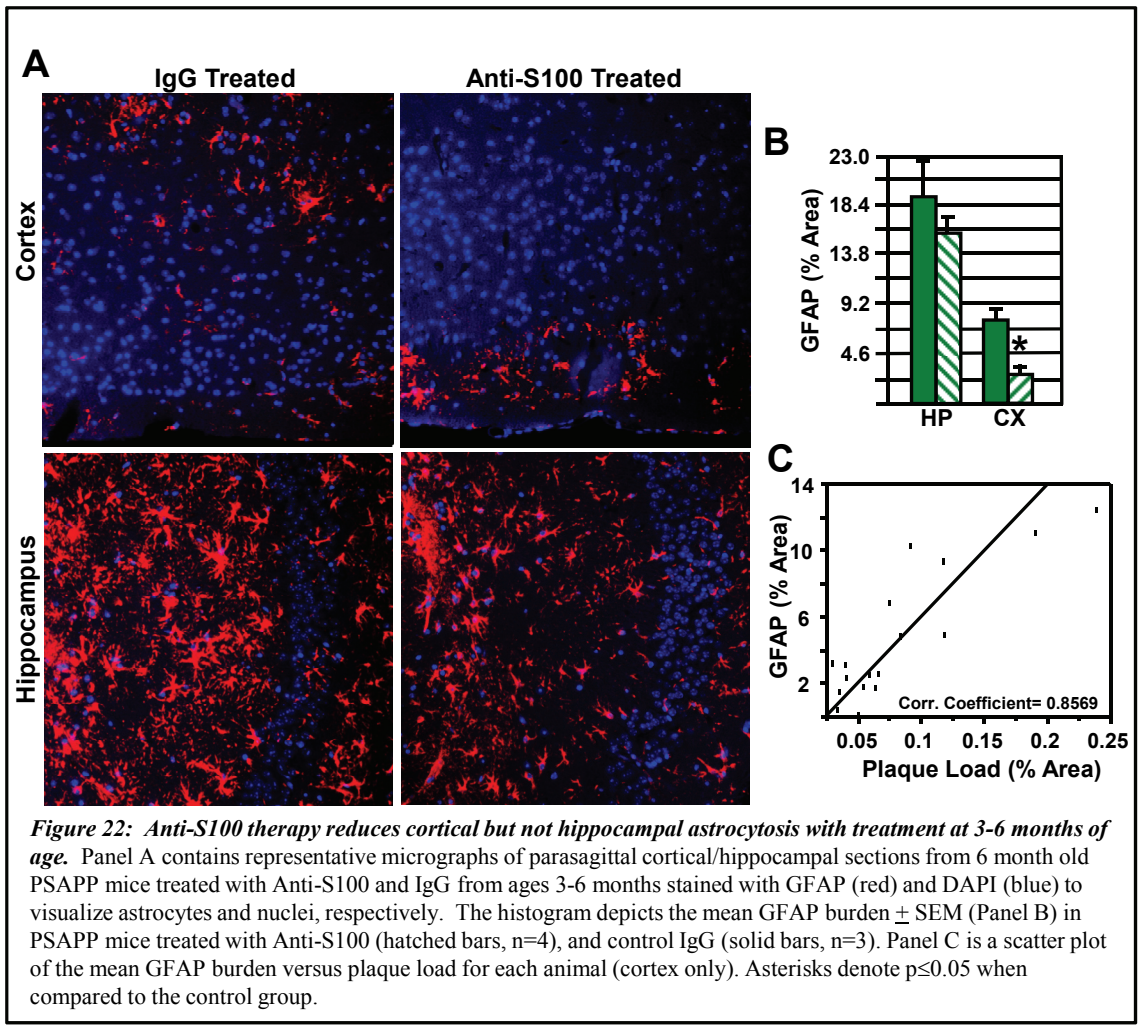

Figure 22: Anti-S100 therapy reduces cortical but not hippocampal astrocytosis with treatment at 3-6 months of age. Panel A contains representative micrographs of parasagittal cortical/hippocampal sections from 6 month old PSAPP mice treated with Anti-S100 and IgG from ages 3-6 months stained with GFAP (red) and DAPI (blue) to visualize astrocytes and nuclei, respectively. The histogram depicts the mean GFAP burden ± SEM (Panel B) in PSAPP mice treated with Anti-S100 (hatched bars, n=4), and control IgG (solid bars, n=3). Panel C is a scatter plot of the mean GFAP burden versus plaque load for each animal (cortex only). Asterisks denote $p \leq 0.05$ when compared to the control group.

determine if plaque reduction in response to passive S100 immunotherapy was accompanied by a decrease in astrocytosis. Hippocampal and cortical GFAP positive astrocytes were observed in all ages of PSAPP mice from both treatment groups. The GFAP staining was associated with cell bodies as well as long processes (Figure 22) and this pattern was indistinguishable from previous reports for AD models ((Mori, et al., 2006; Mori, et al., 2010; Roltsch, et al., 2010). Furthermore, passive S100 immunotherapy in 3-6 month old PSAPP mice resulted in no change in hippocampal

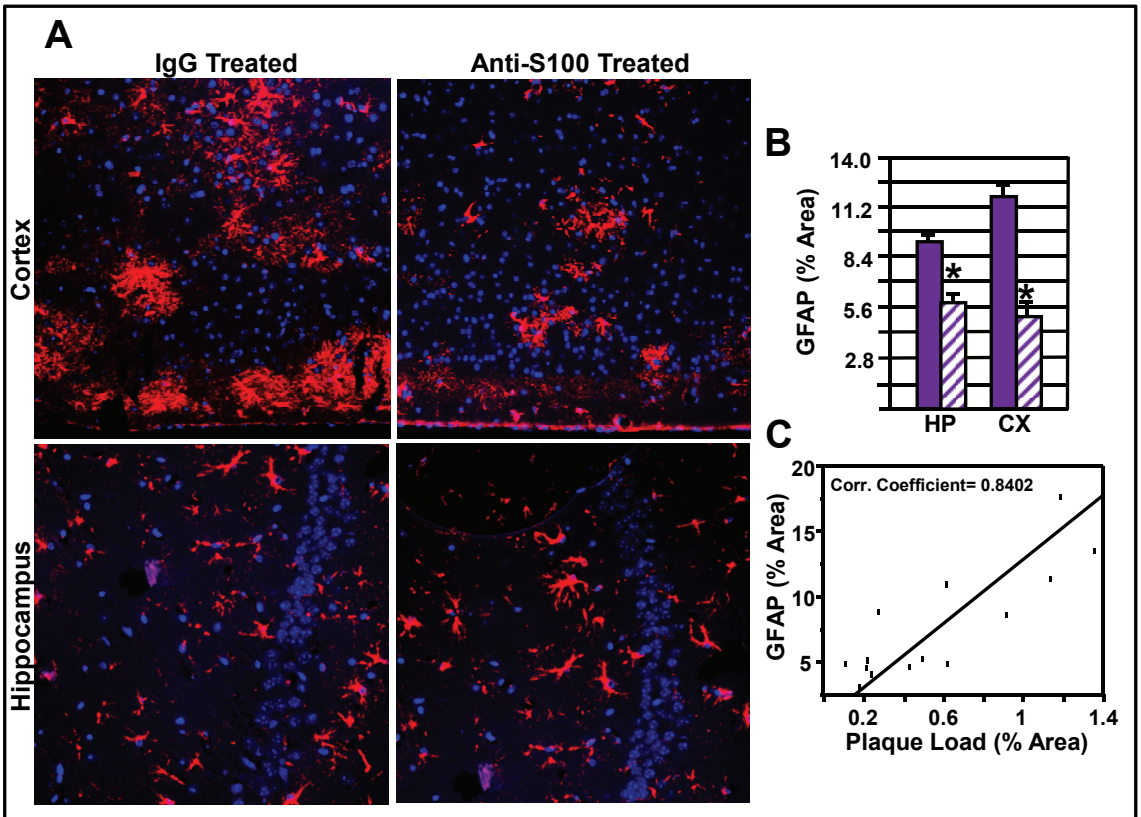

Figure 23: Anti-S100 therapy reduces cortical and hippocampal astrocytosis with treatment at 6-9 months of age. Panel A contains representative micrographs of parasagittal cortical/hippocampal sections from 9 month old PSAPP mice treated with Anti-S100 and IgG from ages 6-9 months stained with GFAP (red) and DAPI (blue) to visualize astrocytes and nuclei, respectively. The histogram depicts the mean GFAP burden ± SEM (Panel B) in PSAPP mice treated with Anti-S100 (hatched bars, n=4), and control IgG (solid bars, n=3). Panel C is a scatter plot of the mean GFAP burden versus plaque load for each animal (cortex and hippocampus). Asterisks denote $p \leq 0.05$ when compared to the control group.

GFAP staining (15.2834 ± 1.9726 vs. 18.9145 ± 3.6069 percent area) when anti-S100 and IgG treated PSAPP mice were compared. In contrast, immunotherapy resulted in a 3.2-fold decrease in cortical GFAP staining (2.2877 ± 0.3881 vs. 7.3870 ± 1.1862 percent area) when anti-S100- and IgG- treated groups were compared. On the other hand, cortical and hippocampal decreases in astrocytosis were observed in PSAPP mice treated with passive S100 immunotherapy from 6-9 months of age. GFAP staining in PSAPP mice was 2.3-fold less in the cortex (5.3442 ± 0.5948 vs. 12.1864 ± 1.5217 percent area) and 1.8-fold less in the hippocampus (5.6562 ± 0.4907 vs. 9.9885 ± 0.6686 percent area) when anti-S100- and IgG- treated groups were compared (Figure 23). Furthermore, in 3-6 and 6-9 month old mice there was a direct correlation between cortical GFAP staining and plaque load (Pearson's Correlation Coefficient 0.8569 and 0.8402 respectively, $p < 0.0005$) (Figure 22C and 23C). Together these results demonstrate that decreased plaque load in response to passive S100 immunotherapy is accompanied by a regionally and temporally selective reduction in astrocytosis.

Discussion

This study definitively demonstrates that passive S100 immunotherapy reduces AD pathology. In fact, PSAPP mice treated with anti-S100 from 3-6 months of age exhibited decreases in plaque load and cortical astrocytosis, while PSAPP mice treated with anti-S100 from 6-9 months of age exhibited reduced cortical, but not hippocampal plaque load with decreases in both cortical and hippocampal astrocytosis. Furthermore, S100 ablation/inhibition has been reported to alter cognitive function in normal animals

(Ackermann, et al., 2006; Kubista, et al., 1999; O'Dowd, et al., 1997) suggesting that S100 ablation/inhibition in AD will impact cognitive function.

It is important to point out that passive S100 immunotherapy results statistically equivalent decrease in cortical but not hippocampal plaque load when anti-S100 treatment from 3-6 month of age is compared to S100A1/S100B ablation at six months of age in PSAPP mice. These differences are not attributable to effects from injection in that control IgG treatment does not increase cortical or hippocampal plaque load. In addition, S100 immunotherapy also results in a statistically equivalent decrease in cortical GFAP staining when anti-S100 in 3-6 month is compared to S100A1/S100B ablation in 6 month old PSAPP mice. The discrepancies between S100 ablation and immunotherapy as well as in regional efficacy suggest that S100A1 and S100B act via dynamic mechanisms in AD.

This is the first report that passive S100 immunotherapy selectively reduces AD pathology. As described in previous studies, S100A1 and S100B are plaque associated proteins in AD mouse models as well as human autopsy tissues (Figures 11 and 13) (Marshak, et al., 1992; Roltsch, et al., 2010; Van Eldik and Griffin, 1994; Van Eldik and Wainwright, 2003). Given that common targets for immunotherapy in AD studies are plaque associated proteins, S100A1 and S100B represent two novel targets for immunotherapy treatment. Collectively, these results suggest that passive S100 immunotherapy combined with other approaches of S100 inhibition, such as small molecules, will effectively delay the progression of AD pathology.

Conclusions

Collectively, these data definitively demonstrate that passive S100A1/S100B immunotherapy is reduces plaque load and astrocytosis in a regionally and temporally selective manner. This study was the second approach that verifies the beneficial effects of S100A1/S100B inhibition. Additional work is needed to determine if this reduction in histopathology will also decrease cognitive impairment exhibited in AD patients. The inhibition of S100A1/S100B represent a novel treatment for AD and continued study of S100A1/S100B targets and mechanisms of action will aid in the development of effective therapeutic strategies for inhibiting S100A1/S100B function in AD treatment as well as other neurological disorders involving Ca^{2+} dysregulation.

CHAPTER V

MiRNA EXPRESSION IS ALTERED IN RESPONSE TO S100A1/S100B MEDIATED REVERSAL OF AD PATHOLOGY

Background

Several neurodegenerative disorders are characterized by miRNA dysregulation, such as frontotemporal dementia, prion diseases, Parkinson's disease, Huntington's disease and Alzheimer's disease (Enciu, et al., 2011; Fiore, et al., 2011; Hebert and De Strooper, 2007; 2009; Lau and de Strooper, 2010; Saugstad, 2010; Sonntag, 2010). MicroRNAs (miRNAs) are a family of small (~21-25 nucleotides) noncoding RNAs that can regulate gene expression at the post-transcriptional level (He and Hannon, 2004). There are currently 1424 human miRNAs and their sequences can be found on miR-Base website (http://www.mirbase.org/cgi-bin/mirna_summary.pl?org=hsa). Most miRNAs are encoded within their own genes and clustered throughout the genome but a subset are encoded for within the introns of pre-mRNAs (Bartel, 2004). Primary miRNA transcripts (pri-miRNAs) can be several thousand base pairs in length and are transcribed by RNA polymerase II or III in the nucleus (Lee, et al., 2004; Winter, et al., 2009). The pri-miRNA is then cleaved by the Drosha-DGCR8 complex and the precursor miRNA (pre-miRNA) is released, which is characterized by a stem and loop structure that is ~70 nucleotides in length. The pre-miRNA is then exported to the cytoplasm by Exportin-5/Ran-GTP and cleaved by Dicer to generate the mature miRNA (Lau and de Strooper, 2010; Winter, et al., 2009). Mature miRNAs function by

recognizing a specific sequence in an mRNA, called the seed region, binding to the mRNA and either triggering degradation or translational repression (Bartel, 2004; He and Hannon, 2004; Lim, et al., 2005). Although mRNAs can, in principle, contain the miRNA "seed region" along their complete length, the most common site is within the 3' untranslated region (UTR) (Ketting, 2010). Recently, studies have indicated the involvement of deregulated miRNA expression in the pathogenesis of AD (Satoh, 2010).

Most studies addressing the role of miRNAs in AD have focused on APP and BACE1 as targets of miRNAs (Delay and Hebert, 2011; Lau and de Strooper, 2010). Recent studies have shown that miR-107, -29a, -29b, -298 and -328 all target BACE1 and miR-17-5p, -20a, -106a, -106b, -520c, -101, -16 and Let-7 all target APP of which miR-107, and miR-29b have been reported as dysregulated in AD (Delay and Hebert, 2011; Hebert, et al., 2008; Lau and de Strooper, 2010; Wang, et al., 2008). Several recent studies have been conducted using post-mortem brain tissues from AD patients and age-matched controls. These studies have shown that a total of 22 miRNAs are dysregulated in the hippocampus, 67 miRNAs are dysregulated in the cortex, and 13 miRNAs are dysregulated in the cerebellum of AD patients (Satoh, 2010). Unfortunately, the majority of these studies are human profiling studies and correlative in nature, they provide little proof of target gene regulation *in vivo* so the AD mouse models will provide a great tool for further dissecting the role of miRNA dysregulation in AD (Delay and Hebert, 2011).

Interestingly, miRNAs have also been implicated in S100 signaling and S100 protein expression (Baudry, et al., 2010; Maru, et al., 2009; Shanmugam, et al., 2008).

Recent studies have shown that S100B binding to the RAGE receptor increases Cyclooxygenase-2 (COX-2) expression and stabilizes COX-2 mRNA (Shanmugam, et al., 2003). Moreover, continued studies demonstrated that S100B significantly decreases miR-16 expression in monocytes which, in turn, blocks the degradation of the inflammatory gene product, COX-2 mRNA (Shanmugam, et al., 2008). Additionally, S100A9 has been shown as a target for miR-196a in the progression of esophageal cancer (Maru, et al., 2009). Together these data suggest that miRNAs are involve in S100 signaling/expression.

In the previous chapters, we have shown that pharmacological inhibition and ablation of S100A1 and/or S100B significantly reduces AD pathology in the PSAPP mouse (Roltsch, et al., 2010). This study examines the role of miRNAs in S100-mediated reversal of pathology. The expression of 15 miRNAs was altered in the hippocampus of 3 month old PSAPP mice. The expression of 14 out of the 15 altered miRNAs was normalized in response to S100A1/S100B ablation in the PSAPP mice. These results suggest that miRNAs are involved in S100A1/S100B contributions to AD pathology and that these miRNAs may be novel therapeutic targets for effectively treating AD.

Methods

PSAPP X S100 knockout mice. The PSAPP double transgenic line was generated by crossing the Tg2576 line ("Swedish" $APP_{K670N/M671L}$ mutation) with the 6.2 line ($PS\text{-}1_{M146L}$) (Gordon, et al., 2001; Gordon, et al., 2002; Holcomb, et al., 1998; Holcomb, et al., 1999). The PSAPP/$S100A1^{-/-}$/$S100B^{-/-}$ line was generated by crossing PSAPP

double transgenic males with S100A1$^{-/-}$/S100B$^{-/-}$ knockout females and subsequent interbreeding of the heterozygous offspring (PSAPP/S100A1$^{+/-}$/S100B$^{+/-}$ X PSAPP/S100A1$^{+/-}$/S100B$^{+/-)}$. To control for genetic background, all experiments used PSAPP/S100A1$^{+/+}$/S100B$^{+/+}$ and PSAPP/S100A1$^{-/-}$/S100B$^{-/-}$littermates. Genotyping was performed as previously described (Gordon, et al., 2001; Prosser, et al., 2008; Roltsch, et al., 2010). All procedures involving animals were approved by the Texas A&M University Institutional Animal Care and Use Committee and comply with the *NIH Guide for the Care and Use of Laboratory Animals*.

MiRNA profiling. Total RNA was isolated from snap frozen hippocampal tissue of PSAPP, PSAPP double knockout and nontransgenic control mice using the MirVana miRNA Isolation Kit (AM1560, Ambion, Foster City, CA). MiRNA expression profiling was performed by Exiqon (Woburn, MA). After quality verification, control and experimental total RNAs will be labeled with Cy3 and Cy5 respectively, hybridized to miRCURY ™ LNA microRNAs, and the data analyzed using the manufacturers protocol.

Post-array validation. MiRNAs that exhibited greatest statistically significant changes in expression were subjected to post-array validation using RT-PCR. RT reactions were performed using the miRCURY LNA ™ Universal RT microRNA PCR Universal cDNA Synthesis kit (Exiqon) and the transcribed cDNA was then used for subsequent PCR amplification. The SYBR Green Universal Master Mix (Exiqon) and miRCURY LNA ™ Universal PCR Primer sets were utilized and reactions run on a MyiQ RT-PCR Detection System (Bio-Rad Laboratory, Hercules, CA), which was optimized for

amplification of small RNAs. All reactions were performed in triplicate and relative expression normalized against endogenous controls using the comparative delta-delta CT method. An independent samples t-test (JMP, Cary, NC) was used to determine the significance of measured differences between the genotypes.

Bioinformatic searches. Each miRNA exhibiting a significant change of expression in both the microarray and post-array validation was subjected to bioinformatics searches for putative target genes (miRWalk) and biological processes (DAVID). MiRWalk is a database of predicted and validated miRNA targets. Searches performed on miRWalk use the miRWalk algorithm on the complete sequence of all know human, mouse and rat genes, as well as information from 8 other established miRNA prediction programs (RNA22, miRanda, miRDB, TargetScan, RNAhybrid, PITA, PICTAR, and Diana-microT) on the 3' UTRs of all known human, mouse and rat genes (http://www.ma.uni-heidelberg.de/apps/zmf/mirwalk/). The generated lists of target genes were then analyzed for pathway enrichment using DAVID (Database for Annotation, Visualization, and Interrogated Discovery) bioinformatics database.

Results

S100A1/S100B ablation normalizes miRNA expression. To identify miRNA's that may play a role in S100A1/S100B mediated reversal of AD pathology we first characterized the expression pattern of miRNA's in the hippocampus of three month old PSAPP, and nontransgenic control mice. The microarray analysis demonstrated that 15 miRNAs were overexpressed in the hippocampus of 3 month old PSAPP mice, including miR-206, miR-34a, miR-195, miR-133a, miR-204, miR-1, miR-10b, miR-133b, miR-

194, miR-34c, miR-192, miR-320, miR-96, miR-486 and miR-448 (Figure 24). Furthermore, all of these miRNAs exhibited overexpression in the PSAPP model.

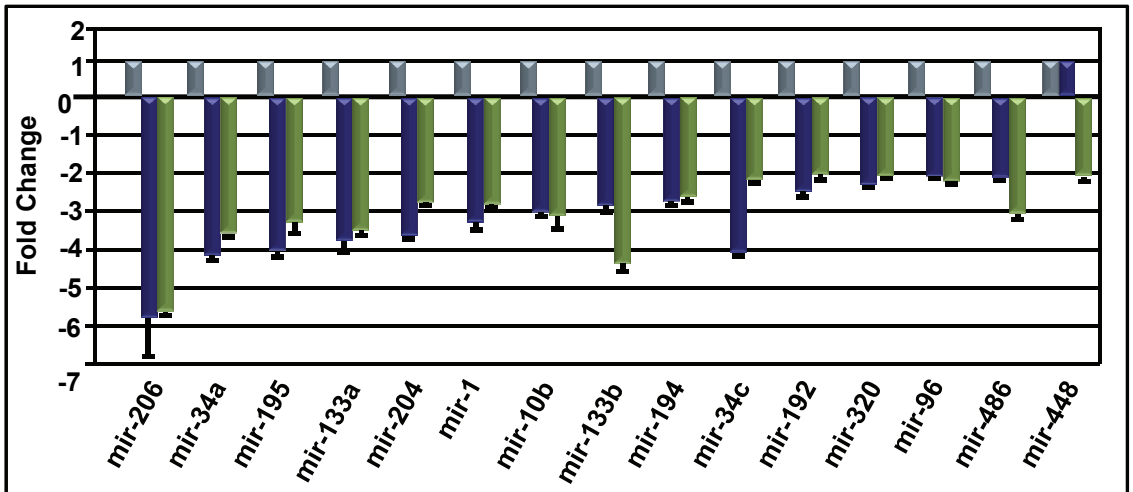

Figure 24. S100A1 and S100B ablation normalize miRNA expression profile. Histogram depicts expression of significantly dysregulated miRNAs in 3 month old hippocampus from PSAPP/S100A1$^{-/-}$/S100B$^{-/-}$ ( ) and non-transgenic ( ) when compared to PSAPP ( ). Means were corrected for nonbiological background contribution and normalized using the LOESS method. miRNAs that passed the filtering criteria (>2 fold change in expression) are expressed as the fold change $\pm$ the SD (n=3) when compared to PSAPP levels.

Additional studies were then completed to determine the miRNA expression profile in response to S100A1/S100B-mediated changes in AD pathology. The expression of 14 out of the 15 altered miRNAs in PSAPP mice were normalized in response to S100A1/S100B ablation in the hippocampus of 3 month old PSAPP mice. Further examination using qRT-PCR to validate the microarray results were confined to seven miRNAs (miR-206, miR-34a, miR-34c, miR-195, miR-133a, miR-204, miR-1 and miR-448) exhibiting the greatest decrease in expression in the PSAPP/S100A1$^{-/-}$/S100B$^{-/-}$ mice. We used miR-124 as an endogenous control to normalize expression which was uniformly expressed within each treatment and highly expressed across all treatment

groups. Five miRNAs exhibited a significant change in expression in the PSAPP/S100A1$^{-/-}$/S100B$^{-/-}$ mice when compared to PSAPP mice, miR-448, miR-133a, miR-204 and miR-206 one miR-34a (Figure 25). Interestingly, only one of the identified miRNAs (miR-34a) has been previously reported in AD (De Smaele, et al., 2010; Delay and Hebert, 2011; Provost, 2010; Satoh, 2010).

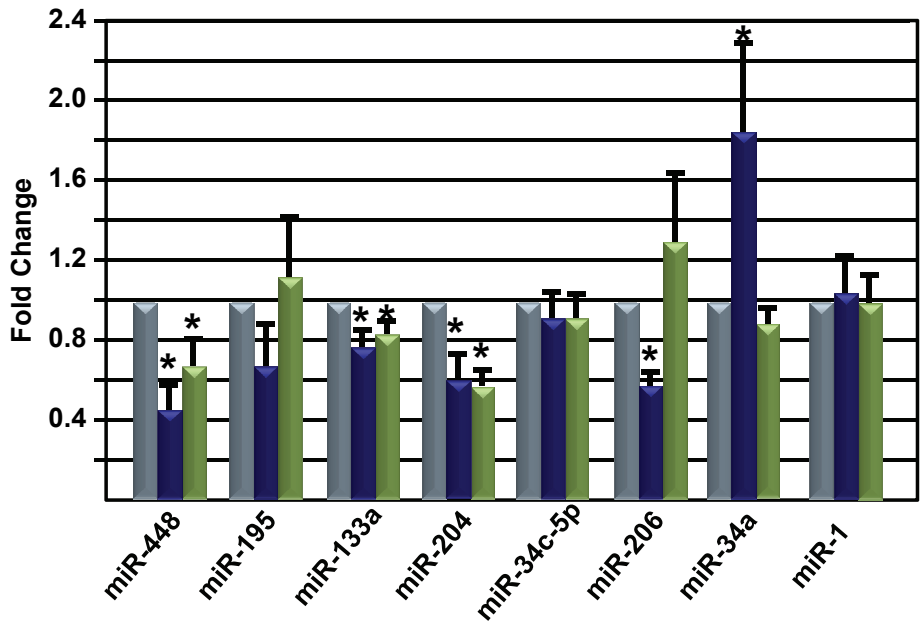

Figure 25. RT-PCR Validation of altered miRNAs. Histogram depicts fold change of miRNA expression in hippocapmus of three month old PSAPP/S100A1$^{-/-}$/S100B$^{-/-}$ (, n=6) and non-transgenic (, n=6) when compared to PSAPP (, n=9). Expression was normalized to miR-124 and expressed as fold change ± SEM relative to PSAPP levels.

Functional analysis of miRNA target genes/pathways. Since miRNAs are thought to regulate target gene expression and pathways it was important to look at the predicted target genes and pathways of the five validated miRNAs. In order to determine the

Table 4. Target and pathway predictions for miRs -448, -204, -133a and -206

miRNA	Total Targets*	Assigned Targets*	KEGG Pathway#	Number of Genes#	Percent#	P-value#	Benjamini#
448	498	5	*No significant pathways*	--	--	--	--
204	818	38	Pathways in cancer	8	21.1	7.50E-05	3.40E-03
			Pancreatic cancer	5	13.2	9.70E-05	2.20E-03
			Chronic myeloid leukemia	5	13.2	1.10E-04	1.70E-03
			Bladder cancer	4	10.5	3.90E-04	4.40E-03
			Colorectal cancer	4	10.5	3.00E-03	2.60E-02
			Prostate cancer	4	10.5	3.50E-03	2.60E-02
133a	418	133	Pathways in cancer	16	15.4	2.10E-07	2.10E-05
			Colorectal cancer	8	7.7	1.30E-05	6.40E-04
			MAPK signaling pathway	10	9.6	8.50E-04	2.80E-02
			TGF-beta signaling pathway	6	5.8	1.40E-03	3.40E-02
			Endometrial cancer	5	4.8	1.50E-03	2.90E-02
			Prostate cancer	6	5.8	1.50E-03	2.50E-02
			Acute myeloid leukemia	5	4.8	2.20E-03	3.10E-02
			Focal adhesion	8	7.7	2.80E-03	3.50E-02
206	567	126	Pancreatic cancer	9	9.8	1.80E-07	1.60E-05
			Pathways in cancer	15	16.3	5.90E-07	2.50E-05
			MAPK signaling pathway	12	13	1.80E-05	5.00E-04
			Focal adhesion	10	10.9	6.10E-05	1.30E-03
			Colorectal cancer	7	7.6	9.40E-05	1.60E-03
			Amyotrophic lateral sclerosis (ALS)	6	6.5	1.00E-04	1.40E-03
			Epithelial cell signaling in Helicobacter pylori infection	6	6.5	3.30E-04	4.00E-03
			Bladder cancer	5	5.4	5.10E-04	5.40E-03
			Chronic myeloid leukemia	6	6.5	5.20E-04	4.90E-03
			Adherens junction	6	6.5	5.90E-04	5.00E-03
			Notch signaling pathway	5	5.4	7.90E-04	6.10E-03
			Non-small cell lung cancer	5	5.4	1.30E-03	9.40E-03
			Dorso-ventral axis formation	4	4.3	1.40E-03	9.00E-03
			Renal cell carcinoma	5	5.4	3.50E-03	2.10E-02
			Melanoma	5	5.4	3.70E-03	2.10E-02
			Neurotrophin signaling pathway	6	6.5	4.90E-03	2.60E-02
			TGF-beta signaling pathway	5	5.4	7.50E-03	3.70E-02
			ErbB signaling pathway	5	5.4	7.50E-03	3.70E-02
			Apoptosis	5	5.4	7.50E-03	3.70E-02
			Cytokine-cytokine receptor interaction	8	8.7	8.50E-03	3.90E-02
			Endometrial cancer	4	4.3	1.10E-02	4.90E-02

*miRWalk (http://www.ma.uni-heidelberg.de/apps/zmf/mirwalk/

#DAVID (http://david.abcc.ncifcrf.gov/

functional significance of these miRNA expression changes, validated target genes were obtained from miRWALK (http://www.ma.uni-heidelberg.de/apps/zmf/mirwalk/, August 8, 2011). The validated target gene lists were then analyzed for each individual miRNA and all miRNAs together using the DAVID Bioinformatics Resources for functional annotation. Functional analysis suggests that miR-204, miR-133a and miR-206 are highly involved in several cancer pathways, while miR-206 is also involved in focal adhesion and MAPK signaling pathways. In contrast, miR-448 was not reported to significantly regulate any KEGG pathway (Table 4). Additionally, Mir-34a was the only miRNA that exhibited an up-regulation in the PSAPP/S100A1$^{-/-}$/S100B$^{-/-}$ mice and similar to the other three miRNAs that were predicted to regulate pathways, functional analysis suggested that miR-34a is highly involved in multiple cancer pathways. In addition, it is predicted to be involved in the cell cycle, p53 signaling pathway and apoptosis (Table 5).

Finally, when the validated target genes of all five miRNAs are grouped together, functional annotation further implicates these miRNAs in multiple cancer pathways such as leukemia, prostate and pancreatic cancers as well as melanoma. In addition, the five altered miRNAs were also implicated in cell cycle pathways, the p53 signaling pathway and apoptosis (Table 6). While these results may seem unexpected, but the fact that these studies were completed in a very early time point in AD pathogenesis and knowing that S100s are involved in stress related pathways, these results are not all together unexpected.

Table 5. Target and pathway predictions for miR-34a

miRNA	Total Targets*	Assigned Targets*	KEGG Pathway#	Number of Genes#	Percent#	P-value#	Benjamini#
34a	600	104	Pathways in cancer	35	19.6	4.80E-17	5.20E-15
			Chronic myeloid leukemia	18	10.1	2.40E-14	1.30E-12
			Melanoma	17	9.5	1.60E-13	5.90E-12
			Prostate cancer	18	10.1	4.90E-13	1.30E-11
			Glioma	15	8.4	7.50E-12	1.60E-10
			Bladder cancer	13	7.3	1.00E-11	1.80E-10
			Small cell lung cancer	15	8.4	4.60E-10	7.00E-09
			Pancreatic cancer	14	7.8	7.10E-10	9.50E-09
			Cell cycle	17	9.5	1.40E-09	1.60E-08
			Non-small cell lung cancer	12	6.7	4.20E-09	4.40E-08
			p53 signaling pathway	13	7.3	4.50E-09	4.30E-08
			Endometrial cancer	11	6.1	4.00E-08	3.50E-07
			Colorectal cancer	13	7.3	5.40E-08	4.40E-07
			Acute myeloid leukemia	10	5.6	1.30E-06	1.00E-05
			Thyroid cancer	7	3.9	1.50E-05	1.10E-04
			Neurotrophin signaling pathway	12	6.7	2.40E-05	1.60E-04
			Focal adhesion	14	7.8	1.20E-04	7.50E-04
			Wnt signaling pathway	11	6.1	6.40E-04	3.80E-03
			T cell receptor signaling pathway	9	5	1.10E-03	6.20E-03
			Apoptosis	8	4.5	1.40E-03	7.50E-03
			ErbB signaling pathway	8	4.5	1.40E-03	7.50E-03
			Renal cell carcinoma	7	3.9	2.20E-03	1.10E-02
			Jak-STAT signaling pathway	10	5.6	3.00E-03	1.40E-02
			VEGF signaling pathway	7	3.9	3.20E-03	1.50E-02
			Toll-like receptor signaling pathway	8	4.5	3.30E-03	1.50E-02
			Progesterone-mediated oocyte maturation	7	3.9	6.30E-03	2.70E-02
			Adipocytokine signaling pathway	6	3.4	9.40E-03	3.80E-02
			Notch signaling pathway	5	2.8	1.30E-02	4.90E-02

*miRWalk (http://www.ma.uni-heidelberg.de/apps/zmf/mirwalk/
#DAVID (http://david.abcc.ncifcrf.gov/

Discussion

In this study, we identified five candidate miRNAs that are differentially regulated in response to S100 mediated reversal of AD pathology and definitively demonstrate that miRNAs are involved in S100-mediated reversal of AD pathology. In addition, the pathways that these five validated miRNAs are predicted to regulate appear

Table 6. Target and pathway predictions for all validated miRNAs

miRNA	Total Targets*	Assigned Targets*	KEGG Pathway#	Number of Genes#	Percent#	P-value#	Benjamini#
All	3061	424	Pathways in cancer	52	15.4	3.80E-22	4.90E-20
			Chronic myeloid leukemia	24	7.1	6.40E-17	7.10E-15
			Pancreatic cancer	23	6.8	3.50E-16	1.40E-14
			Prostate cancer	22	6.5	5.40E-13	1.80E-11
			Melanoma	20	5.9	6.40E-13	1.70E-11
			Colorectal cancer	21	6.2	1.70E-12	3.60E-11
			Bladder cancer	16	4.7	1.80E-12	3.30E-11
			Glioma	18	5.3	9.80E-12	1.60E-10
			Non-small cell lung cancer	15	4.4	1.30E-09	1.90E-08
			Endometrial cancer	14	4.1	8.40E-09	1.10E-07
			Cell cycle	20	5.9	2.10E-08	2.50E-07
			Small cell lung cancer	16	4.7	7.80E-08	8.40E-07
			MAPK signaling pathway	28	8.3	1.50E-07	1.50E-06
			p53 signaling pathway	14	4.1	2.60E-07	2.40E-06
			Focal adhesion	22	6.5	2.50E-06	2.20E-05
			Neurotrophin signaling pathway	17	5	2.80E-06	2.30E-05
			Acute myeloid leukemia	11	3.3	1.70E-05	1.30E-04
			TGF-beta signaling pathway	13	3.8	2.60E-05	1.90E-04
			Adherens junction	12	3.6	4.10E-05	2.80E-04
			T cell receptor signaling pathway	14	4.1	5.30E-05	3.40E-04
			Apoptosis	12	3.6	1.30E-04	8.00E-04
			Wnt signaling pathway	16	4.7	1.30E-04	7.90E-04
			Thyroid cancer	7	2.1	3.20E-04	1.80E-03
			Adipocytokine signaling pathway	10	3	3.40E-04	1.80E-03
			Cytokine-cytokine receptor interaction	21	6.2	4.00E-04	2.10E-03
			Renal cell carcinoma	10	3	4.70E-04	2.40E-03
			ErbB signaling pathway	11	3.3	5.80E-04	2.80E-03
			Notch signaling pathway	8	2.4	8.40E-04	3.90E-03
			Dorso-ventral axis formation	6	1.8	1.20E-03	5.40E-03
			Amyotrophic lateral sclerosis (ALS)	8	2.4	1.70E-03	7.40E-03
			Epithelial cell signaling in Helicobacter pylori infection	9	2.7	1.80E-03	7.30E-03
			VEGF signaling pathway	9	2.7	3.30E-03	1.30E-02
			Type II diabetes mellitus	7	2.1	4.40E-03	1.70E-02
			Insulin signaling pathway	12	3.6	5.20E-03	2.00E-02
			Jak-STAT signaling pathway	13	3.8	5.40E-03	2.00E-02
			Toll-like receptor signaling pathway	10	3	6.30E-03	2.20E-02
			B cell receptor signaling pathway	8	2.4	1.20E-02	4.20E-02

*miRWalk (http://www.ma.uni-heidelberg.de/apps/zmf/mirwalk/

#DAVID (http://david.abcc.ncifcrf.gov/

to be related to previously reported S100 functions. Interestingly, out of the five validated miRNAs, only miR-34a has been previously identified in AD (Wang, et al., 2009). Wang, et al. (2009) reported that miR-34a was up-regulated in their double transgenic AD mouse model when compared to nontransgenic mice. In contrast, we found that miR-34a was not up-regulated in the PSAPP AD mouse model, but was up-regulated in response to S100A1/S100B ablation. A possible reason for this discrepancy is the brain region used in the studies. Wang, et al. (2009) conducted their studies in the cortex while this study was conducted in the hippocampus of 3 month old mice.

MiR-34a is a member of the miR-34 family and, in mice, is expressed throughout most tissue types with highest expression in the brain (Aranha, et al., 2011). It has been suggested that miR-34a possesses cell cycle regulatory potential and anti-proliferative capacity through p53 dependent and independent mechanisms (Chang, et al., 2007; He, et al., 2007; Tarasov, et al., 2007). In fact, miR-34a is a direct transcriptional target of p53 which positively regulates miR-34a expression (He, et al., 2007; Raver-Shapira, et al., 2007; Tarasov, et al., 2007). Increased expression of miR-34a has also been reported to induce cell cycle arrest in G_1 by inhibiting G_1/S phase transition through negative regulation of cyclin D1 (CCDN1) and cyclin dependent kinase 6 (CDK6) (Sun, et al., 2008; Tarasov, et al., 2007). Furthermore, p63 also directly targets, and represses miR-34a expression, which has been shown to restore cell cycle progression and expression of CCND1 and CDK6 (Antonini, et al., 2010). Interestingly, it has been suggested that aberrant cell cycle re-entry by mature neurons leads to the apoptotic neuronal loss exhibited in AD (Lopes, et al., 2009). Collectively, these studies implicate miR-34a in

apoptosis and cell cycle progression/inhibition suggesting that miR-34a represents a possible target for inhibiting the aberrant cell cycle re-entry of neurons as seen in AD.

Additionally, we found that miR-448 was down regulated in response to S100A1/S100B ablation in PSAPP mice. Interestingly, our bioinformatics searches were unable to identify any significant KEGG pathway predictions and only five validated gene targets for miR-448 (Table 4). MiR-448 is located within the fourth intron of the Serotonin receptor 2C (Htr2c) and recent reports have suggested that miR-448 regulates adipocyte differentiation through translational repression of Kruppel-like Factor 5 (KLF5), a known transcription factor that induces adipocyte differentiation (Kinoshita, et al., 2010; Millan, 2011). In addition, NF-κB has been reported to suppress miR-448 expression in breast tumors undergoing chemotherapy-induced epithelial-mesenchymal transition (Li, et al., 2011). Recent studies have also suggested that interferon beta (IFNβ) upregulates miR-448 which directly targets the genomic RNA of the hepatitis C virus (HCV) and is capable of inhibiting HCV infection and replication (Pedersen, et al., 2007). Furthermore, miR-448 was also identified in bovine alveolar macrophages (Xu, et al., 2009). Together, these studies implicate miR-448 both cell differentiation and immune response (Pedersen and David, 2008; Xu, et al., 2009) suggesting it may have a role in the detrimental inflammation in the brain of AD patients.

We also observed a decrease in miR-204 expression in response to S100A1/S100B ablation in PSAPP mice. A recent study characterized miR-204 as significantly enriched in the distal axons of primary sympathetic neurons when

compared to cell bodies (Natera-Naranjo, et al., 2010). MiR-204 was also reported to be expressed in multiple structures of the human fetal eye, including the retina, lens and ciliary body as well as being the most highly expressed miRNA (with miR-211) in the retinal pigment epithelium (Wang, et al., 2010). Multiple studies have suggested that miR-204 in an important factor in epithelial differentiation, but miR-204 has also been reported to be involved in the differentiation of other cell types such as mesenchymal stem cells, bone marrow stromal cells and mouse embryonic stem cells (Conte, et al., 2010; Huang, et al., 2010; Saunders, et al., 2010). In addition, miR-204 has been reported to suppress SIRT1 during mESC differentiation and maintain the low levels in adult tissues (Saunders, et al., 2010). Interestingly, SIRT1 activation is reported to be beneficial in neurodegeneration. In fact, SIRT1 activators have been shown to slow *in vitro* cell death and *in vivo* neurodegeneration as well as lead to anti-inflammatory activity by suppressing NF-κB activity (Lavu, et al., 2008). SIRT1 also deactivates p53 and p73 through deacetylation, effectively controlling the transcriptional activities of, and apoptosis induced by p53 and p73 (Dai, et al., 2007; Vaziri, et al., 2001). Increased miR-204 has also been reported to also regulate apoptosis and cell death due to oxidative and ER stress as well as a decrease in the expression of inflammatory factors (Li, et al., 2011) as well as regulating autophagy (Xiao, et al., 2011). Collectively, these studies suggest that miR-204 has a role in cell differentiation and p53 pathways as well as inflammation.

Finally, we also saw a decrease of expression in two muscle specific miRNAs, miR-133a and miR-206. Interestingly, neither of these miRNA's has been previously

studied in the brain. In fact, miR-206 has been reported as a skeletal muscle-specific miRNA (McCarthy, 2008). Interestingly, as in the other miRNAs, miR-206 and miR-133a are involved in human muscle cell differentiation (Koutsoulidou, et al., 2011). TGF-β targets both miR-206 and miR-133a, but miR-206 overexpression *in vitro* is reported to promote myogenic differentiation, while miR-133a overexpression enhances myoblast proliferation and represses differentiation (Dey, et al., 2011; Koutsoulidou, et al., 2011; Townley-Tilson, et al., 2010; Winbanks, et al., 2011). MyoD is a transcription factor that regulates the transcription of miR-206 and miR-MyoD also acts as a proapoptotic factor by negatively regulating Pax3 expression through translational activation of miR-206 (Hirai, et al., 2010). This regulation of Pax3/7 also regulated proliferation, differentiation and apoptosis in adult muscle stem cells (Chen, et al., 2010; Goljanek-Whysall, et al., 2011; Hirai, et al., 2010). In addition, in renal cell carcinoma maxillary sinus squamous cell carcinoma, and bladder cancer, miR-133a targets TAGLN2, and increased expression inhibits proliferation and invasion, as well as increases cell cycle arrest and apoptosis (Kawakami, et al., 2011; Nohata, et al., 2011; Yoshino, et al., 2011). In addition to TAGLN2, miR-133a also targets GSTP1 in bladder cancer inducing apoptosis (Uchida, et al., 2011). While they have been studied in different tissue types, miR-206 and miR-133a exhibit apoptotic, proliferative and cell cycle regulative properties suggesting they may have a role in the neuronal cell death and aberrant cell cycle re-entry exhibited in AD pathology.

Conclusions

Collectively, these data suggest that a specific subset of miRNAs contribute to the S100-mediated reversal of AD pathobiology in the PSAPP mouse model. PSAPP/S100A1$^{-/-}$/S100B$^{-/-}$ mice exhibited a significant decrease in the expression of four miRNAs (miR-448, miR-133a, miR-204 and miR-206), and a significant increase in the expression of one, miR-34a. Interestingly, the common predicted pathways for these miRNAs are cancer related suggesting that cancer and AD share some disease pathways. These alterations provide evidence that miRNA expression/inhibition is involved in S100A1/S100B-mediated reversal of histopathology in AD and provide novel targets for therapeutic intervention. Finally, the beneficial effects of inhibiting S100A1/S100B, including miRNA expression/inhibition, may extend to other neurological diseases involving disruptions in cell cycle, p53 and/or differentiation.

CHAPTER VI

CONCLUSIONS

Collectively, these data demonstrate that S100A1 and S100B inhibition represents a novel avenue for AD therapy. This study used two different approaches to show that S100A1/S100B inhibition reduces plaque load and inflammation in the PSAPP mouse model of AD. We demonstrated that S100A1 and/or S100B ablation synergistically reduces plaque load, astrocytosis and microgliosis. Additionally, this S100-mediated reduction in pathology involves changes in miRNA expression. Furthermore, passive S100 immunotherapy mimics the results of ablation in cortical plaque load and astrocytosis. These studies illustrate that the net effect of S100A1/S100B inhibition in AD is a reduction in histopathology, suggesting that S100A1 and S100B are involved in the onset/progression of AD pathology in patients. An early event in AD pathology is the destabilization of Ca^{2+} homeostasis, which causes an alteration in S100 signaling and detrimental gain of function that promotes AD pathology. We hypothesize that S100A1 and S100B are involved in a p53 stress response pathway that contributes to the onset and progression of AD pathology (Figure 26). Although S100A1/S100B inhibition did not halt AD pathology all together, these studies suggest that this inhibition significantly slows the disease progression and it is predicted that slowing the progression of AD by as little as one year will reduce health care costs by $250 billion per year (Alzheimer's Association, et al., 2011). Unfortunately, the only current treatments for AD "temporarily slow worsening of

symptoms for about six to 12 months, on average, for about half the individuals that take them" (Alzheimer's Association, et al., 2011). The results of this study suggest that the

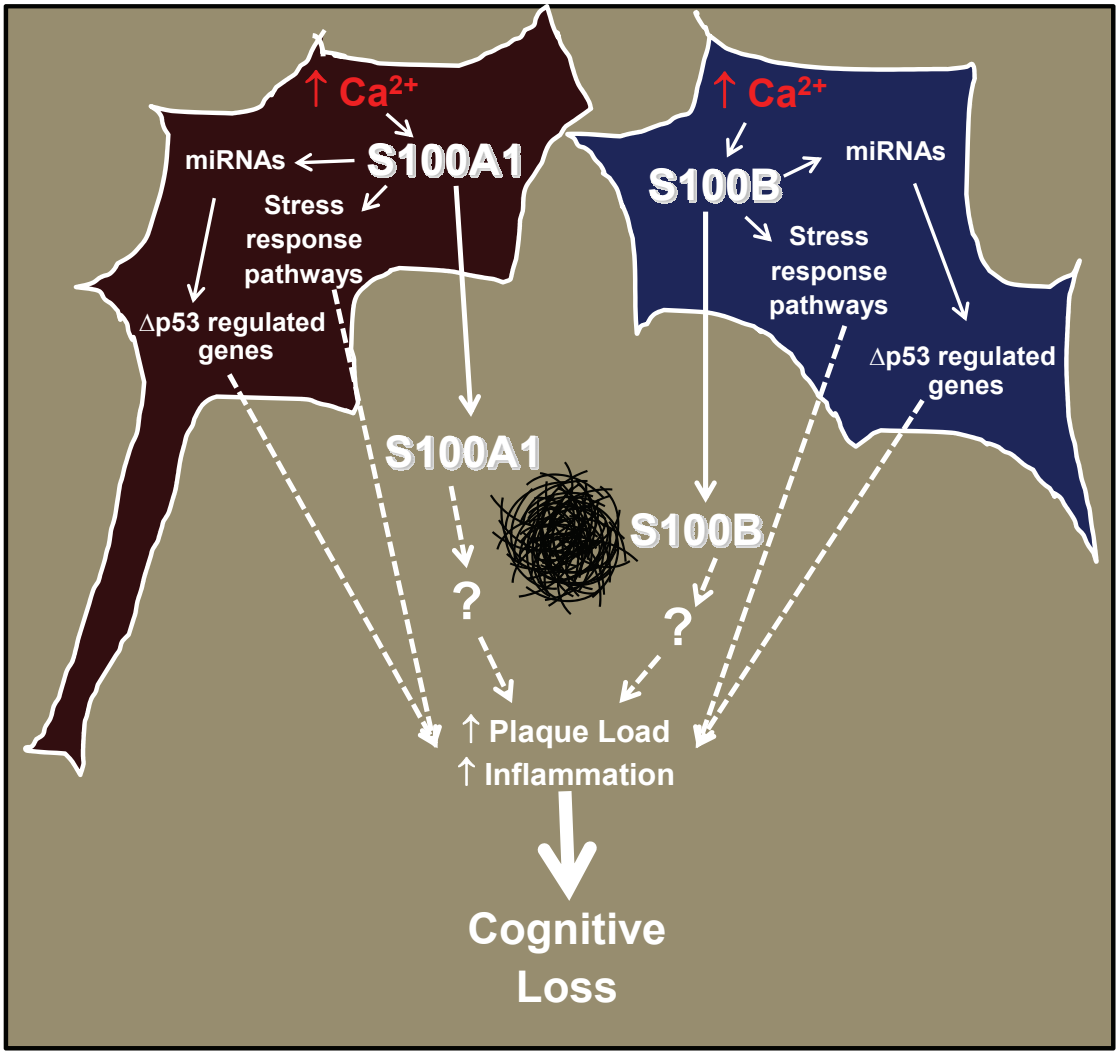

Figure 26. S100A1 and S100B in AD. Above model describes possible mechanisms of S100A1/S100B mediated increases in AD pathology. Solid line denotes known events and dotted line denotes hypothesized pathways.

inhibition of S100A1/S100B function through a combination of multiple approaches (passive immunotherapy, small molecule inhibitors, etc.) will significantly delay the

progression of AD pathology as well as improve cognitive decline in patients and perhaps aid in the treatment of other neurological diseases that involve the dysregulation of Ca^{2+} homeostasis as well.

REFERENCES

Ackermann GE, Marenholz I, Wolfer DP, Chan WY, Schafer B, Erne P, Heizmann CW (2006) S100A1-deficient male mice exhibit increased exploratory activity and reduced anxiety-related responses. Biochim Biophys Acta 1763:1307-1319.

Alzheimer's Association, Thies W, Bleiler L (2011) 2011 Alzheimer's disease facts and figures. Alzheimers Dement 7:208-244.

Anderson PJ, Watts HR, Jen S, Gentleman SM, Moncaster JA, Walsh DT, Jen LS (2009) Differential effects of interleukin-1beta and S100B on amyloid precursor protein in rat retinal neurons. Clin Ophthalmol 3:235-242.

Antonini D, Russo MT, De Rosa L, Gorrese M, Del Vecchio L, Missero C (2010) Transcriptional repression of miR-34 family contributes to p63-mediated cell cycle progression in epidermal cells. J Invest Dermatol 130:1249-1257.

Aranha MM, Santos DM, Sola S, Steer CJ, Rodrigues CM (2011) MiR-34a regulates mouse neural stem cell differentiation. PLoS One 6:e21396 Aug 3. [Epub ahead of print]

Arcuri C, Bianchi R, Brozzi F, Donato R (2005) S100B increases proliferation in PC12 neuronal cells and reduces their responsiveness to nerve growth factor via Akt activation. J Biol Chem 280:4402-4414.

Asano T, Mori T, Shimoda T, Shinagawa R, Satoh S, Yada N, Katsumata S, Matsuda S, Kagamiishi Y, Tateishi N (2005) Arundic acid (ONO-2506) ameliorates delayed ischemic brain damage by preventing astrocytic overproduction of S100B. Curr Drug Targets CNS Neurol Disord 4:127-142.

Atwood CS, Martins RN, Smith MA, Perry G (2002) Senile plaque composition and posttranslational modification of amyloid-beta peptide and associated proteins. Peptides 23:1343-1350.

Bartel DP (2004) MicroRNAs: genomics, biogenesis, mechanism, and function. Cell 116:281-297.

Baudier J, Briving C, Deinum J, Haglid K, Sorskog L, Wallin M (1982) Effect of S-100 proteins and calmodulin on Ca2+-induced disassembly of brain microtubule proteins in vitro. FEBS Lett 147:165-168.

Baudry A, Mouillet-Richard S, Schneider B, Launay JM, Kellermann O (2010) MiR-16 targets the serotonin transporter: a new facet for adaptive responses to antidepressants. Science 329:1537-1541.

Bekris LM, Yu CE, Bird TD, Tsuang DW (2010) Genetics of Alzheimer disease. J Geriatr Psychiatry Neurol 23:213-227.

Benfenati F, Ferrari R, Onofri F, Arcuri C, Giambanco I, Donato R (2004) S100A1 codistributes with synapsin I in discrete brain areas and inhibits the F-actin-bundling activity of synapsin I. J Neurochem 89:1260-1270.

Berridge MJ (1998) Neuronal calcium signaling. Neuron 21:13-26.

Berridge MJ (2010) Calcium hypothesis of Alzheimer's disease. Pflugers Arch 459:441-449.

Berridge MJ (2011) Calcium signalling and Alzheimer's disease. Neurochem Res 36:1149-1156.

Bertram L, Lill CM, Tanzi RE (2010) The genetics of Alzheimer disease: back to the future. Neuron 68:270-281.

Boom A, Pochet R, Authelet M, Pradier L, Borghgraef P, Van Leuven F, Heizmann CW, Brion JP (2004) Astrocytic calcium/zinc binding protein S100A6 over expression in Alzheimer's disease and in PS1/APP transgenic mice models. Biochim Biophys Acta 1742:161-168.

Boutajangout A, Ingadottir J, Davies P, Sigurdsson EM (2011) Passive immunization targeting pathological phospho-tau protein in a mouse model reduces functional decline and clears tau aggregates from the brain. J Neurochem 118:658-667.

Brozzi F, Arcuri C, Giambanco I, Donato R (2009) S100B protein regulates astrocyte shape and migration via interaction with src kinase: implications for astrocyte development, activation, and tumor growth. J Biol Chem 284:8797-8811.

Bruno AM, Huang JY, Bennett DA, Marr RA, Hastings ML, Stutzmann GE (2011) Altered ryanodine receptor expression in mild cognitive impairment and Alzheimer's disease. Neurobiol Aging Apr 29. [Epub ahead of print]

Cameron B, Landreth GE (2010) Inflammation, microglia, and Alzheimer's disease. Neurobiol Dis 37:503-509.

Castellani RJ, Lee HG, Siedlak SL, Nunomura A, Hayashi T, Nakamura M, Zhu X, Perry G, Smith MA (2009) Reexamining Alzheimer's disease: evidence for a protective role for amyloid-beta protein precursor and amyloid-beta. J Alzheimers Dis 18:447-452.

Castellani RJ, Rolston RK, Smith MA (2010) Alzheimer disease. Dis Mon 56:484-546.

Chang TC, Wentzel EA, Kent OA, Ramachandran K, Mullendore M, Lee KH, Feldmann G, Yamakuchi M, Ferlito M, Lowenstein CJ, Arking DE, Beer MA, Maitra A, Mendell JT (2007) Transactivation of miR-34a by p53 broadly influences gene expression and promotes apoptosis. Mol Cell 26:745-752.

Chaves ML, Camozzato AL, Ferreira ED, Piazenski I, Kochhann R, Dall'Igna O, Mazzini GS, Souza DO, Portela LV (2010) Serum levels of S100B and NSE proteins in Alzheimer's disease patients. J Neuroinflammation 7:6-12.

Chen JF, Tao Y, Li J, Deng Z, Yan Z, Xiao X, Wang DZ (2010) MicroRNA-1 and microRNA-206 regulate skeletal muscle satellite cell proliferation and differentiation by repressing Pax7. J Cell Biol 190:867-879.

Cherny RA, Atwood CS, Xilinas ME, Gray DN, Jones WD, McLean CA, Barnham KJ, Volitakis I, Fraser FW, Kim Y, Huang X, Goldstein LE, Moir RD, Lim JT, Beyreuther K, Zheng H, Tanzi RE, Masters CL, Bush AI (2001) Treatment with a copper-zinc chelator markedly and rapidly inhibits beta-amyloid accumulation in Alzheimer's disease transgenic mice. Neuron 30:665-676.

Chow SK, Yu D, Macdonald CL, Buibas M, Silva GA (2010) Amyloid beta-peptide directly induces spontaneous calcium transients, delayed intercellular calcium waves and gliosis in rat cortical astrocytes. ASN Neuro 2:15-23.

Citron M (2010) Alzheimer's disease: strategies for disease modification. Nat Rev Drug Discov 9:387-398.

Combs CK (2009) Inflammation and microglia actions in Alzheimer's disease. J Neuroimmune Pharmacol 4:380-388.

Conte I, Carrella S, Avellino R, Karali M, Marco-Ferreres R, Bovolenta P, Banfi S (2010) miR-204 is required for lens and retinal development via Meis2 targeting. Proc Natl Acad Sci U S A 107:15491-15496.

Costa DA, Nilsson LN, Bales KR, Paul SM, Potter H (2004) Apolipoprotein is required for the formation of filamentous amyloid, but not for amorphous abeta deposition, in an APP/PS double transgenic mouse model of Alzheimer's disease. J Alzheimers Dis 6:509-514.

Craft JM, Watterson DM, Marks A, Van Eldik LJ (2005) Enhanced susceptibility of S-100B transgenic mice to neuroinflammation and neuronal dysfunction induced by intracerebroventricular infusion of human beta-amyloid. Glia 51:209-216.

Dai JM, Wang ZY, Sun DC, Lin RX, Wang SQ (2007) SIRT1 interacts with p73 and suppresses p73-dependent transcriptional activity. J Cell Physiol 210:161-166.

De Smaele E, Ferretti E, Gulino A (2010) MicroRNAs as biomarkers for CNS cancer and other disorders. Brain Res 1338:100-111.

Deane R, Zlokovic BV (2007) Role of the blood-brain barrier in the pathogenesis of Alzheimer's disease. Curr Alzheimer Res 4:191-197.

Delay C, Hebert SS (2011) MicroRNAs and Alzheimer's disease mouse models: current insights and future research avenues. Int J Alzheimers Dis 2011: article ID 894938.

Delrieu J, Ousset PJ, Caillaud C, Vellas B (2011) "Clinical trials in Alzheimer's disease": immunotherapy approaches. J Neurochem Aug 30. [Epub ahead of print]

Demuro A, Parker I, Stutzmann GE (2010) Calcium signaling and amyloid toxicity in Alzheimer disease. J Biol Chem 285:12463-12468.

Dey BK, Gagan J, Dutta A (2011) MiR-206 and -486 induce myoblast differentiation by downregulating Pax7. Mol Cell Biol 31:203-214.

Dolev I, Michaelson DM (2004) A nontransgenic mouse model shows inducible amyloid-beta (Abeta) peptide deposition and elucidates the role of apolipoprotein E in the amyloid cascade. Proc Natl Acad Sci U S A 101:13909-13914.

Donato R (2001) S100: a multigenic family of calcium-modulated proteins of the EF-hand type with intracellular and extracellular functional roles. Int J Biochem Cell Biol 33:637-668.

Donato R, Sorci G, Riuzzi F, Arcuri C, Bianchi R, Brozzi F, Tubaro C, Giambanco I (2009) S100B's double life: intracellular regulator and extracellular signal. Biochim Biophys Acta 1793:1008-1022.

Eikelenboom P, van Exel E, Hoozemans JJ, Veerhuis R, Rozemuller AJ, van Gool WA (2010) Neuroinflammation - an early event in both the history and pathogenesis of Alzheimer's disease. Neurodegener Dis 7:38-41.

Elder GA, Gama Sosa MA, De Gasperi R (2010) Transgenic mouse models of Alzheimer's disease. Mt Sinai J Med 77:69-81.

Enciu AM, Popescu BO, Gheorghisan-Galateanu A (2011) MicroRNAs in brain development and degeneration. Mol Biol Rep Jun 5. [Epub ahead of print]

Eriksson S, Janciauskiene S, Lannfelt L (1995) Alpha 1-antichymotrypsin regulates Alzheimer beta-amyloid peptide fibril formation. Proc Natl Acad Sci U S A 92:2313-2317.

Esposito G, Scuderi C, Lu J, Savani C, De Filippis D, Iuvone T, Steardo L, Jr., Sheen V, Steardo L (2008) S100B induces tau protein hyperphosphorylation via Dickopff-1 up-regulation and disrupts the Wnt pathway in human neural stem cells. J Cell Mol Med 12:914-927.

Fiore R, Khudayberdiev S, Saba R, Schratt G (2011) MicroRNA function in the nervous system. Prog Mol Biol Transl Sci 102:47-100.

Fraser PE, Nguyen JT, McLachlan DR, Abraham CR, Kirschner DA (1993) Alpha 1-antichymotrypsin binding to Alzheimer abeta peptides is sequence specific and induces fibril disaggregation in vitro. J Neurochem 61:298-305.

Friend WC, Clapoff S, Landry C, Becker LE, O'Hanlon D, Allore RJ, Brown IR, Marks A, Roder J, Dunn RJ (1992) Cell-specific expression of high levels of human S100 beta in transgenic mouse brain is dependent on gene dosage. J Neurosci 12:4337-4346.

Fuhrmann M, Bittner T, Jung CK, Burgold S, Page RM, Mitteregger G, Haass C, LaFerla FM, Kretzschmar H, Herms J (2010) Microglial Cx3cr1 knockout prevents neuron loss in a mouse model of Alzheimer's disease. Nat Neurosci 13:411-413.

Fulle S, Pietrangelo T, Mariggio MA, Lorenzon P, Racanicchi L, Mozrzymas J, Guarnieri S, Zucconi-Grassi G, Fano G (2000) Calcium and fos involvement in brain-derived Ca(2+)-binding protein (S100)-dependent apoptosis in rat phaeochromocytoma cells. Exp Physiol 85:243-453.

Garbuglia M, Verzini M, Rustandi RR, Osterloh D, Weber DJ, Gerke V, Donato R (1999) Role of the C-terminal extension in the interaction of S100A1 with GFAP,

tubulin, the S100A1- and S100B-inhibitory peptide, TRTK-12, and a peptide derived from p53, and the S100A1 inhibitory effect on GFAP polymerization. Biochem Biophys Res Commun 254:36-41.

Giunta B, Hou H, Zhu Y, Rrapo E, Tian J, Takashi M, Commins D, Singer E, He J, Fernandez F, Tan J (2009) HIV-1 Tat contributes to Alzheimer's disease-like pathology in PSAPP mice. Int J Clin Exp Pathol 2:433-443.

Glabe CG (2008) Structural classification of toxic amyloid oligomers. J Biol Chem 283:29639-29643.

Goljanek-Whysall K, Sweetman D, Abu-Elmagd M, Chapnik E, Dalmay T, Hornstein E, Munsterberg A (2011) MicroRNA regulation of the paired-box transcription factor Pax3 confers robustness to developmental timing of myogenesis. Proc Natl Acad Sci U S A 108:11936-11941.

Gomez-Isla T, Price JL, McKeel DW, Jr., Morris JC, Growdon JH, Hyman BT (1996) Profound loss of layer II entorhinal cortex neurons occurs in very mild Alzheimer's disease. J Neurosci 16:4491-4500.

Gordon MN, King DL, Diamond DM, Jantzen PT, Boyett KV, Hope CE, Hatcher JM, DiCarlo G, Gottschall WP, Morgan D, Arendash GW (2001) Correlation between cognitive deficits and Abeta deposits in transgenic APP+PS1 mice. Neurobiol Aging 22:377-385.

Gordon MN, Holcomb LA, Jantzen PT, DiCarlo G, Wilcock D, Boyett KW, Connor K, Melachrino J, O'Callaghan JP, Morgan D (2002) Time course of the development of

Alzheimer-like pathology in the doubly transgenic PS1+APP mouse. Exp Neurol 173:183-195.

Gorelick PB (2010) Role of inflammation in cognitive impairment: results of observational epidemiological studies and clinical trials. Ann N Y Acad Sci 1207:155-162.

Gotz J, Ittner LM (2008) Animal models of Alzheimer's disease and frontotemporal dementia. Nat Rev Neurosci 9:532-544.

Green KN, Demuro A, Akbari Y, Hitt BD, Smith IF, Parker I, LaFerla FM (2008) SERCA pump activity is physiologically regulated by presenilin and regulates amyloid beta production. J Cell Biol 181:1107-1116.

Griffin WS (2006) Inflammation and neurodegenerative diseases. Am J Clin Nutr 83:470S-474S.

Grill JD, Cummings JL (2010) Current therapeutic targets for the treatment of Alzheimer's disease. Expert Rev Neurother 10:711-728.

Haass C, Selkoe DJ (2007) Soluble protein oligomers in neurodegeneration: lessons from the Alzheimer's amyloid beta-peptide. Nat Rev Mol Cell Biol 8:101-112.

Hardy J, Allsop D (1991) Amyloid deposition as the central event in the aetiology of Alzheimer's disease. Trends Pharmacol Sci 12:383-388.

Hardy JA, Higgins GA (1992) Alzheimer's disease: the amyloid cascade hypothesis. Science 256:184-185.

Hartley DM, Zhao C, Speier AC, Woodard GA, Li S, Li Z, Walz T (2008) Transglutaminase induces protofibril-like amyloid beta-protein assemblies that are protease-resistant and inhibit long-term potentiation. J Biol Chem 283:16790-16800.

He L, Hannon GJ (2004) MicroRNAs: small RNAs with a big role in gene regulation. Nat Rev Genet 5:522-531.

He L, He X, Lowe SW, Hannon GJ (2007) microRNAs join the p53 network--another piece in the tumour-suppression puzzle. Nat Rev Cancer 7:819-822.

Hebert SS, De Strooper B (2007) Molecular biology. miRNAs in neurodegeneration. Science 317:1179-1180.

Hebert SS, Horre K, Nicolai L, Papadopoulou AS, Mandemakers W, Silahtaroglu AN, Kauppinen S, Delacourte A, De Strooper B (2008) Loss of microRNA cluster miR-29a/b-1 in sporadic Alzheimer's disease correlates with increased BACE1/beta-secretase expression. Proc Natl Acad Sci U S A 105:6415-6420.

Hebert SS, De Strooper B (2009) Alterations of the microRNA network cause neurodegenerative disease. Trends Neurosci 32:199-206.

Heizmann CW, Cox JA (1998) New perspectives on S100 proteins: a multi-functional Ca(2+)-, Zn(2+)- and Cu(2+)-binding protein family. Biometals 11:383-397.

Heneka MT, Nadrigny F, Regen T, Martinez-Hernandez A, Dumitrescu-Ozimek L, Terwel D, Jardanhazi-Kurutz D, Walter J, Kirchhoff F, Hanisch UK, Kummer MP (2010) Locus ceruleus controls Alzheimer's disease pathology by modulating microglial functions through norepinephrine. Proc Natl Acad Sci U S A 107:6058-6063.

Heneka MT, O'Banion MK, Terwel D, Kummer MP (2010) Neuroinflammatory processes in Alzheimer's disease. J Neural Transm 117:919-947.

Hirai H, Verma M, Watanabe S, Tastad C, Asakura Y, Asakura A (2010) MyoD regulates apoptosis of myoblasts through microRNA-mediated down-regulation of Pax3. J Cell Biol 191:347-365.

Hofmann MA, Drury S, Fu C, Qu W, Taguchi A, Lu Y, Avila C, Kambham N, Bierhaus A, Nawroth P, Neurath MF, Slattery T, Beach D, McClary J, Nagashima M, Morser J, Stern D, Schmidt AM (1999) RAGE mediates a novel proinflammatory axis: a central cell surface receptor for S100/calgranulin polypeptides. Cell 97:889-901.

Holcomb L, Gordon MN, McGowan E, Yu X, Benkovic S, Jantzen P, Wright K, Saad I, Mueller R, Morgan D, Sanders S, Zehr C, O'Campo K, Hardy J, Prada CM, Eckman C, Younkin S, Hsiao K, Duff K (1998) Accelerated Alzheimer-type phenotype in transgenic mice carrying both mutant amyloid precursor protein and presenilin 1 transgenes. Nat Med 4:97-100.

Holcomb LA, Gordon MN, Jantzen P, Hsiao K, Duff K, Morgan D (1999) Behavioral changes in transgenic mice expressing both amyloid precursor protein and presenilin-1 mutations: lack of association with amyloid deposits. Behav Genet 29:177-185.

Holcomb LA, Dhanasekaran M, Hitt AR, Young KA, Riggs M, Manyam BV (2006) Bacopa monniera extract reduces amyloid levels in PSAPP mice. J Alzheimers Dis 9:243-251.

Holmes C, Boche D, Wilkinson D, Yadegarfar G, Hopkins V, Bayer A, Jones RW, Bullock R, Love S, Neal JW, Zotova E, Nicoll JA (2008) Long-term effects of Abeta42 immunisation in Alzheimer's disease: follow-up of a randomised, placebo-controlled phase I trial. Lancet 372:216-223.

Hoppmann S, Steinbach J, Pietzsch J (2010) Scavenger receptors are associated with cellular interactions of S100A12 in vitro and in vivo. Int J Biochem Cell Biol 42:651-661.

Hu J, Castets F, Guevara JL, Van Eldik LJ (1996) S100 beta stimulates inducible nitric oxide synthase activity and mRNA levels in rat cortical astrocytes. J Biol Chem 271:2543-2547.

Huang J, Zhao L, Xing L, Chen D (2010) MicroRNA-204 regulates Runx2 protein expression and mesenchymal progenitor cell differentiation. Stem Cells 28:357-364.

Huttunen HJ, Kuja-Panula J, Sorci G, Agneletti AL, Donato R, Rauvala H (2000) Coregulation of neurite outgrowth and cell survival by amphoterin and S100 proteins through receptor for advanced glycation end products (RAGE) activation. J Biol Chem 275:40096-40105.

Hyman BT, Van Hoesen GW, Damasio AR, Barnes CL (1984) Alzheimer's disease: cell-specific pathology isolates the hippocampal formation. Science 225:1168-1170.

Isaacs AM, Senn DB, Yuan M, Shine JP, Yankner BA (2006) Acceleration of amyloid beta-peptide aggregation by physiological concentrations of calcium. J Biol Chem 281:27916-27923.

Iwatsubo T, Odaka A, Suzuki N, Mizusawa H, Nukina N, Ihara Y (1994) Visualization of Abeta 42(43) and Abeta 40 in senile plaques with end-specific abeta monoclonals: evidence that an initially deposited species is Abeta 42(43). Neuron 13:45-53.

Janus C, Pearson J, McLaurin J, Mathews PM, Jiang Y, Schmidt SD, Chishti MA, Horne P, Heslin D, French J, Mount HT, Nixon RA, Mercken M, Bergeron C, Fraser PE, St George-Hyslop P, Westaway D (2000) Abeta peptide immunization reduces behavioural impairment and plaques in a model of Alzheimer's disease. Nature 408:979-982.

Jarrett JT, Berger EP, Lansbury PT, Jr. (1993) The carboxy terminus of the beta amyloid protein is critical for the seeding of amyloid formation: implications for the pathogenesis of Alzheimer's disease. Biochemistry 32:4693-4697.

Karran E, Mercken M, Strooper BD (2011) The amyloid cascade hypothesis for Alzheimer's disease: an appraisal for the development of therapeutics. Nat Rev Drug Discov 10:698-712.

Kawakami K, Enokida H, Chiyomaru T, Tatarano S, Yoshino H, Kagara I, Gotanda T, Tachiwada T, Nishiyama K, Nohata N, Seki N, Nakagawa M (2011) The functional significance of miR-1 and miR-133a in renal cell carcinoma. Eur J Cancer Jul 9. [Epub ahead of print]

Ketting RF (2010) MicroRNA biogenesis and function. An overview. Adv Exp Med Biol 700:1-14.

Kinghorn KJ, Crowther DC, Sharp LK, Nerelius C, Davis RL, Chang HT, Green C, Gubb DC, Johansson J, Lomas DA (2006) Neuroserpin binds abeta and is a

neuroprotective component of amyloid plaques in Alzheimer disease. J Biol Chem 281:29268-29277.

Kinoshita M, Ono K, Horie T, Nagao K, Nishi H, Kuwabara Y, Takanabe-Mori R, Hasegawa K, Kita T, Kimura T (2010) Regulation of adipocyte differentiation by activation of serotonin (5-HT) receptors 5-HT2AR and 5-HT2CR and involvement of microRNA-448-mediated repression of KLF5. Mol Endocrinol 24:1978-1987.

Kotilinek LA, Bacskai B, Westerman M, Kawarabayashi T, Younkin L, Hyman BT, Younkin S, Ashe KH (2002) Reversible memory loss in a mouse transgenic model of Alzheimer's disease. J Neurosci 22:6331-6335.

Koutsoulidou A, Mastroyiannopoulos NP, Furling D, Uney JB, Phylactou LA (2011) Expression of miR-1, miR-133a, miR-133b and miR-206 increases during development of human skeletal muscle. BMC Dev Biol 11:34-42.

Kubista H, Donato R, Hermann A (1999) S100 calcium binding protein affects neuronal electrical discharge activity by modulation of potassium currents. Neuroscience 90:493-508.

Lambert JC, Ferreira S, Gussekloo J, Christiansen L, Brysbaert G, Slagboom E, Cottel D, Petit T, Hauw JJ, DeKosky ST, Richard F, Berr C, Lendon C, Kamboh MI, Mann D, Christensen K, Westendorp R, Amouyel P (2007) Evidence for the association of the S100beta gene with low cognitive performance and dementia in the elderly. Mol Psychiatry 12:870-880.

Lau P, de Strooper B (2010) Dysregulated microRNAs in neurodegenerative disorders. Semin Cell Dev Biol 21:768-773.

Lavu S, Boss O, Elliott PJ, Lambert PD (2008) Sirtuins--novel therapeutic targets to treat age-associated diseases. Nat Rev Drug Discov 7:841-853.

Leclerc E, Sturchler E, Vetter SW, Heizmann CW (2009) Crosstalk between calcium, amyloid beta and the receptor for advanced glycation endproducts in Alzheimer's disease. Rev Neurosci 20:95-110.

Leclerc E, Sturchler E, Vetter SW (2010) The S100B/RAGE axis in Alzheimer's disease. Cardiovasc Psychiatry Neurol 2010: article ID 539581.

Lee CY, Landreth GE (2010) The role of microglia in amyloid clearance from the AD brain. J Neural Transm 117:949-960.

Lee Y, Kim M, Han J, Yeom KH, Lee S, Baek SH, Kim VN (2004) MicroRNA genes are transcribed by RNA polymerase II. EMBO J 23:4051-4060.

Lee YJ, Han SB, Nam SY, Oh KW, Hong JT (2010) Inflammation and Alzheimer's disease. Arch Pharm Res 33:1539-1556.

Lemere CA, Beierschmitt A, Iglesias M, Spooner ET, Bloom JK, Leverone JF, Zheng JB, Seabrook TJ, Louard D, Li D, Selkoe DJ, Palmour RM, Ervin FR (2004) Alzheimer's disease abeta vaccine reduces central nervous system abeta levels in a non-human primate, the Caribbean vervet. Am J Pathol 165:283-297.

Li C, Zhao R, Gao K, Wei Z, Yin MY, Lau LT, Chui D, Hoi Yu AC (2011) Astrocytes: implications for neuroinflammatory pathogenesis of Alzheimer's disease. Curr Alzheimer Res 8:67-80.

Li G, Luna C, Qiu J, Epstein DL, Gonzalez P (2011) Role of miR-204 in the regulation of apoptosis, endoplasmic reticulum stress response, and inflammation in human trabecular meshwork cells. Invest Ophthalmol Vis Sci 52:2999-3007.

Li QQ, Chen ZQ, Cao XX, Xu JD, Xu JW, Chen YY, Wang WJ, Chen Q, Tang F, Liu XP, Xu ZD (2011) Involvement of NF-kappaB/miR-448 regulatory feedback loop in chemotherapy-induced epithelial-mesenchymal transition of breast cancer cells. Cell Death Differ 18:16-25.

Lim LP, Lau NC, Garrett-Engele P, Grimson A, Schelter JM, Castle J, Bartel DP, Linsley PS, Johnson JM (2005) Microarray analysis shows that some microRNAs downregulate large numbers of target mRNAs. Nature 433:769-773.

Lopes JP, Oliveira CR, Agostinho P (2009) Cell cycle re-entry in Alzheimer's disease: a major neuropathological characteristic? Curr Alzheimer Res 6:205-212.

Marenholz I, Heizmann CW, Fritz G (2004) S100 proteins in mouse and man: from evolution to function and pathology (including an update of the nomenclature). Biochem Biophys Res Commun 322:1111-1122.

Marenholz I, Lovering RC, Heizmann CW (2006) An update of the S100 nomenclature. Biochim Biophys Acta 1763:1282-1283.

Markowitz J, MacKerell AD, Jr., Weber DJ (2007) A search for inhibitors of S100B, a member of the S100 family of calcium-binding proteins. Mini Rev Med Chem 7:609-616.

Marshak DR, Pesce SA, Stanley LC, Griffin WS (1992) Increased S100 beta neurotrophic activity in Alzheimer's disease temporal lobe. Neurobiol Aging 13:1-7.

Maru DM, Singh RR, Hannah C, Albarracin CT, Li YX, Abraham R, Romans AM, Yao H, Luthra MG, Anandasabapathy S, Swisher SG, Hofstetter WL, Rashid A, Luthra R (2009) MicroRNA-196a is a potential marker of progression during Barrett's metaplasia-dysplasia-invasive adenocarcinoma sequence in esophagus. Am J Pathol 174:1940-1948.

Matute C (2010) Calcium dyshomeostasis in white matter pathology. Cell Calcium 47:150-157.

McCarthy JJ (2008) MicroRNA-206: the skeletal muscle-specific myomiR. Biochim Biophys Acta 1779:682-691.

Millan MJ (2011) MicroRNA in the regulation and expression of serotonergic transmission in the brain and other tissues. Curr Opin Pharmacol 11:11-22.

Monsonego A, Weiner HL (2003) Immunotherapeutic approaches to Alzheimer's disease. Science 302:834-838.

Moore BW (1965) A soluble protein characteristic of the nervous system. Biochem Biophys Res Commun 19:739-744.

Morgan D (2006) Modulation of microglial activation state following passive immunization in amyloid depositing transgenic mice. Neurochem Int 49:190-194.

Morgan D (2011) Immunotherapy for Alzheimer's disease. J Intern Med 269:54-63.

Mori T, Town T, Tan J, Yada N, Horikoshi Y, Yamamoto J, Shimoda T, Kamanaka Y, Tateishi N, Asano T (2006) Arundic acid ameliorates cerebral amyloidosis and gliosis in Alzheimer transgenic mice. J Pharmacol Exp Ther 318:571-578.

Mori T, Koyama N, Arendash GW, Horikoshi-Sakuraba Y, Tan J, Town T (2010) Overexpression of human S100B exacerbates cerebral amyloidosis and gliosis in the Tg2576 mouse model of Alzheimer's disease. Glia 58:300-314.

Morrissette DA, Parachikova A, Green KN, LaFerla FM (2009) Relevance of transgenic mouse models to human Alzheimer disease. J Biol Chem 284:6033-6037.

Most P, Remppis A, Pleger ST, Katus HA, Koch WJ (2007) S100A1: a novel inotropic regulator of cardiac performance. Transition from molecular physiology to pathophysiological relevance. Am J Physiol Regul Integr Comp Physiol 293:R568-R577.

Mrak RE, Griffin WS (2004) Trisomy 21 and the brain. J Neuropathol Exp Neurol 63:679-685.

Natera-Naranjo O, Aschrafi A, Gioio AE, Kaplan BB (2010) Identification and quantitative analyses of microRNAs located in the distal axons of sympathetic neurons. RNA 16:1516-1529.

Nedergaard M, Rodriguez JJ, Verkhratsky A (2010) Glial calcium and diseases of the nervous system. Cell Calcium 47:140-149.

Nelson PT, Braak H, Markesbery WR (2009) Neuropathology and cognitive impairment in Alzheimer disease: a complex but coherent relationship. J Neuropathol Exp Neurol 68:1-14.

Nishiyama H, Knopfel T, Endo S, Itohara S (2002) Glial protein S100B modulates long-term neuronal synaptic plasticity. Proc Natl Acad Sci U S A 99:4037-4042.

Nogueira MI, Abbas SY, Campos LG, Allemandi W, Lawson P, Takada SH, Azmitia EC (2009) S100beta protein expression: gender- and age-related daily changes. Neurochem Res 34:1355-1362.

Nohata N, Hanazawa T, Kikkawa N, Sakurai D, Sasaki K, Chiyomaru T, Kawakami K, Yoshino H, Enokida H, Nakagawa M, Okamoto Y, Seki N (2011) Identification of novel molecular targets regulated by tumor suppressive miR-1/miR-133a in maxillary sinus squamous cell carcinoma. Int J Oncol 39:1099-1107.

O'Dowd BS, Zhao WQ, Ng KT, Robinson SR (1997) Chicks injected with antisera to either S-100 alpha or S-100 beta protein develop amnesia for a passive avoidance task. Neurobiol Learn Mem 67:197-206.

Okada M, Hatakeyama T, Itoh H, Tokuta N, Tokumitsu H, Kobayashi R (2004) S100A1 is a novel molecular chaperone and a member of the Hsp70/Hsp90 multichaperone complex. J Biol Chem 279:4221-4233.

Opazo C, Barria MI, Ruiz FH, Inestrosa NC (2003) Copper reduction by copper binding proteins and its relation to neurodegenerative diseases. Biometals 16:91-98.

Orgogozo JM, Gilman S, Dartigues JF, Laurent B, Puel M, Kirby LC, Jouanny P, Dubois B, Eisner L, Flitman S, Michel BF, Boada M, Frank A, Hock C (2003) Subacute meningoencephalitis in a subset of patients with AD after abeta42 immunization. Neurology 61:46-54.

Pedersen I, David M (2008) MicroRNAs in the immune response. Cytokine 43:391-394.

Pedersen IM, Cheng G, Wieland S, Volinia S, Croce CM, Chisari FV, David M (2007) Interferon modulation of cellular microRNAs as an antiviral mechanism. Nature 449:919-922.

Pena LA, Brecher CW, Marshak DR (1995) Beta-amyloid regulates gene expression of glial trophic substance S100 beta in C6 glioma and primary astrocyte cultures. Brain Res Mol Brain Res 34:118-126.

Perrone L, Peluso G, Melone MA (2008) RAGE recycles at the plasma membrane in S100B secretory vesicles and promotes Schwann cells morphological changes. J Cell Physiol 217:60-71.

Perry VH, Nicoll JA, Holmes C (2010) Microglia in neurodegenerative disease. Nat Rev Neurol 6:193-201.

Pham N, Fazio V, Cucullo L, Teng Q, Biberthaler P, Bazarian JJ, Janigro D (2010) Extracranial sources of S100B do not affect serum levels. PLoS One 5:e12691.

Pinto SS, Gottfried C, Mendez A, Goncalves D, Karl J, Goncalves CA, Wofchuk S, Rodnight R (2000) Immunocontent and secretion of S100B in astrocyte cultures from different brain regions in relation to morphology. FEBS Lett 486:203-207.

Prosser BL, Wright NT, Hernandez-Ochoa EO, Varney KM, Liu Y, Olojo RO, Zimmer DB, Weber DJ, Schneider MF (2008) S100A1 binds to the calmodulin-binding site of ryanodine receptor and modulates skeletal muscle excitation-contraction coupling. J Biol Chem 283:5046-5057.

Prosser BL, Hernandez-Ochoa EO, Schneider MF (2011) S100A1 and calmodulin regulation of ryanodine receptor in striated muscle. Cell Calcium 50:323-331.

Provost P (2010) MicroRNAs as a molecular basis for mental retardation, Alzheimer's and prion diseases. Brain Res 1338:58-66.

Qin W, Ho L, Wang J, Peskind E, Pasinetti GM (2009) S100A7, a novel Alzheimer's disease biomarker with non-amyloidogenic alpha-secretase activity acts via selective promotion of ADAM-10. PLoS One 4:e4183.

Querfurth HW, LaFerla FM (2010) Alzheimer's disease. N Engl J Med 362:329-344.

Quincozes-Santos A, Rosa RB, Leipnitz G, de Souza DF, Seminotti B, Wajner M, Goncalves CA (2010) Induction of S100B secretion in C6 astroglial cells by the major metabolites accumulating in glutaric acidemia type I. Metab Brain Dis 25:191-198.

Radde R, Duma C, Goedert M, Jucker M (2008) The value of incomplete mouse models of Alzheimer's disease. Eur J Nucl Med Mol Imaging 35 Suppl 1:S70-S74.

Raver-Shapira N, Marciano E, Meiri E, Spector Y, Rosenfeld N, Moskovits N, Bentwich Z, Oren M (2007) Transcriptional activation of miR-34a contributes to p53-mediated apoptosis. Mol Cell 26:731-743.

Rebaudo R, Melani R, Balestrino M, Cupello A, Haglid K, Hyden H (2000) Antiserum against S-100 protein prevents long term potentiation through a cAMP-related mechanism. Neurochem Res 25:541-545.

Reitz C, Brayne C, Mayeux R (2011) Epidemiology of Alzheimer disease. Nat Rev Neurol 7:137-152.

Ricobaraza A, Cuadrado-Tejedor M, Perez-Mediavilla A, Frechilla D, Del Rio J, Garcia-Osta A (2009) Phenylbutyrate ameliorates cognitive deficit and reduces tau

pathology in an Alzheimer's disease mouse model. Neuropsychopharmacology 34:1721-1732.

Roltsch E, Holcomb L, Young KA, Marks A, Zimmer DB (2010) PSAPP mice exhibit regionally selective reductions in gliosis and plaque deposition in response to S100B ablation. J Neuroinflammation 7:78-90.

Romito-DiGiacomo RR, Menegay H, Cicero SA, Herrup K (2007) Effects of Alzheimer's disease on different cortical layers: the role of intrinsic differences in Abeta susceptibility. J Neurosci 27:8496-8504.

Ruse M, Lambert A, Robinson N, Ryan D, Shon KJ, Eckert RL (2001) S100A7, S100A10, and S100A11 are transglutaminase substrates. Biochemistry 40:3167-3173.

Sakatani S, Seto-Ohshima A, Itohara S, Hirase H (2007) Impact of S100B on local field potential patterns in anesthetized and kainic acid-induced seizure conditions in vivo. Eur J Neurosci 25:1144-1154.

Sakatani S, Seto-Ohshima A, Shinohara Y, Yamamoto Y, Yamamoto H, Itohara S, Hirase H (2008) Neural-activity-dependent release of S100B from astrocytes enhances kainate-induced gamma oscillations in vivo. J Neurosci 28:10928-10936.

Salloway S, Sperling R, Gilman S, Fox NC, Blennow K, Raskind M, Sabbagh M, Honig LS, Doody R, van Dyck CH, Mulnard R, Barakos J, Gregg KM, Liu E, Lieberburg I, Schenk D, Black R, Grundman M (2009) A phase 2 multiple ascending dose trial of bapineuzumab in mild to moderate Alzheimer disease. Neurology 73:2061-2070.

Santamaria-Kisiel L, Rintala-Dempsey AC, Shaw GS (2006) Calcium-dependent and -independent interactions of the S100 protein family. Biochem J 396:201-214.

Satoh J (2010) MicroRNAs and their therapeutic potential for human diseases: aberrant microRNA expression in Alzheimer's disease brains. J Pharmacol Sci 114:269-275.

Saugstad JA (2010) MicroRNAs as effectors of brain function with roles in ischemia and injury, neuroprotection, and neurodegeneration. J Cereb Blood Flow Metab 30:1564-1576.

Saunders LR, Sharma AD, Tawney J, Nakagawa M, Okita K, Yamanaka S, Willenbring H, Verdin E (2010) MiRNAs regulate SIRT1 expression during mouse embryonic stem cell differentiation and in adult mouse tissues. Aging (Albany NY) 2:415-431.

Schenk D (2002) Amyloid-beta immunotherapy for Alzheimer's disease: the end of the beginning. Nat Rev Neurosci 3:824-828.

Schulte-Herbruggen O, Hortnagl H, Ponath G, Rothermundt M, Hellweg R (2008) Distinct regulation of brain-derived neurotrophic factor and noradrenaline in S100B knockout mice. Neurosci Lett 442:100-103.

Sen J, Belli A (2007) S100B in neuropathologic states: the CRP of the brain? J Neurosci Res 85:1373-1380.

Serrano-Pozo A, Frosch MP, Masliah E, Hyman BT (2011) Neuropathological alterations in Alzheimer disease. Cold Spring Harb Perspect Biol 3:a006189.

Shanmugam N, Kim YS, Lanting L, Natarajan R (2003) Regulation of cyclooxygenase-2 expression in monocytes by ligation of the receptor for advanced glycation end products. J Biol Chem 278:34834-34844.

Shanmugam N, Reddy MA, Natarajan R (2008) Distinct roles of heterogeneous nuclear ribonuclear protein K and microRNA-16 in cyclooxygenase-2 RNA stability induced by S100b, a ligand of the receptor for advanced glycation end products. J Biol Chem 283:36221-36233.

Sheng JG, Mrak RE, Rovnaghi CR, Kozlowska E, Van Eldik LJ, Griffin WS (1996) Human brain S100 beta and S100 beta mRNA expression increases with age: pathogenic implications for Alzheimer's disease. Neurobiol Aging 17:359-363.

Shepherd CE, Goyette J, Utter V, Rahimi F, Yang Z, Geczy CL, Halliday GM (2006) Inflammatory S100A9 and S100A12 proteins in Alzheimer's disease. Neurobiol Aging 27:1554-1563.

Small SA, Duff K (2008) Linking Abeta and tau in late-onset Alzheimer's disease: a dual pathway hypothesis. Neuron 60:534-542.

Solomon B, Frenkel D (2010) Immunotherapy for Alzheimer's disease. Neuropharmacology 59:303-309.

Sonntag KC (2010) MicroRNAs and deregulated gene expression networks in neurodegeneration. Brain Res 1338:48-57.

Sorci G, Bianchi R, Riuzzi F, Tubaro C, Arcuri C, Giambanco I, Donato R (2010) S100B protein, a damage-associated molecular pattern protein in the brain and heart, and beyond. Cardiovasc Psychiatry Neurol 2010: article ID 656481.

Srikanth V, Maczurek A, Phan T, Steele M, Westcott B, Juskiw D, Munch G (2011) Advanced glycation endproducts and their receptor RAGE in Alzheimer's disease. Neurobiol Aging 32:763-777.

Steiner J, Walter M, Guest P, Myint AM, Schiltz K, Panteli B, Brauner M, Bernstein HG, Gos T, Herberth M, Schroeter ML, Schwarz MJ, Westphal S, Bahn S, Bogerts B (2010) Elevated S100B levels in schizophrenia are associated with insulin resistance. Mol Psychiatry 15:3-4.

Steiner J, Schroeter ML, Schiltz K, Bernstein HG, Muller UJ, Richter-Landsberg C, Muller WE, Walter M, Gos T, Bogerts B, Keilhoff G (2010) Haloperidol and clozapine decrease S100B release from glial cells. Neuroscience 167:1025-1031.

Steiner J, Bogerts B, Schroeter ML, Bernstein HG (2011) S100B protein in neurodegenerative disorders. Clin Chem Lab Med 49:409-424.

Sun F, Fu H, Liu Q, Tie Y, Zhu J, Xing R, Sun Z, Zheng X (2008) Downregulation of CCND1 and CDK6 by miR-34a induces cell cycle arrest. FEBS Lett 582:1564-1568.

Supnet C, Bezprozvanny I (2010) Neuronal calcium signaling, mitochondrial dysfunction, and Alzheimer's disease. J Alzheimers Dis 20 Suppl 2:S487-S498.

Supnet C, Bezprozvanny I (2010) The dysregulation of intracellular calcium in Alzheimer disease. Cell Calcium 47:183-189.

Takeuchi M, Yamagishi S (2008) Possible involvement of advanced glycation end-products (AGEs) in the pathogenesis of Alzheimer's disease. Curr Pharm Des 14:973-978.

Tarasov V, Jung P, Verdoodt B, Lodygin D, Epanchintsev A, Menssen A, Meister G, Hermeking H (2007) Differential regulation of microRNAs by p53 revealed by massively parallel sequencing: miR-34a is a p53 target that induces apoptosis and G1-arrest. Cell Cycle 6:1586-1593.

Thind K, Sabbagh MN (2007) Pathological correlates of cognitive decline in Alzheimer's disease. Panminerva Med 49:191-195.

Tomiyama T, Matsuyama S, Iso H, Umeda T, Takuma H, Ohnishi K, Ishibashi K, Teraoka R, Sakama N, Yamashita T, Nishitsuji K, Ito K, Shimada H, Lambert MP, Klein WL, Mori H (2010) A mouse model of amyloid beta oligomers: their contribution to synaptic alteration, abnormal tau phosphorylation, glial activation, and neuronal loss in vivo. J Neurosci 30:4845-4856.

Townley-Tilson WH, Callis TE, Wang D (2010) MicroRNAs 1, 133, and 206: critical factors of skeletal and cardiac muscle development, function, and disease. Int J Biochem Cell Biol 42:1252-1255.

Tramontina F, Tramontina AC, Souza DF, Leite MC, Gottfried C, Souza DO, Wofchuk ST, Goncalves CA (2006) Glutamate uptake is stimulated by extracellular S100B in hippocampal astrocytes. Cell Mol Neurobiol 26:81-86.

Uchida Y, Chiyomaru T, Enokida H, Kawakami K, Tatarano S, Kawahara K, Nishiyama K, Seki N, Nakagawa M (2011) MiR-133a induces apoptosis through direct regulation of GSTP1 in bladder cancer cell lines. Urol Oncol Mar 9. [Epub ahead of print]

van Dieck J, Fernandez-Fernandez MR, Veprintsev DB, Fersht AR (2009) Modulation of the oligomerization state of p53 by differential binding of proteins of the S100 family to p53 monomers and tetramers. J Biol Chem 284:13804-13811.

Van Eldik LJ, Griffin WS (1994) S100 beta expression in Alzheimer's disease: relation to neuropathology in brain regions. Biochim Biophys Acta 1223:398-403.

Van Eldik LJ, Wainwright MS (2003) The janus face of glial-derived S100B: beneficial and detrimental functions in the brain. Restor Neurol Neurosci 21:97-108.

Vangheluwe P, Raeymaekers L, Dode L, Wuytack F (2005) Modulating sarco(endo)plasmic reticulum Ca2+ ATPase 2 (SERCA2) activity: cell biological implications. Cell Calcium 38:291-302.

Vaziri H, Dessain SK, Ng Eaton E, Imai SI, Frye RA, Pandita TK, Guarente L, Weinberg RA (2001) hSIR2(SIRT1) functions as an NAD-dependent p53 deacetylase. Cell 107:149-159.

Verkhratsky A, Olabarria M, Noristani HN, Yeh CY, Rodriguez JJ (2010) Astrocytes in Alzheimer's disease. Neurotherapeutics 7:399-412.

Verma R, Cutler DJ, Holmans P, Knowles JA, Crowe RR, Scheftner WA, Weissman MM, DePaulo JR, Jr., Levinson DF, Potash JB (2007) Investigating the role of p11 (S100A10) sequence variation in susceptibility to major depression. Am J Med Genet B Neuropsychiatr Genet 144B:1079-1082.

Wang FE, Zhang C, Maminishkis A, Dong L, Zhi C, Li R, Zhao J, Majerciak V, Gaur AB, Chen S, Miller SS (2010) MicroRNA-204/211 alters epithelial physiology. FASEB J 24:1552-1571.

Wang WX, Rajeev BW, Stromberg AJ, Ren N, Tang G, Huang Q, Rigoutsos I, Nelson PT (2008) The expression of microRNA miR-107 decreases early in Alzheimer's disease and may accelerate disease progression through regulation of beta-site amyloid precursor protein-cleaving enzyme 1. J Neurosci 28:1213-1223.

Wang X, Liu P, Zhu H, Xu Y, Ma C, Dai X, Huang L, Liu Y, Zhang L, Qin C (2009) MiR-34a, a microRNA up-regulated in a double transgenic mouse model of Alzheimer's disease, inhibits bcl2 translation. Brain Res Bull 80:268-273.

Whitaker-Azmitia PM, Murphy R, Azmitia EC (1990) Stimulation of astroglial 5-HT1A receptors releases the serotonergic growth factor, protein S-100, and alters astroglial morphology. Brain Res 528:155-158.

Winbanks CE, Wang B, Beyer C, Koh P, White L, Kantharidis P, Gregorevic P (2011) TGF-beta regulates miR-206 and miR-29 to control myogenic differentiation through regulation of HDAC4. J Biol Chem 286:13805-13814.

Winter J, Jung S, Keller S, Gregory RI, Diederichs S (2009) Many roads to maturity: microRNA biogenesis pathways and their regulation. Nat Cell Biol 11:228-234.

Wright NT, Cannon BR, Zimmer DB, Weber DJ (2009) S100A1: structure, function, and therapeutic potential. Curr Chem Biol 3:138-145.

Wyss-Coray T, Mucke L (2002) Inflammation in neurodegenerative disease--a double-edged sword. Neuron 35:419-432.

Xiao J, Zhu X, He B, Zhang Y, Kang B, Wang Z, Ni X (2011) MiR-204 regulates cardiomyocyte autophagy induced by ischemia-reperfusion through LC3-II. J Biomed Sci 18:35-40.

Xiong Z, O'Hanlon D, Becker LE, Roder J, MacDonald JF, Marks A (2000) Enhanced calcium transients in glial cells in neonatal cerebellar cultures derived from S100B null mice. Exp Cell Res 257:281-289.

Xu G, Zhang Y, Jia H, Li J, Liu X, Engelhardt JF, Wang Y (2009) Cloning and identification of microRNAs in bovine alveolar macrophages. Mol Cell Biochem 332:9-16.

Yan SD, Chen X, Fu J, Chen M, Zhu H, Roher A, Slattery T, Zhao L, Nagashima M, Morser J, Migheli A, Nawroth P, Stern D, Schmidt AM (1996) RAGE and amyloid-beta peptide neurotoxicity in Alzheimer's disease. Nature 382:685-691.

Yan SD, Bierhaus A, Nawroth PP, Stern DM (2009) RAGE and Alzheimer's disease: a progression factor for amyloid-beta-induced cellular perturbation? J Alzheimers Dis 16:833-843.

Yoshino H, Chiyomaru T, Enokida H, Kawakami K, Tatarano S, Nishiyama K, Nohata N, Seki N, Nakagawa M (2011) The tumour-suppressive function of miR-1 and miR-133a targeting TAGLN2 in bladder cancer. Br J Cancer 104:808-818.

Zhang YW, Thompson R, Zhang H, Xu H (2011) APP processing in Alzheimer's disease. Mol Brain 4:3-16.

Zimmer DB, Landar A (1995) Analysis of S100A1 expression during skeletal muscle and neuronal cell differentiation. J Neurochem 64:2727-2736.

Zimmer DB, Cornwall EH, Landar A, Song W (1995) The S100 protein family: history, function, and expression. Brain Res Bull 37:417-429.

Zimmer DB, Cornwall EH, Reynolds PD, Donald CM (1998) S100A1 regulates neurite organization, tubulin levels, and proliferation in PC12 cells. J Biol Chem 273:4705-4711.

Zimmer DB, Wright Sadosky P, Weber DJ (2003) Molecular mechanisms of S100-target protein interactions. Microsc Res Tech 60:552-559.

Zimmer DB, Chaplin J, Baldwin A, Rast M (2005) S100-mediated signal transduction in the nervous system and neurological diseases. Cell Mol Biol (Noisy-le-grand) 51:201-214.

Zimmer DB, Weber DJ (2010) The calcium-dependent interaction of S100B with its protein targets. Cardiovasc Psychiatry Neurol 2010: article ID 728052.

VITA

Name: Emily Anna Roltsch

Education: Ph.D., Veterinary Microbiology, Texas A&M University, 2011
M.S., Veterinary Medical Sciences, Texas A&M University, 2007
B.S., Biomedical Sciences, Texas A&M University, 2005

Address: IBBR
C/O Dr. Danna Zimmer
9600 Gudelsky Drive
Rockville, MD 20850

Email Address: eroltsch@me.com